

Development of real-time mechanistic tools for the elucidation of catalytic reaction mechanisms

by

Rhonda Louise Stoddard
B. Sc., Dalhousie University, 2011

A Thesis Submitted in Partial Fulfillment
of the Requirements for the Degree of

Master of Science

in the Department of Chemistry

© Rhonda Louise Stoddard, 2014

University of Victoria

All rights reserved. This thesis may not be reproduced in whole or in part, by photocopy or other means, without the permission of the author.

Supervisory Committee

Development of real-time mechanistic tools for the elucidation of catalytic reaction mechanisms

by

Rhonda Louise Stoddard
B. Sc., Dalhousie University, 2011

Supervisory Committee

Dr. J. Scott McIndoe, Department of Chemistry
Supervisor

Dr. David J. Berg, Department of Chemistry
Departmental Member

Abstract

Supervisory Committee

Dr. J. Scott McIndoe, Department of Chemistry

Supervisor

Dr. David J. Berg, Department of Chemistry

Departmental Member

The mechanism of a conjugate addition of an alcohol to an alkynic acid ester using a phosphine catalyst was investigated using pressurized sample infusion electrospray ionization mass spectrometry (PSI-ESI-MS) and proton and phosphorus nuclear magnetic resonance (NMR) experiments. Since ESI-MS only detects charged species, and only the phosphonium intermediates and by-products were visible by ESI-MS, ^1H NMR was used to track the disappearance of the starting alkyne and the appearance of the conjugate addition product over time. ^{31}P NMR was used to quantify the ESI-MS results. By-product formation was shown to out-compete product formation upon fast addition of alkyne, but with dropwise addition of alkyne, product was shown to dominate. A detailed numerical model was developed using PowerSim software to test mechanistic hypotheses. The experimental results were shown to be consistent with the mechanism proposed by Inanaga, and the cycle was elaborated to account for by-product formation.

Piers' catalyst, a ruthenium complex with a phosphonium-functionalized carbene ligand, is a fast-initiating living catalyst for a number of olefin metathesis reactions, including ring-opening metathesis polymerization (ROMP) and cross metathesis (CM). Catalyst speciation was monitored in real-time for the ROMP of norbornene and the CM of 1-hexene using PSI-ESI-MS. The expected mass distribution of charged polymer-catalyst species were not observed, but merely catalyst and decomposition species were visible by ESI-MS. NMR and gel permeation chromatography (GPC) were used to determine quantitatively the presence of polymer and the polydispersity index, respectively. The results suggest that while Piers' catalyst is indeed fast-initiating, the propagation rate greatly outstrips the initiation rate.

In a foray into the area of chemical education, a well-known pH-induced colour change exhibited by the anthocyanins in red cabbage was developed into a simple – and ingestible – classroom demonstration.

Table of Contents

Supervisory Committee	ii
Abstract	iii
Table of Contents	iv
List of Schemes	vi
List of Figures	vii
List of Abbreviations	x
Acknowledgments	xii
Dedication	xiii
Chapter 1. Overview of online reaction monitoring by ESI-MS	1
1.1 The path of the ions	2
1.2 PSI-ESI-MS	6
1.3 Collision Induced Dissociation	7
1.4 Organic and Organometallic Catalysis Reaction Studies by ESI-MS	8
1.5 Protection from oxygen and moisture	9
Chapter 2. Phosphine Catalysis	13
2.1 Introduction	13
2.2. Results and Discussion	20
Table 1. List of numbered species for phosphine catalysis.	20
2.2.1. ¹ H NMR	21
2.2.2 ³¹ P NMR	27
2.2.3 PSI-ESI-MS	29
2.2.4. Numerical modeling	33
2.2.5. Drop-wise addition of alkyne	44
2.2.6 Effect of a sterically hindered alcohol on product yield	45
2.3 Conclusions	48
2.4 Experimental	48
Chapter 3: Olefin Metathesis	51
3.1 Overview of Olefin Metathesis	51
3.2 Living polymerization and polydispersity index	53
3.3 Ring Opening Metathesis Polymerization	55
3.4 Development of ROMP catalysts	56
3.4.1 Ill-defined ruthenium metathesis catalysts for ROMP	56
3.4.2 Well-defined ruthenium catalysts for ROMP	56
3.4.3 Ruthenium Catalyst Decomposition	59
3.5 Piers' Catalyst for ROMP	61
3.6 Results and Discussion for ROMP	63
Table 2. List of numbered species for ROMP and CM.	63
3.6.1 ESI-MS	63
3.6.2 ¹ H NMR	72
3.6.3 Polydispersity Index by Gel Permeation Chromatography	74
3.7 Conclusions	75
3.8 Cross Metathesis	76

3.8.1 Introduction.....	76
3.8.2 Results and Discussion for CM.....	77
3.8.3 ¹ H NMR with 1-hexene	82
3.9 Conclusions.....	89
3.10 Future work.....	90
3.11 Experimental.....	90
Chapter 4: The Colour-Changing Sports Drink	93
4.1 Introduction.....	93
4.2 Results and Discussion	95
4.3 Experimental.....	96
4.3.1 Red Cabbage	96
4.3.2 Blueberries	97
4.4 Conclusions.....	98
Bibliography	99
Appendix A NMR spectra for phosphine catalysis.....	103
³¹ P NMR spectra for phosphine catalysis with ethyl-butynoate and ethanol in CD ₃ CN....	107
ESI-MS spectra	110
Parameter optimization with Copasi.....	111

List of Schemes

Scheme 1. Morita's first reported phosphine catalysis of acrylonitrile with an aldehyde to form an allylic alcohol; depiction of the zwitterion in "carbinol addition".....	14
Scheme 2. Morita-Baylis-Hillman reaction of an aldehyde with an α - β -unsaturated ketone and 1,4-diazabicyclo[2.2.2]octane (DABCO) catalyst to generate an allylic alcohol.....	14
Scheme 3. After the phosphine attacks the β -carbon of the olefin, electron density is directed towards either the α - or γ -carbon, allowing for regioselective attack on the substrate under different reaction conditions.	15
Scheme 4. A selection of phosphine-mediated reactions.....	16
Scheme 5. Mechanisms in phosphine catalysis demonstrating (top) γ -carbon umpolung with a protic nucleophile, and (bottom) super-reactivity of an allenolate.	17
Scheme 6. Iterative use of a phosphine-mediated addition, leading to a radical cascade precursor.	18
Scheme 7. Proposed catalytic cycle for the tributylphosphine-catalyzed addition of ethanol to ethyl butynoate.....	19
Scheme 8: Proposed mechanism suggested by ^1H NMR, ^{31}P NMR, and PSI-ESI-MS.....	32
Scheme 9. Reaction scheme including generation of by-products, and the numerically modelled forward and reverse rate constants in green and red, respectively.	41
Scheme 10. Mechanism accounting for the exchange of the two alkoxides present in solution and the formation of the phosphonium intermediates detected by PSI-ESI-MS.....	47
Scheme 11. Top depicts the proposed "pairwise" breakage of C=C bonds to form a metal coordinated cyclobutene followed by construction of new C=C bonds. Bottom depicts the now established [2 +2] cycloaddition to form the metallacycle followed by cycloreversion to form the new olefin and metal carbene.	52
Scheme 12. Synthesis (top) of the first well-defined ruthenium (II) metathesis catalyst, and (bottom) reaction with the norbornene monomer and functionalization of the growing polynorbornene.	57
Scheme 13. Regeneration of the starting phosphonium olefin.	81
Scheme 14. List of reactions detected by ESI-MS and by ^1H NMR	88

List of Figures

Figure 1.1. The desolvation process in electrospray ionization.....	2
Figure 1.2. Setup for the ion path through the source.....	3
Figure 1.3. Ion path through the mass analyser to the time-of-flight (ToF).	5
Figure 1.4. Path for ions of the same mass given same kinetic energy through the reflectron.	6
Figure 1.5. PSI sample delivery setup.	7
Figure 1.6. Setup for PSI-ESI-MS in the glovebox using a party balloon.....	10
Figure 1.7. Setup for tandem glovebox-MS.....	10
Figure 1.8. High concentration of hydrolyzed AlMe ₃	11
Figure 2.1. Reaction progress as seen with ¹ H NMR.	22
Figure 2.2. Multiple peak formation in the ester and ether range as seen with ¹ H NMR.....	23
Figure 2.3. Illustration of change in chemical shift for starting alkyne ester protons	25
Figure 2.4. Starting alkyne ethylene peak monitored by ¹ H NMR over 4 hours.....	26
Figure 2.5. ³¹ P NMR stacked plot showing the dynamic progress of phosphonium oligomer peaks.	28
Figure 2.6. Intensity traces generated by quantitative ³¹ P NMR.	28
Figure 2.7 Positive ion mass spectrum 20 minutes after catalyst addition..	29
Figure 2.8. Reaction progress according to PSI-ESI-MS.	30
Figure 2.9. Simple example with PowerSim Studio 9 Academic software..	34
Figure 2.10. PowerSim models for three proposed mechanisms.....	35
Figure 2.11. Differential equations generated by Copasi for the proposed mechanism.	40
Figure 2.12. Numerical model output for the substrate, product, key phosphonium intermediates and decomposition oligomers	42

Figure 2.13. Experimental results for ^1H NMR compared to the numerical model for the starting alkyne and product traces.....	43
Figure 2.14. Drop-wise addition of alkyne to ethanol and tributylphosphine catalyst, compared with Copasi model	44
Figure 2.15. MS data for the reaction of ethyl-2-butynoate with neopentyl alcohol and $^n\text{Bu}_3\text{P}$ catalyst.	46
Figure 3.1. Example of molecular weight distribution for polymer chains	54
Figure 3.2. Example of a Schrock metathesis catalyst, Grubbs' first and second generation metathesis catalysts, and Hoyveda-Grubbs second generation metathesis catalyst.	58
Figure 3. 3. Grubbs' 2 nd generation catalysts characterized by X-ray crystallography, and ^1H and ^{31}P NMR.....	61
Figure 3. 4. Reaction of Piers' catalyst with ethylene at -50°C generating the vinylphosphonium salt and parent ruthenacycle in high yield.....	62
Figure 3.5. Depiction of possible ruthenium decomposition partners	65
Figure 3.6. Normalized plot showing the decomposition of Piers' catalyst with heat in acetonitrile solvent	65
Figure 3.7. Combined spectra of oligomers.....	66
Figure 3.8. 1% catalyst loading with Piers' catalyst and norbornene in MeCN solvent at reflux temperature..	67
Figure 3.9. 1% catalyst loading with Piers' catalyst and norbornene in MeCN solvent at reflux temperature showing all oligomers.....	68
Figure 3.10. 1% catalyst loading for three reactions with norbornene	69
Figure 3.11. Norbornene with 1% catalyst loading in MeCN at reflux showing abundance traces for the catalyst and isotope patterns for decomposed Ruthenium.	71
Figure 3.12. Normalized plots showing the constant intensity of Piers' catalyst in CH_2Cl_2 at RT with isotope patterns.	72
Figure 3.13. Stacked ^1H NMR plot for ROMP with norbornene and Piers' catalyst.	73

Figure 3.14. LALS GPC plot for the ROMP of Piers' catalyst and norbornene, generating polynorbornene and depiction of incomplete activation of catalyst and chain propagation as determined by GPC.....	75
Figure 3.15. Optimization of statistical isomers by design, through careful choice of starting olefin partners.	77
Figure 3.16. Appearance of charged product and by-product with disappearance of catalyst. 0.05% catalyst loading and 0.04M 1-hexene were used.....	78
Figure 3.17. 0.5% catalyst loading with 1-hexene in CH ₂ Cl ₂ observed by ESI-MS.....	79
Figure 3.18. Reaction of Piers' catalyst with 1-hexene-6-triphenylphosphonium hexafluorophosphate in CH ₂ Cl ₂	80
Figure 3.19. 100% catalyst loading with charge-tagged 1-hexene showing depletion of the charged catalyst and regeneration of the tagged hexene over 80 minutes at RT.....	82
Figure 3.20. 1-hexene in CDCl ₃ , before catalyst addition.....	83
Figure 3.21. 9 minutes after catalyst addition.....	84
Figure 3.22. 10 minutes after catalyst addition.....	84
Figure 3.23. 45 minutes after catalyst addition.....	85
Figure 3.24. ¹ H NMR expansion showing the appearance of ethene and of cis- and trans- decene	85
Figure 4.1. pH-causing transitional forms of cyanidin in red cabbage.....	94
Figure 4.2. Changing pH causing protonation and rearrangement of the π-bonds in the anthocyanins from red cabbage change the colour in the sports drink.....	95
Figure 4.3. The three solutions used in the red cabbage experiment: blue + clear = pink.....	97
Figure 4.4. The three solutions used in the blueberry experiment: purple + clear = green.	98

1 List of Abbreviations

^1H	proton nuclear magnetic resonance
^{31}P	phosphorus nuclear magnetic resonance
AcOH	acetic acid
AIBN	azobisisobutyronitrile
a.m.u	atomic mass units
a.u.	arbitrary units
CID	collision induced dissociation
CM	cross metathesis
COD	cyclooctadiene
Da	Daltons
DC	direct current
DIBAL-H	diisobutylaluminum hydride
EI	electron impact or electron ionization
E_k	kinetic energy
ESI	Electrospray Ionization
Et	ethyl
EWG	electron withdrawing group
GPC	Gel permeation chromatography
ID	inner diameter
LALS	low angle light scattering
LSODA	Livermore solver for ordinary differential equations
MBH	Morita-Baylis-Hillman
MCP	micro-channel plate
Me	methyl
mes	mesityl
M_n	number average molecular weight
MS	mass spectrometry / mass spectrometer / mass spectrum
MS/MS	tandem mass spectrometry
MW	molecular weight
M_w	weight average molecular weight
m/z	mass-to-charge ratio
NaOAc	sodium acetate
NHC	<i>N</i> -Heterocyclic carbene
NMR	nuclear magnetic resonance
Np	neopentyl
Nu	nucleophile
$^n\text{Bu}_3\text{P}$	<i>n</i> -tributylphosphine
OPBu ₃	tributylphosphine oxide
PCy ₃	tricyclohexylphosphine
PEEK	poly ether ether ketone
PDI	polydispersity index

Ph	phenyl
PMe ₃	trimethylphosphine
PPh ₃	triphenylphosphine
psi	pounds per square inch
PSI	pressurized sample infusion
Q-ToF	quadrupole-time-of-flight
rf	radio frequency
ROMP	ring-opening metathesis polymerization
RT	room temperature
SPS	solvent purification system
T1	spin-lattice relaxation time
TIC	total ion count
ToF	time-of-flight
Ts	tosyl

Acknowledgments

I wish to thank Dr. J. Scott McIndoe for allowing me the opportunity to work in his research group and to learn from him. He has been a very patient teacher and mentor, and has encouraged me, but not overshadowed me, which I appreciate a great deal. His greatest skills lie in recognizing opportunities and niches that others have not seen and encouraging others to successfully implement them, and to be excited about what they can achieve. For an apprehensive, chemically timid grad student, he knew how best embolden me to attain those towering, far-away goals and I thank him earnestly for that.

Ori Granot and Chris Barr I thank heartily for teaching me about mass spec and NMR. You are both extremely knowledgeable and easy to work with and you have both helped me to solve difficult puzzles in my research.

I would also like to thank my group members, Zohrab and Jingwei for teaching and mentoring me in everything involved with grad school. You both made my time fruitful and enjoyable and I wouldn't have gotten this far without both of you. My other group members, Eric, Lars, Robin, Jessamyn, Tsuki, Natalie, Steven, Amelia, Karlee, James, Kristen, Tengfei, Yaneris, Tony, and Christine for making the lab environment an easy place to come to work every day.

Minnie and Mac, Ruth and Donald you all gave me your love, intelligence and work ethic. Pharah, you have been my close friend most of my life, and I am grateful for you.

Mom, you are the first and last, most important encourager and supporter with the largest heart, and you are always at the forefront of my mind when I worry I can't do something. You have always told me I can, and you always tell me the truth.

Dedication

For all the chemists who dedicate their lives
To helping mankind
Even if most men are oblivious to the
Truths of science:

THERE are hermit souls that live withdrawn
In the place of their self-content;
There are souls like stars, that dwell apart,
In a fellowless firmament;
There are pioneer souls that blaze the paths
Where highways never ran-
But let me live by the side of the road
And be a friend to man.

Let me live in my house by the side of the road,
Where the race of men go by-
They are good, they are bad, they are weak, they are strong,
Wise, foolish - so am I.
Then why should I sit in the scorner's seat,
Or hurl the cynic's ban?
Let me live in my house by the side of the road
And be a friend to man.

Sam Walter Foss

Chapter 1. Overview of online reaction monitoring by ESI-MS

ESI-MS was developed by John Fenn and subsequently published in *Science* in 1989.¹ He won the Nobel Prize in Chemistry in 2002 for his work. Until that time, the main method of ionization was electron ionization (EI) which used a metal filament with an applied electrical current, producing heat. Electrons are pulled off the analyte molecule, creating an ion, but fragmentation of analyte occurs to such an extent that the unfragmented molecular ion is rarely seen, and EI is considered to be a “hard” ionization technique.² In contrast, ESI is a “soft” ionization method as fragmentation rarely occurs and the molecular ion is easily discerned.³ Additionally, cations and anions alike may be analyzed by this technique which is not true for EI-MS, which is an ionization technique that only creates cations (an electron capture variant exists but is not of broad utility). ESI-MS is ideally suited to the analysis of organometallic compounds and catalysis,⁴ as fragmentation rarely occurs making this method of ionization highly conducive to study of these delicate systems.⁵ Some main advantages include: it is especially capable of separating complex reaction mixtures, containing reactants, products, intermediates, resting states, by-products, and decomposed species; it is sensitive,⁶ allowing for trace intermediates to be easily discerned; and it has a dynamic range⁷ in which the abundance of species can be measured across many orders of magnitude. Reactions can be monitored using this technique over a period of minutes or hours and the acquisition of one spectrum can take less than one second. When these spectra are combined into abundance traces, the numerous individual snapshots flow into a time-resolved composite that provides more than just instantaneous relative concentrations of many species. The shape of each concentration versus time curve tells us about the kinetics of each species.

1.1 The path of the ions

The reaction solution is directed through a stainless steel capillary at atmospheric pressure which is given either a positive or negative charge of 2500-4000V. At this high voltage, the solvent rapidly aerosolizes into a spray of fine droplets that carry an excess of positive (or negative) charge, due to oxidative (reductive) electrochemical processes occurring at the capillary. These processes are oxidation (reduction) of the solvent, the capillary itself, or sometimes the analyte itself. The excess positive charges repel one another, so as the droplet shrinks under the influence of a warm desolvation gas, ions evaporate from the surface of the droplet (Figure 1.1).

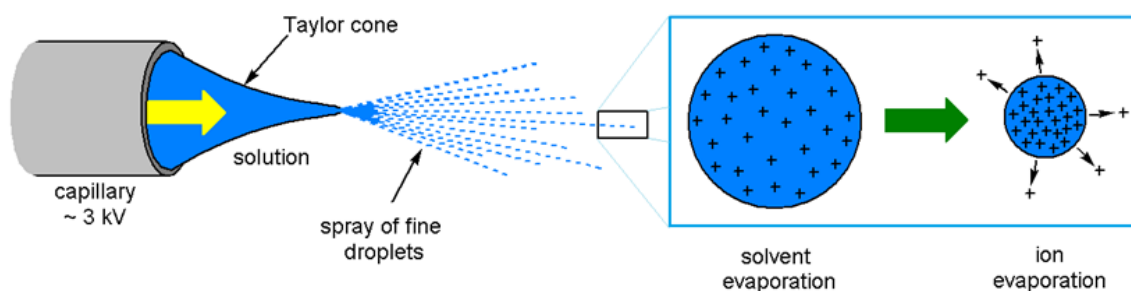


Figure 1.1. The desolvation process in electrospray ionization.

The now desolvated analyte ions, in the gas phase, are drawn into the mass spectrometer and the solvent and desolvation gases are pumped away as the ions come under the influence of the multipole ion guides at the entrance to the instrument (Figure 1.2).

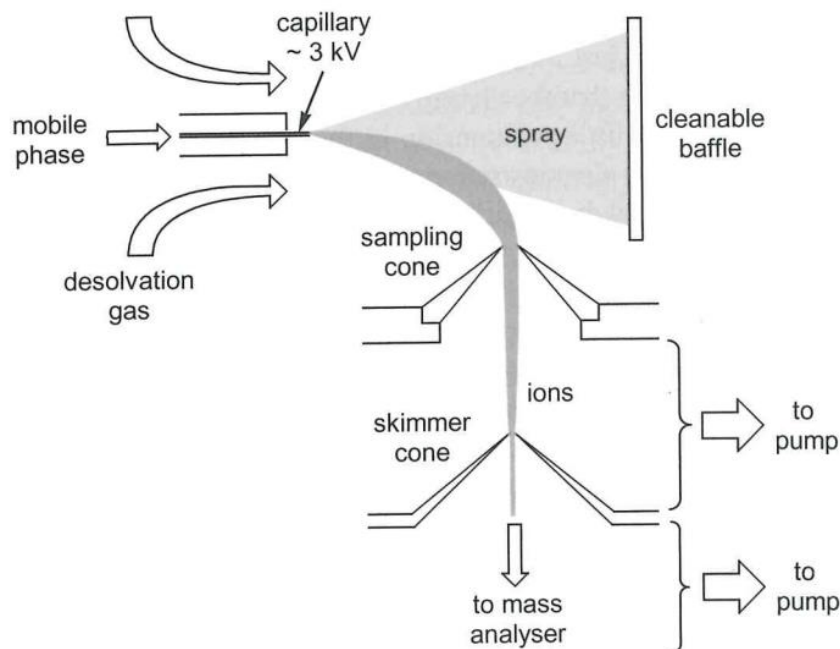


Figure 1.2. Setup for the ion path through the source. Ions leave the capillary, most strike the baffle, the remainder entering the sampling and skimmer cones before being directed by differential pressure to the first mass analyser.

From that point on, vacuum pumps decrease the pressure through a series of differentially pumped chambers. The vacuum is important to prevent collisions between ions as they move to the detector and aids in ensuring that all ions of the same mass to charge ratio (m/z) will reach the detector at the same time.

The ions next move through a hexapole (6 parallel metal rods) that focuses the ions into the first mass analyzer, a quadrupole (4 parallel metal rods) with an applied rf and DC voltage. Each rod is paired electrically with the rod opposite and the pair holds an opposite polarity to the other pair. The polarity rapidly switches back and forth and as the ions enter, they are drawn to one of the rods with the opposite charge. As the polarity of the rods switch, so the path of the ion switches trajectory. When the quadrupole is used as a mass filter, the influence of the field imposes complex trajectories on the ions. The rf potential can be changed by the user to allow

passage of ions with stable trajectories to the detector, but those with unstable trajectories will fall out of the path.

Between the quadrupole and the ToF (time-of-flight) lies the collision cell (which is at a pressure of $\sim 1 \times 10^{-3}$ torr) that allows for fragmentation of chosen ions (MS/MS). When not being used for fragmentation purposes, it merely serves to guide the ions to the ToF chamber.

A Micromass Quadrupole Time of Flight (Q-ToF) Micro tandem mass spectrometer was the mass spectrometer used for the research in this thesis. The ToF is the second mass analyser and the chamber is under a very low pressure, which is differentially pumped to $\sim 2 \times 10^{-7}$ mbar, from atmospheric pressure, and the low vacuum draws the gas phase ions into the ToF chamber. Since the Newtonian formula for kinetic energy is

$$E_k = \frac{1}{2} mv^2 \quad (1)$$

it is known that ions of different masses will have different velocities. If the energy and path length (~ 1 meter in our instrument) are held constant, then two ions with the same mass should reach the detector at the same time. The mass of each ion is therefore determined by how long it takes to travel down the flight tube to the detector. This mass analyzer takes its name, “Time of Flight” (ToF) from this equation. An electric pulse accelerates the ions from the source into a drift region, which must be free of magnetic and electric fields and at high vacuum.

Kinetic energy can also be related to charge with the equation:

$$E_k = zeV \quad (2)$$

Where z is the charge on the ion, e is the charge of an electron in coulombs, and V is the strength of the electric field in volts. Relating (1) and (2), gives

$$zeV = \frac{1}{2} mv^2 \quad (3)$$

$$zeV = \frac{1}{2} m (dx/dt)^2 \quad (4)$$

Rearranging this equation, one can determine the m/z for an ion:

$$m/z = 2eV \Delta t^2 / \Delta x^2 \quad (5)$$

m is mass in kg, Δt is the flight time and Δx is the flight path length in meters. The pulse gives all ions of the same charge the same energy, so the ions separate according to their m/z value, the ions with lower m/z values reaching the detector first (Figure 1.3).

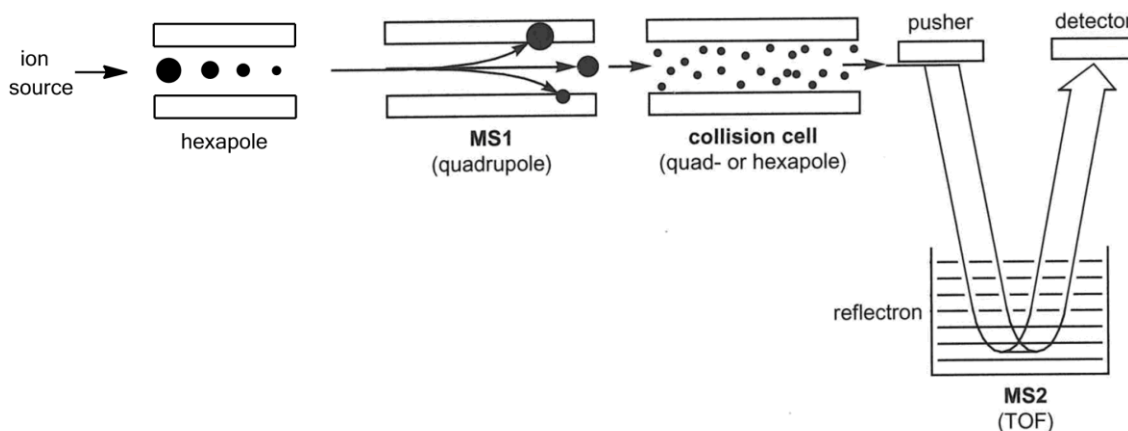


Figure 1.3. Ion path through the mass analyser to the time-of-flight (ToF).

The ToF chamber is under a very high vacuum to ensure a long mean free path for each ion. Ions with the same m/z can have different initial kinetic energies and to ensure that ions of the same mass reach the detector at the same time, each ion is pushed on an orthogonal trajectory toward a reflectron, which is a series of strong electric field gradients that behaves like a mirror. The ions spread out after being accelerated from the pusher and those with greater kinetic energy (faster moving) penetrate more deeply into the reflectron field, taking longer to return to the detector, however on the trip from the reflectron, all ions of the same mass spend the same amount of time in the ToF chamber and arrive at the detector at the same instant (Figure 1.4). This enhances detection at the micro-channel plate (MCP).

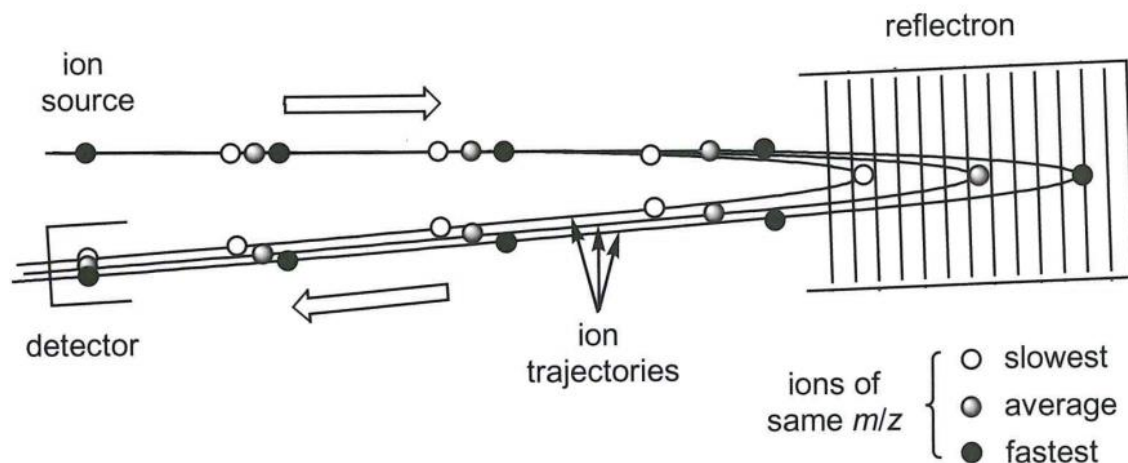


Figure 1.4. Path for ions of the same mass; given the same kinetic energy through the reflectron.

The MCP is an array detector that is equipped with thousands of electron multiplier tubes. The array effectively captures the spread out ions travelling from the reflectron, and serves to enhance resolution still further. A cascade of electrons is triggered when hit by an ion, which converts the kinetic energy of the ion into an electronic signal.

1.2 PSI-ESI-MS

Pressurized sample infusion electrospray ionization mass spectrometry (PSI-ESI-MS) is a method of sample introduction⁸ to the source of the mass spectrometer where ionization occurs. Instead of using a syringe pump for solution delivery, an inert gas with a slight overpressure of about 3 psi is applied to a Schlenk flask containing the reaction solution. PEEK tubing is inserted through a septum in the top of the flask and the overpressure of gas pushes the reaction solution up through the PEEK tubing and directly into the capillary of the source (Figure 1.5).

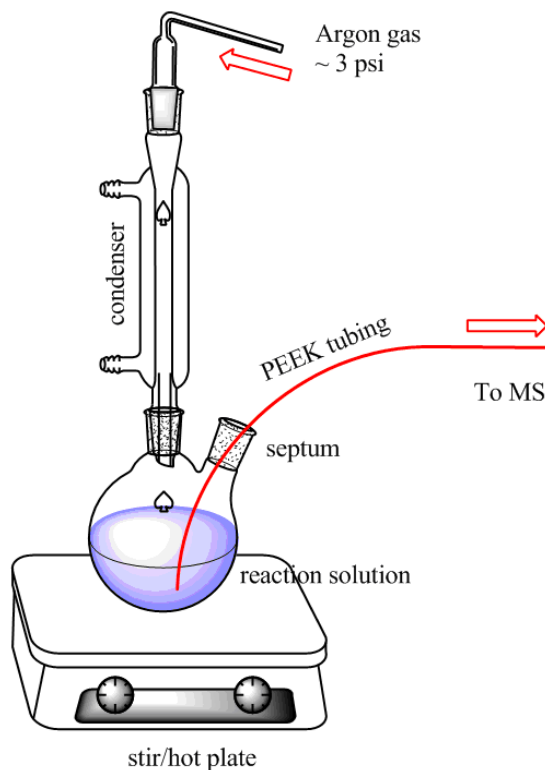


Figure 1.5. PSI sample delivery setup.

A relationship exists in fluid dynamics between relative pressure and laminar flow rate in a long, cylindrical tube, as seen in the Hagen-Poiseuille equation:

$$\Delta P = (128\mu LQ) / (\pi d^4) \quad (6)$$

where ΔP is the loss of pressure, μ is the dynamic viscosity, L is the tube length, Q is the volumetric flow rate and d is the inner diameter of the tube. Flow rates observed for 0.005" ID PEEK tubing for water, methanol, acetonitrile and dichloromethane at an overpressure of 3 psi produced flow rates of 20-90 $\mu\text{L}/\text{min}$, which was within a useable range for our investigations.⁸

1.3 Collision Induced Dissociation

Collision-induced-dissociation (CID) is a method of causing diagnostic fragmentation in a selected species in the gas phase. An ion is accelerated using a specific radio frequency which

increases its kinetic energy. When this fast-moving ion collides with a neutral gas, such as nitrogen or argon, the kinetic energy becomes vibrational energy, causing the ion to split into fragments.⁹ Fragmentation can be a useful tool to elucidate the structure of an ion. Weaker bonds break with less energy, allowing the m/z of each product ion to be detected and showing loss of a neutral species. Functional groups will fragment in a characteristic manner and the fragments can be reassembled using valence rules to determine structure. Effectively, this involves selection of a desired species by mass, and increasing the collision voltage until fragmentation occurs. There are 2 steps involved in CID: the collision between the ion and the immobile neutral target (fast step); the unimolecular decomposition of the excited ion into daughter ions and neutral fragments (slow step). Fragmentation of larger ions using CID is more difficult as they have more vibrational modes that can accommodate more energy than smaller ions can.¹⁰

1.4 Organic and Organometallic Catalysis Reaction Studies by ESI-MS

There are numerous examples of mechanistic studies of organic¹¹ and organometallic catalysis¹² reactions probed by ESI-MS. In the book, *Reactive Intermediates. MS Investigations in Solution*,¹³ on pp. 46-48, there is a table listing reactions spanning the years 1993-2008. It includes mechanistic investigations of gas phase reactions such as the Baylis-Hillman reaction, C-H or N-H activation, Diels-Alder reactions, Fischer Indole synthesis, Grubbs metathesis reaction, Heck reaction, Raney-nickel-catalyzed coupling, Suzuki reaction, Wittig reaction, and Pd-catalyzed C-C bond formation. Proposed intermediates and reaction pathways were confirmed, and new catalysts were suggested and synthesized based on said mechanistic pathways gleaned, as was demonstrated by Chen and co-workers.¹⁴ The results for these mechanistic studies were obtained using spectra obtained every few minutes or found using CID

investigations. Mechanistic investigations in our group are accomplished in a similar manner, however the number of data points has greatly increased (1/s), and we can monitor all of the charged species present in the reaction solution in real time by infusing the solution slowly into the MS over the course of the reaction. As ESI is a soft ionization technique, it is amenable to observation of molecular ions, but for our method of investigation, it is necessary to be able to constantly and consistently observe charged starting materials, products, intermediates and by-products. It is unlikely that sufficient charged species will be present and detectable in the reaction solution, unless charged species are produced during the reaction, or unless a charged “tag” is affixed to one of the reactants, such that we may follow it and any species it becomes bonded to. In the group, aryl phosphonium tags are most often employed as the instrument is sensitive to their presence.

1.5 Protection from oxygen and moisture

For extremely air-sensitive work, a glovebox adjacent to the mass spectrometer is most handy. The reaction is conducted in solution inside the glovebox which may then be pushed through either PEEK or fused silica tubing through a feedthrough in the glovebox and directly into the mass spectrometer. Decomposition is limited by the length and inner diameter of the tubing. Either a syringe pump may be used to inject diluted aliquots of the reacting solution over time intervals directly into the MS, or a pressurized sample infusion setup may be utilized to monitor the reacting solution in the same manner that is used outside the glovebox (Figure 1.5). For the PSI setup inside the glovebox, the over-pressurization comes from a simple party balloon which can be easily inflated using a cheap balloon inflator, all done inside the glovebox. The reaction can be done in a Schlenk flask or sample vial, with the balloon attached using a syringe needle and a septum. The glovebox atmosphere is pushed into the balloon using the inflator and a

steady pressure of ~ 1 psi is delivered continuously (Figure 1.6), which is sufficient to push the reacting solution through the tubing and into the MS for constant analysis of any charged species (Figure 1.7).



Figure 1.6. Setup for PSI-ESI-MS in the glovebox using a party balloon which provides the over-pressure of nitrogen while the solution is pushed out through the PEEK tubing to the MS.

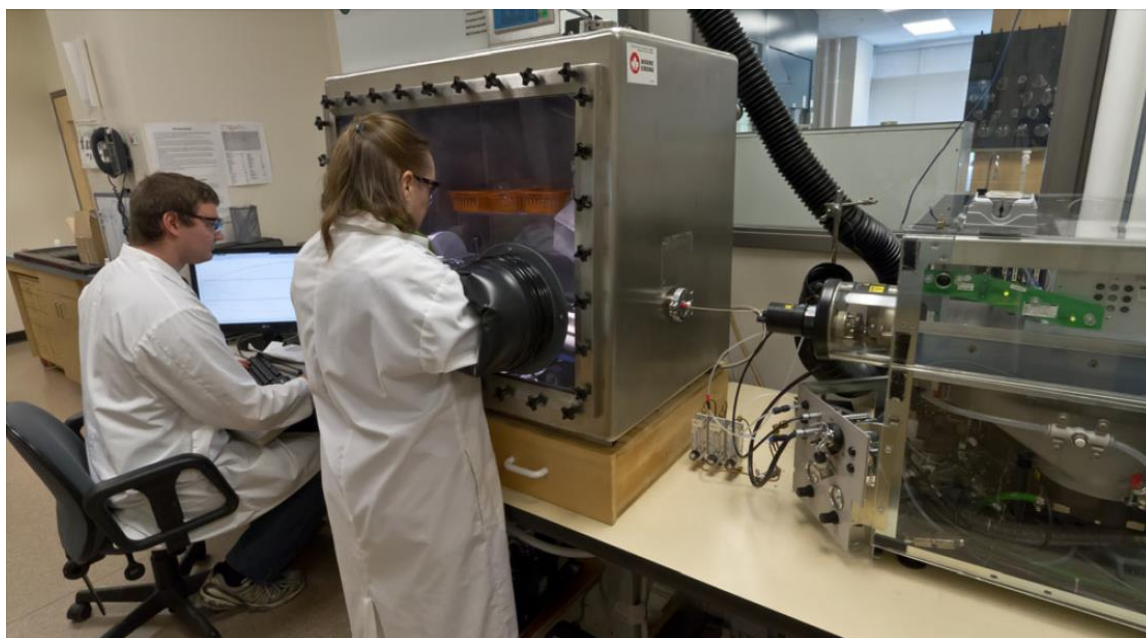


Figure 1.7. Setup for tandem glovebox-MS, connected by ~ 1 foot of tubing¹⁵.

Since MS is such a sensitive technique, and can detect species at the ppm level, solvents must be scrupulously dry. Ordinary distillation and SPS will dry solvents to ~ 5 ppm water, which is insufficient for our analysis. After distillation using an alkali metal, the solvent must sit in the glovebox for 4 days over molecular sieves which have been heated under vacuum for 5 days. The apparatus used in the analysis, including flasks, tubing, syringes, sample vials, and septa must be thoroughly vacuum dried before being placed in the glovebox. The source must also be kept free of water and oxygen, and this can be done through the use of heating tape wrapped around the source housing to eliminate water, and by connecting nitrogen to the housing with an over-pressure of gas applied to keep air out. These techniques were demonstrated to be very effective in the elimination of both air and moisture in monitoring olefin polymerization with the reactive species, $[\text{AlMe}_2]^+$. Large quantities of AlMe_3 are also present and are easily hydrolysed by water to form Al-OH groups, which can despoil MS results and cause capillary clogging, thus preventing ions from reaching the detector (Figure 1.8).

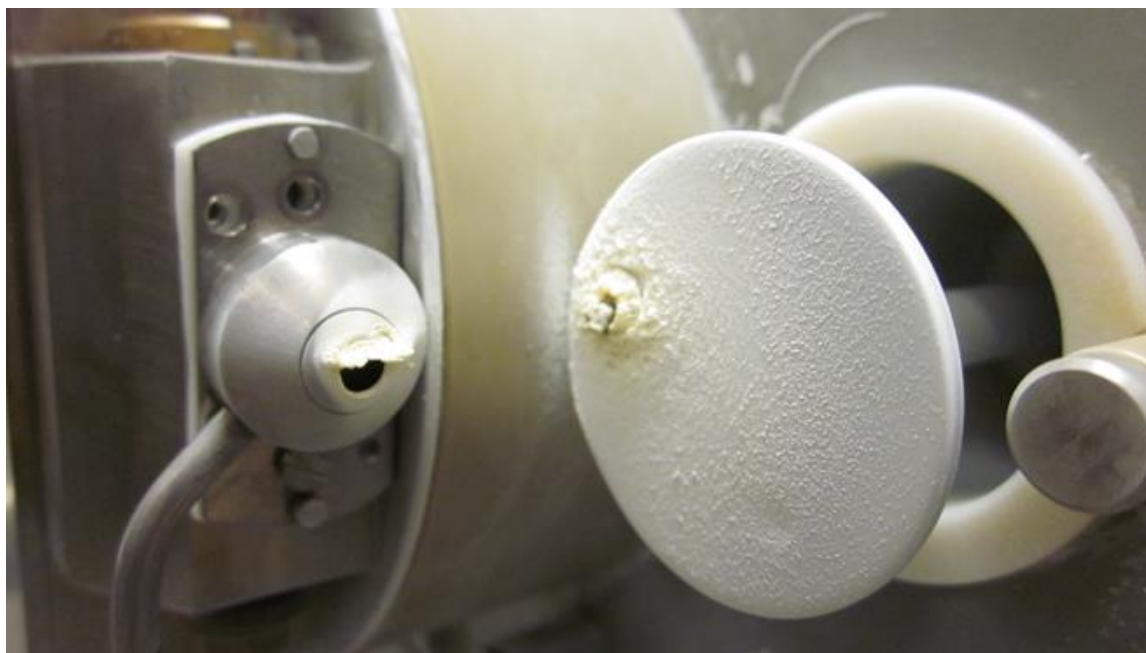


Figure 1.8. High concentration of hydrolyzed AlMe_3 , due to water in the source; the solid caused extensive clogging of both tubing and capillary.

Another issue that arises from the presence of air is the production of unwanted species that interfere with analysis. One example is our studies with charged-tagging species using phosphines to generate phosphonium ions. Phosphines make great nucleophiles, but are weak bases, and the presence of a miniscule amount of air will easily generate phosphine oxides which associate strongly with protons or alkali metals, and have much greater ionization efficiencies than phosphonium ions. Phosphine oxides in low concentration may not be detected by ^{31}P NMR, but if it is present in the MS sample, it will dominate the MS spectrum, which again establishes the need for stringent precautions in our analysis.

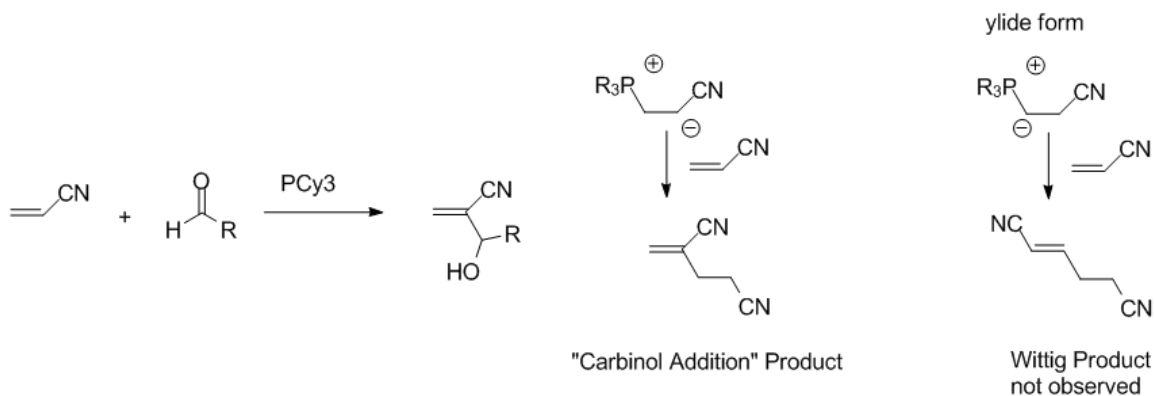
Chapter 2. Phosphine Catalysis

2.1 Introduction

Precious metals including platinum, palladium and rhodium are becoming increasingly scarce and costly¹⁶ as demand for their employment in electronics, auto- and industrial catalysis increases. Metal-free catalysis is becoming correspondingly popular as a method for effecting organic transformations.¹⁷ Phosphines have an increasingly larger niche in catalysis with the number of publications having risen steadily since the mid 1990's, with over 1600 citations per year of "phosphine-catalyzed" papers on Web of Knowledge as of 2014, up from 90 in 1995.¹⁸ Phosphine-catalyzed reactions are able to effect the synthesis of a variety of complex cyclic and heterocyclic products¹⁹ required in the preparation of pharmaceuticals.²⁰

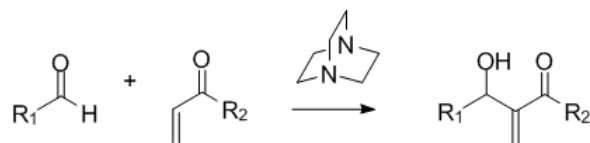
Morita was a pioneer of phosphine-catalyzed reactions, using tricyclohexylphosphine with acrylonitriles and methacrylates.²¹ In 1968, he discovered that the conjugate addition of an aldehyde occurred in place of the oligomerization, which had been previously reported by Baizer and Anderson.²² Morita reported a β -hydroxy- α -methylene compound using a catalytic amount of tricyclohexylphosphine. It was noted by Baizer and Anderson that in the presence of a polar solvent, such as ethanol, water, or acetonitrile, oligomerization of the starting acrylonitrile occurred. Morita, however, made a distinction in which dimerization occurred when using alkylphosphines but not with arylphosphines. Morita wanted to confirm the product of dimerization of the acrylonitrile with the phosphine catalyst. He supposed that interconversion of the zwitterion to the ylide form did not occur for the alkylphosphine, as no product of a Wittig olefination appeared (Scheme 1.), in which attack came from the carbon closest to the

phosphonium of the zwitterion. Instead, he saw what he called the “carbinol addition” product, where attack came from the carbon *beta* to the phosphonium of the zwitterion, thus confirming the first reported instance of phosphine catalysis.



Scheme 1. Morita’s first reported phosphine catalysis of acrylonitrile with an aldehyde to form an allylic alcohol; depiction of the zwitterion in “carbinol addition”.

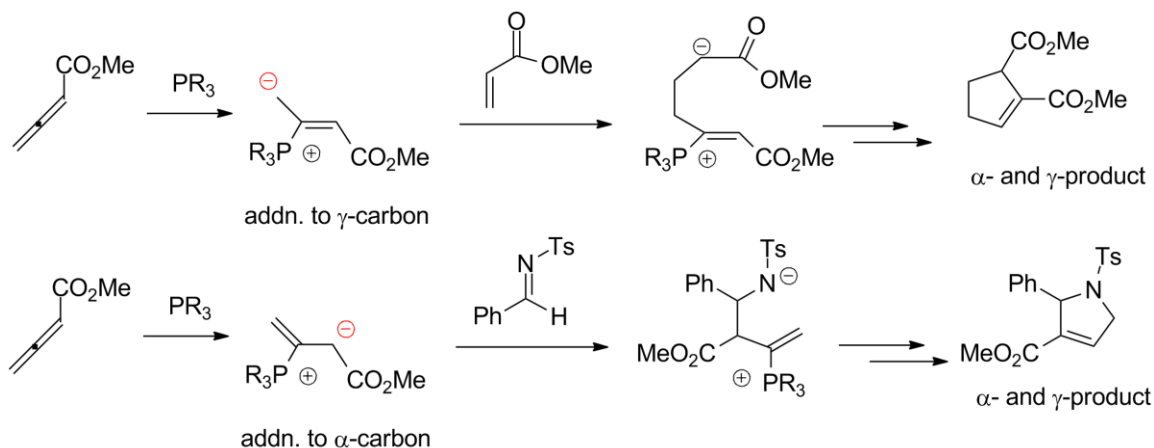
Baylis and Hillman improved upon the yield of this conjugate addition a few years later, using a tertiary amine catalyst and an α,β -unsaturated ketone with an olefin substrate containing an electron-withdrawing group,²³ Scheme 2.



Scheme 2. Morita-Baylis-Hillman reaction of an aldehyde with an α,β -unsaturated ketone and 1,4-diazabicyclo[2.2.2]octane (DABCO) catalyst to generate an allylic alcohol.

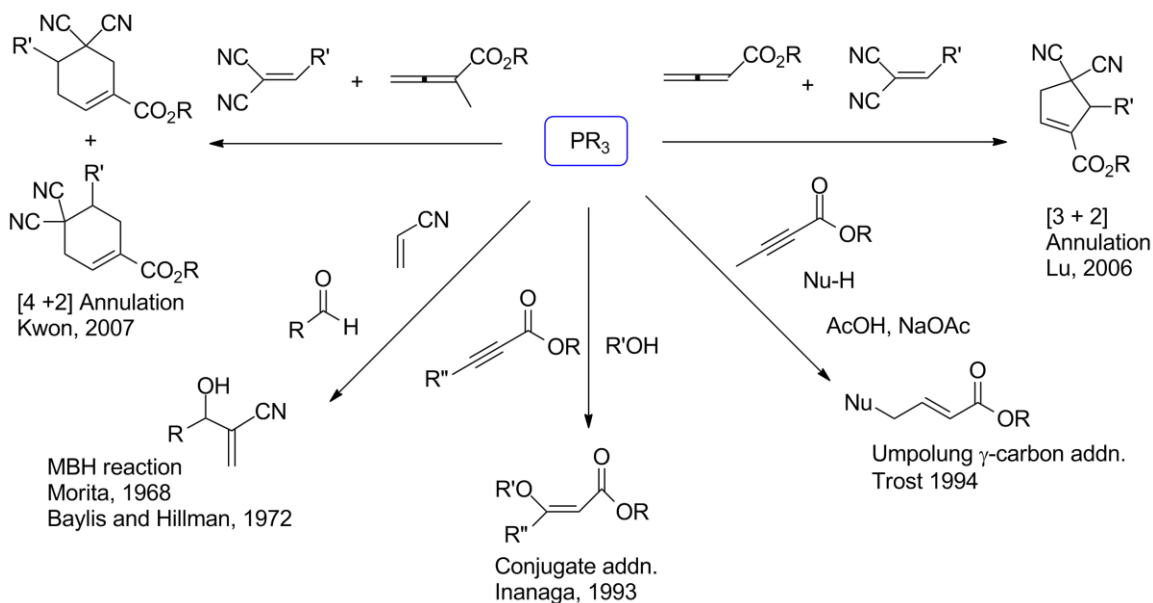
As has been repeatedly demonstrated with more recent phosphine catalysis, the nucleophilic phosphine reliably reacts with the electrophilic β -carbon of an allenolate or alkynic acid ester,²⁴

thus pushing electron density either towards the ester, creating an nucleophilic carbon in the α -position relative to the carbonyl, or towards the γ -carbon, Scheme 3.²⁵



Scheme 3. After the phosphine attacks the β -carbon of the olefin, electron density is directed towards either the α - or γ -carbon, allowing for regioselective attack on the substrate under different reaction conditions.

An electron-withdrawing group such as an ester or nitrile is required to facilitate the formation of the zwitterion.²⁶ Two distinct types of reactions can occur: Reaction with an electrophile or addition of a nucleophile for conjugate addition (Scheme 4).²⁷ There is an extensive volume of work with electrophiles in annulation reactions,²⁸ including those that focus on carbocycle formation,²⁹ and those that involve the production of heterocycles.³⁰ Annulation reactions can be also be facilitated with chiral phosphines that promote enantioselectivity,³¹ Kwon has been especially prominent in developing phosphine-catalyzed annulations to produce heterocycles,³² including highly functionalized 5-, 6-, and even 8-membered nitrogen heterocycles,³³ cyclohexenes from activated olefins,³⁴ and in the total synthesis of natural products.³⁵ The Kwon group also recently developed a so-called “ β' -Umpolung” addition to allenes.³⁶

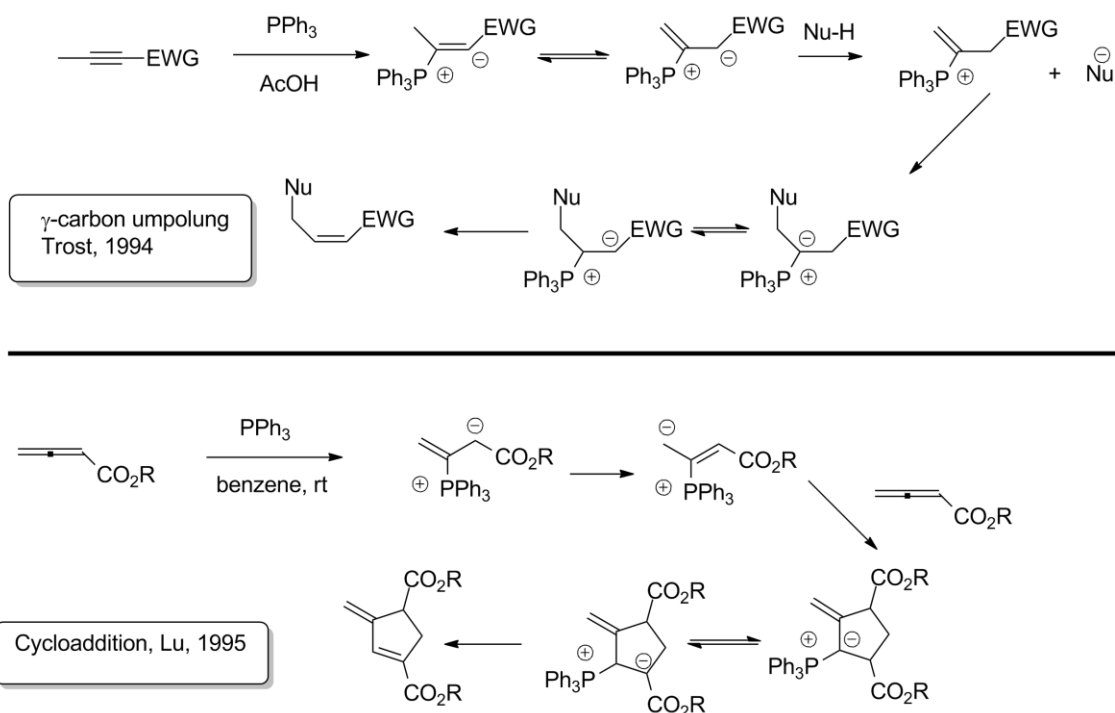


Scheme 4. A selection of phosphine-mediated reactions.

In 1993, Inanaga first probed the conjugate addition of alcohols to α,β -unsaturated alkyne acid esters using alkyl and aryl phosphines,³⁷ and noted that the yield of the *E* over the *Z* isomer was dependent upon the type of solvent and phosphine used. A non-protic solvent with a more nucleophilic phosphine favored the *E* isomer, whereas sterically bulky alcohols increased product yield. Scheme 4 has a selection of phosphine-mediated catalytic reactions, for which Inanaga's addition of an alcohol to an alkyne acid ester carries the most relevance to this project.

In 1994, Barry Trost's homonuclear addition demonstrated umpolung of the γ -carbon with an arylphosphine catalyst to an alkyne acid ester with an acid co-catalyst in toluene.³⁸ Good to excellent yields of the *trans* product were generated with the arylphosphine. However, when an alkyl phosphine was used, oligomeric by-products were discovered, and he explained that this was due to the increased nucleophilicity of the catalyst, whereas the less nucleophilic

arylphosphines did not readily undergo oligomerization (Scheme 5). In 1995, Zhang and Lu³⁹ noted that a self-cycloaddition reaction occurred with PPh_3 and ethyl-2,3-butadienoate in benzene, indicating that it was more reactive than other olefins like 1-hexene or methyl methacrylate. They also noted a reduced yield with an alkylphosphine and the presence of dimers (Scheme 5.).

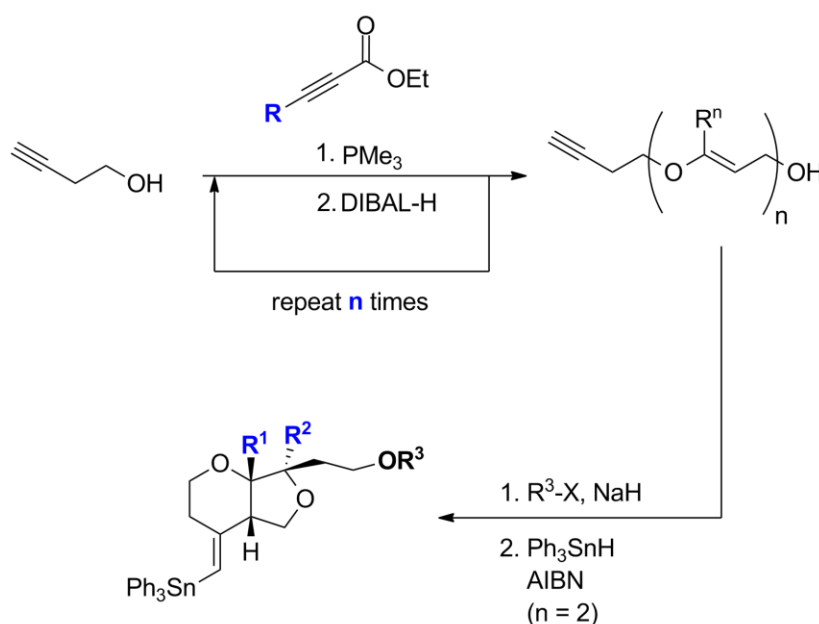


Scheme 5. Mechanisms in phosphine catalysis demonstrating (top) γ -carbon umpolung with a protic nucleophile, and (bottom) super-reactivity of an allenolate.

While it is true that alkylphosphines have greater nucleophilicity than arylphosphines, a substituent at the α - or γ -position requires a more nucleophilic catalyst for the zwitterion to form. For conjugate addition, both Inanaga and Trost noted that the yield is improved by use of a more sterically bulky protic nucleophile. There is general agreement from Lu, Trost and Inanaga that

the *E*-isomer is favored but Inanaga noted that result was dependent on the solvent used and not the nucleophile. This lent credence to earlier results being influenced by the presence of a protic species, solvent or starting material, and whether oligomers or conjugate addition products would dominate.

In 2011, the Wulff group began investigations into phosphine-catalyzed conjugate addition of alcohols to an alkyne acid ester for use in a cascade reaction (Scheme 6).⁴⁰

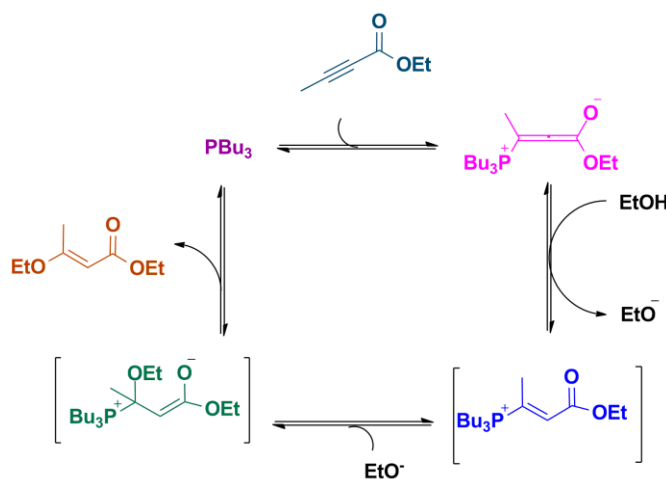


Scheme 6. Iterative use of a phosphine-mediated addition, leading to a radical cascade precursor.

They also encountered the presence of oligomers. Upon investigation of the mechanism of this synthesis,⁴¹ they noticed a wide variation in product yield that was dependent on a number of parameters, which was not heavily influenced by the type of alkyl or arylphosphine used. Use of a more sterically bulky alcohol in addition to the drop-wise addition of alkyne acid ester, non-coordinating solvent, all would increase the product yield, as was known previously. Since the main focus of research in the McIndoe group is to dynamically measure the charged species

present in a catalytic cycle, determine information about the turnover-limiting step(s), and to establish the identity of by-products, resting states and decomposition products, a collaboration was desired that sought to address the factors affecting product yield in the conjugation addition of alcohols to activated alkynes.

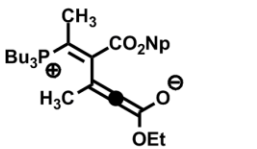
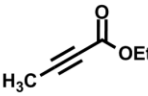
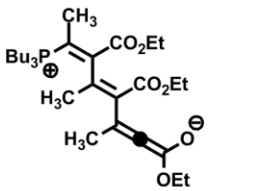
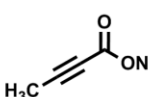
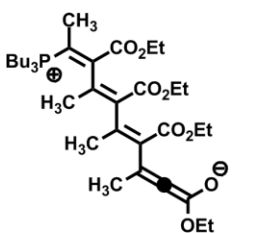
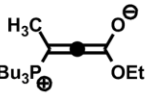
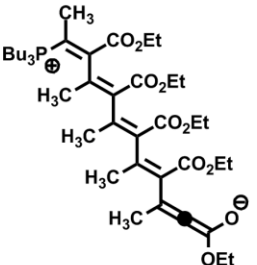
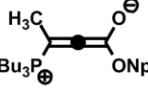
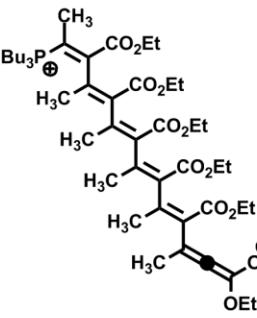
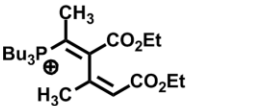
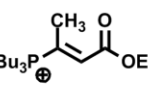
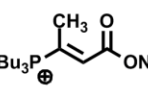
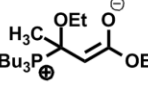
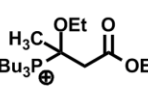
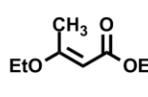
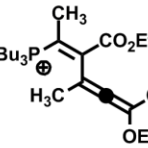
The McIndoe group accomplishes real-time monitoring of reaction mixtures using pressurized sample infusion electrospray ionization mass spectrometry (PSI-ESI-MS): a method of gathering data regarding charged species in solution, over minutes, or even hours.⁴² Instead of injecting a product into the mass spectrometer via syringe to merely obtain a snapshot of the reaction process, the reacting solution is continuously injected into the mass spectrometer, with spectra collected every second, if required. For the reaction being studied, it was found that several phosphonium species were readily produced and no charged tags were required. PSI-ESI-MS was therefore useful in helping to flesh out charged phosphonium intermediates and by-products that are difficult to detect by other methods, as the first phosphonium zwitterion was characterized by x-ray crystallography in 2007 by Kwon's group.⁴³ A reaction mechanism was proposed based on Inanaga's suggested mechanism (Scheme 7.) and was the basis for the mechanistic study in this project.

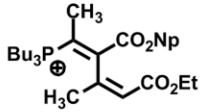
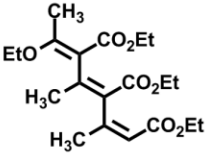
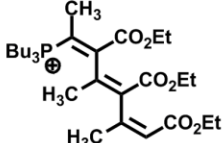
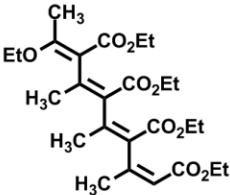
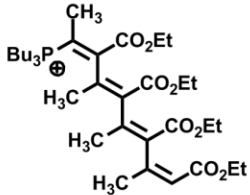
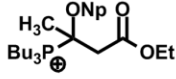
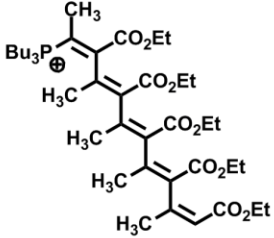
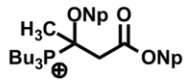
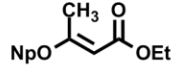
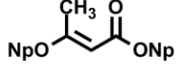
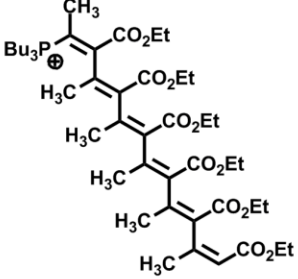
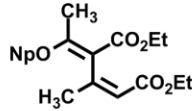
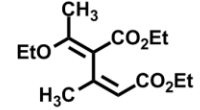
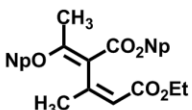


Scheme 7. Proposed catalytic cycle for the tributylphosphine-catalyzed addition of ethanol to ethyl butynoate.

2.2. Results and Discussion

Table 1. List of numbered species for phosphine catalysis.

Species #	Species	<i>m/z</i>	Species #	Species	<i>m/z</i>
1	PBu ₃		10A		
2			11		
2A			12		
3			12A		
3A			12B		
4	EtOH		13		<i>m/z</i> 427
5	EtO [⊖]				
6		<i>m/z</i> 315			
6A		<i>m/z</i> 357			
7					
8		<i>m/z</i> 361			
9					
10					

Species #	Species	<i>m/z</i>	Species #	Species	<i>m/z</i>
13A		<i>m/z</i> 469	17		
14		<i>m/z</i> 539	18		
15		<i>m/z</i> 651	19		<i>m/z</i> 403
15A		<i>m/z</i> 764	19A		<i>m/z</i> 445
			20		
			20A		
15B		<i>m/z</i> 877	21	NpOH	
			22	NpO [⊖]	
			23		
16			23A		

2.2.1. ^1H NMR

Proton NMR allowed for the tracking of the rate of disappearance of the alkyne and the rate of appearance of the conjugate addition product. It is of limited use in analyzing the role of the $^n\text{Bu}_3\text{P}$ catalyst, since the butyl protons do not shift diagnostically upon changes at phosphorus, and we expect to see an intractable mixture of intermediates. The most useful protons on the alkyne starting material are the $\text{H}_3\text{C}-\text{C}_{sp}$ protons, which become $\text{H}_3\text{C}-\text{C}_{sp^2}$ protons in the product. The remaining signals suffer from overlap problems that make them less useful for accurately establishing the rate of reaction. Disappearance of ethanol could also be monitored, but this reactant was used in excess so the change in intensity is more subtle. To quantify the reaction accurately, diphenylacetylene was used as an internal standard, and the reaction was run under conditions that enabled quantitative data to be obtained (long relaxation times).

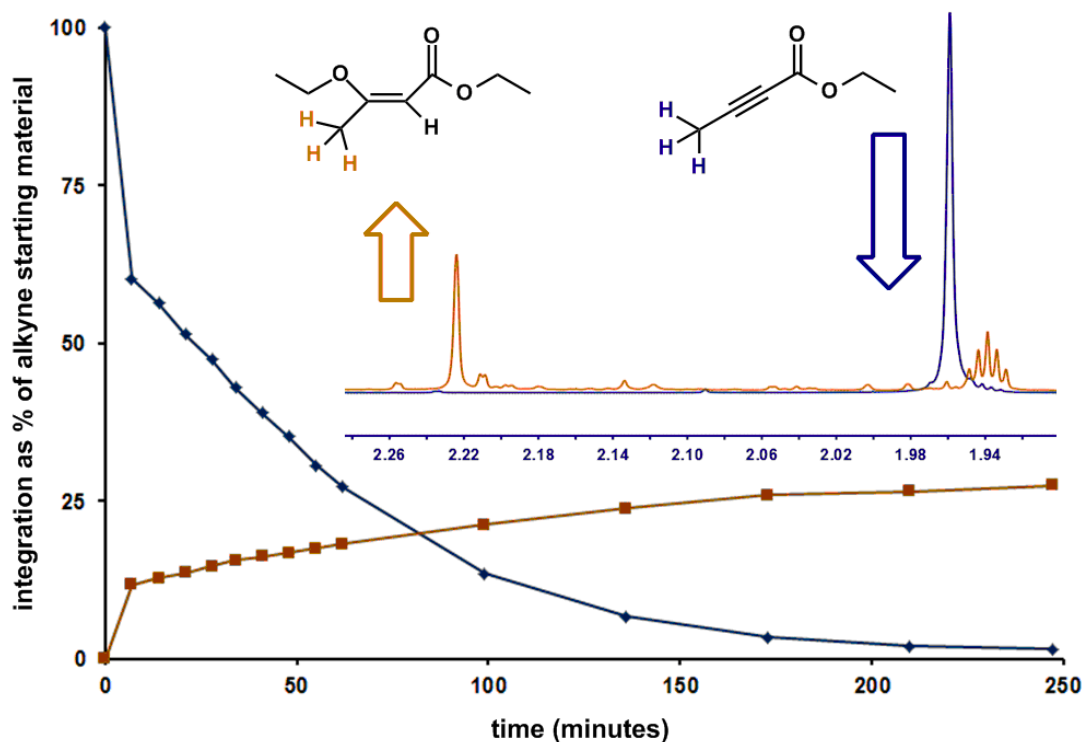


Figure 2.1. Reaction progress as seen with ^1H NMR. Inset shows methyl protons in the starting alkyne at 1.96 ppm and the methyl protons in the product at 2.22 ppm.

The alkyne is entirely consumed after about four hours, following approximately first order kinetics after an initial burst of activity responsible for consuming about one-third of the starting material in the first 10 minutes (Figure 2.1).

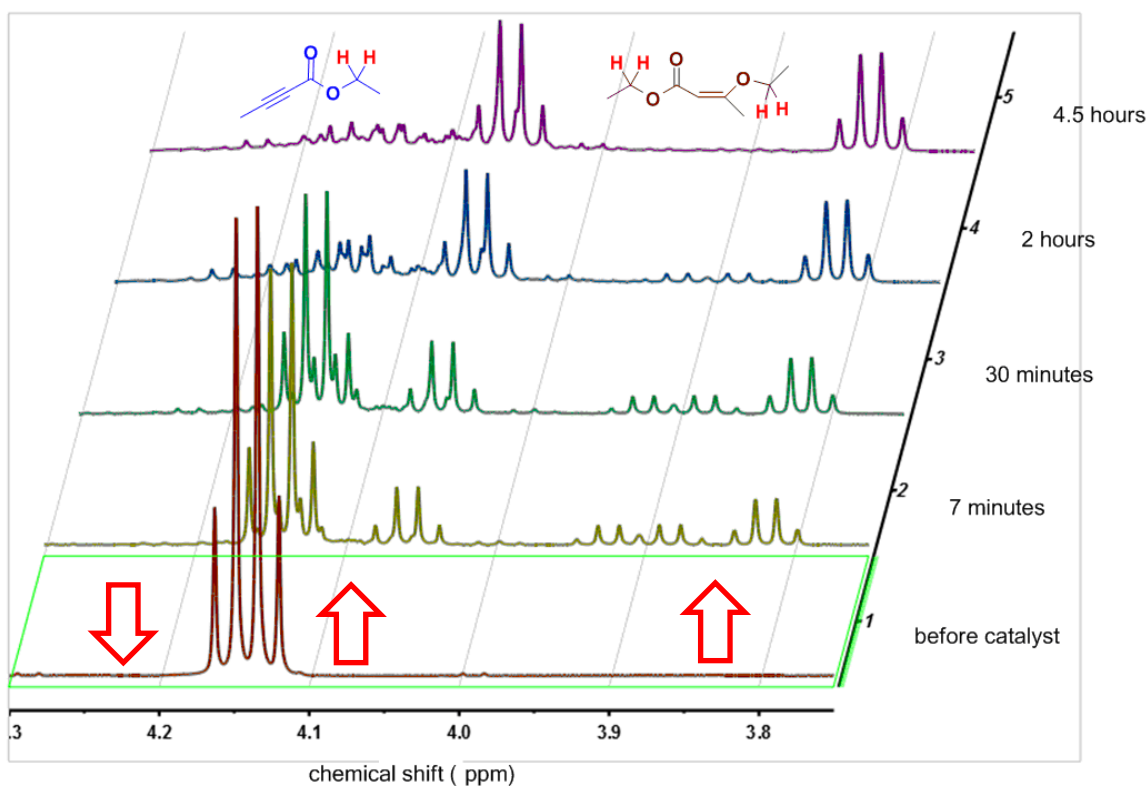


Figure 2.2. Multiple peak formation in the ester and ether range as seen with ¹H NMR. From the bottom up, red trace is before addition of catalyst; yellow trace is 7 minutes after catalyst is added; green trace is 30 minutes later; blue trace is after 120 minutes; violet trace is 244 minutes after catalyst addition.

As seen in Figure 2.2, the bottom red trace shows the methylene CH₂ of the ester at 4.14 ppm in the starting alkyne. The catalyst is added by syringe and 7 minutes later the first ¹H NMR spectrum is obtained (yellow trace) which shows the gradual disappearance of the ester CH₂ protons, and the appearance of another quartet appearing underneath. This new peak corresponds to the CH₂ protons in the double addition product, **13** which have a slightly different

chemical shift. Also present are the product peaks in **9**, two quartets at 4.06 and 3.82 ppm corresponding to the ester and ether CH₂ protons, respectively. At 3.93 and 3.89 ppm a close pair of quartets is also seen to appear and grow during the first 30 minutes of the reaction, only to disappear again. These peaks correspond to the CH₂ protons from the addition of alcohol to the off-cycle by-products of the reaction, **14** and **15**. These protons are in a more de-shielded environment due to the ester groups withdrawing electron density through the π -bonds, resulting in a more downfield chemical shift than the product counterpart. It is also likely that **15A** is either not present in high enough concentration to be detected, or that it is a solid. This is also the likely reason for the drop in signal at 3.93 and 3.89 ppm in that **14** and **15** are slowly becoming solids and dropping out of solution. As the reaction progresses, there are a number of peaks forming in the range of 4.25-4.10 ppm (Figure 2.3) corresponding to a number of ester CH₂ protons in the by-product oligomers. The protons in the starting alkyne disappear entirely after 4 hours.

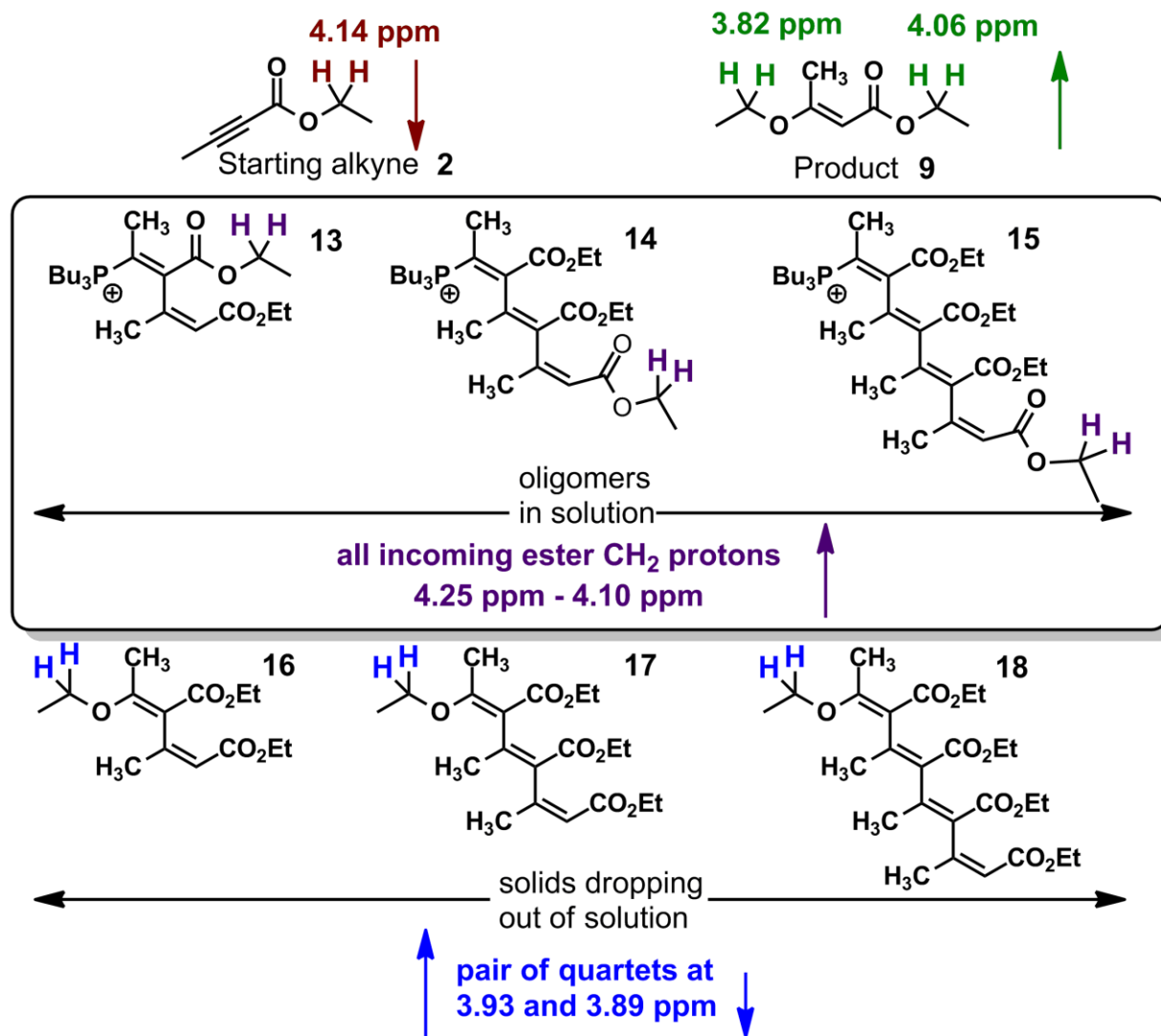


Figure 2.3. Illustration of change in chemical shift for starting alkyne protons (ester); product protons (ester and ether) – top; chemical shift range of methylene esters in the intermediate oligomers appearing in the spectra over 4 hours – center; chemical shifts of quartet pair from ether methylenes in the off-cycle by-products – bottom.

To test whether an alcohol was intrinsic to formation of oligomers, the reaction was done in an NMR tube without the presence of alcohol, using diphenylacetylene as an internal standard, and with the same starting alkyne and catalyst concentrations (0.4 M and 0.04 M, respectively) as previous NMR studies, under the same reaction conditions. The resultant data (Figure 2.4) showed that in relation to the internal standard, just over 98% of the starting alkyne was present

after 4 hours. Small amounts of additional peaks appeared at the same chemical shift value as for the oligomers, only after the addition of the catalyst. Solids were present in the bottom of the NMR tube after the reaction and those were filtered through a 2 micron syringe filter and dried in the fumehood for 3 days. At the end, those dried brown solids accounted for 0.86% of the starting mass of the entire reacting solution.

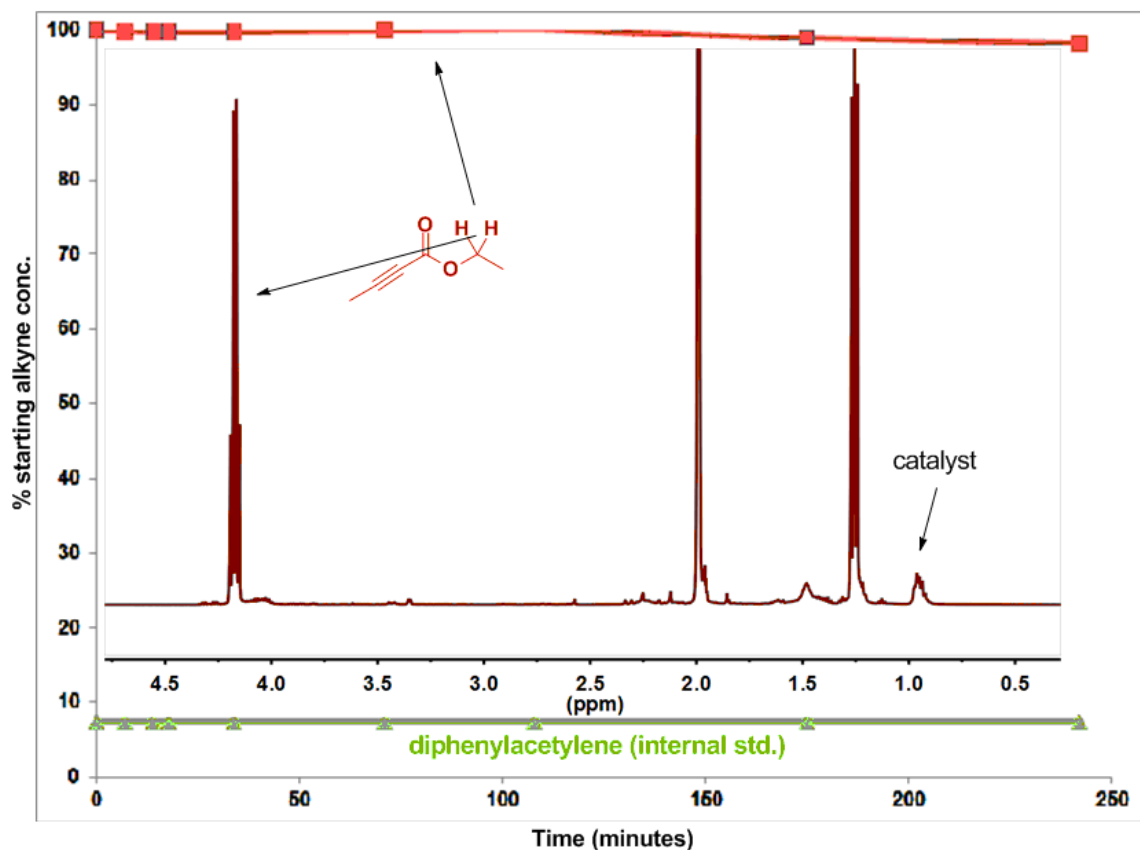


Figure 2.4. Starting alkyne ethylene peak monitored by ^1H NMR over 4 hours in CD_3CN , without alcohol. NMR inset shows the final spectrum after 4 hours and the presence of unknown peaks near the baseline with the same chemical shift as for oligomers when alcohol is present.

2.2.2 ^{31}P NMR

Phosphorus NMR allows the reaction to be tracked from the perspective of the $^n\text{Bu}_3\text{P}$ catalyst, but quantitative ^{31}P NMR requires very long relaxation times (D1 delay time for $^n\text{Bu}_3\text{P}$ was determined to be 90 seconds, indicating that a spin-lattice relaxation time of 5 T1s was needed), and each ^{31}P scan took 29 minutes. The complexity of the spectrum was unexpectedly high; no $^n\text{Bu}_3\text{P}$ is observed, but approximately 10 other species of reasonable intensity appear over the course of the four hour reaction (Figure 2.5). Some oxidized phosphine, OPBu_3 , is readily identifiable at 58.3 ppm; its abundance is essentially constant throughout. The other peaks all appear at chemical shifts consistent with characterization as phosphonium salts, as expected from the mechanism. However, elucidating exactly what they are is not possible, even though we can measure their abundance over time; a single peak is simply not diagnostic enough, and too little is known about the influence of chemical structure on ^{31}P chemical shift to distinguish between closely related species. However, in using quantitative NMR we were able to track the intensity of the peaks over time to generate traces (Figure 2.6) which allowed us to make a correlation to the ESI-MS results.

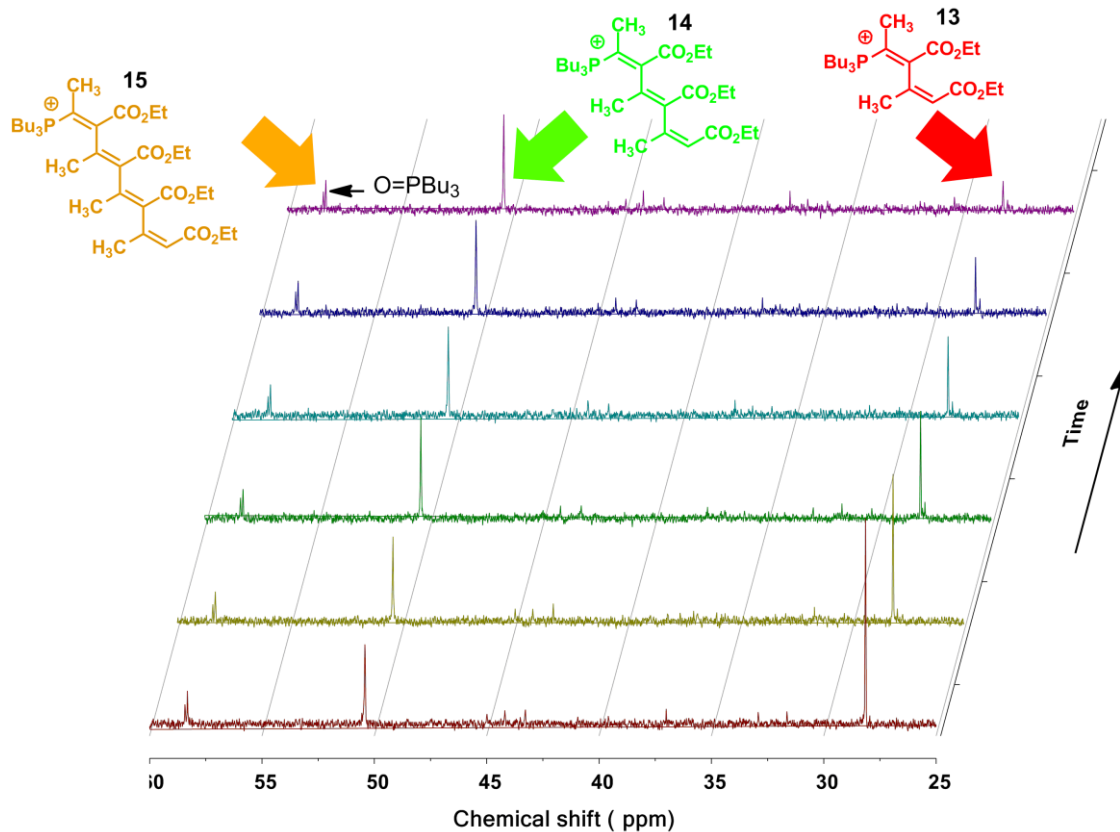


Figure 2.5. ^{31}P NMR stacked plot showing the dynamic progress of phosphonium oligomer peaks. The first spectrum (bottom) was taken 30 minutes after the catalyst was added, and the last spectrum (top) was taken 4.5 hours after catalyst addition.

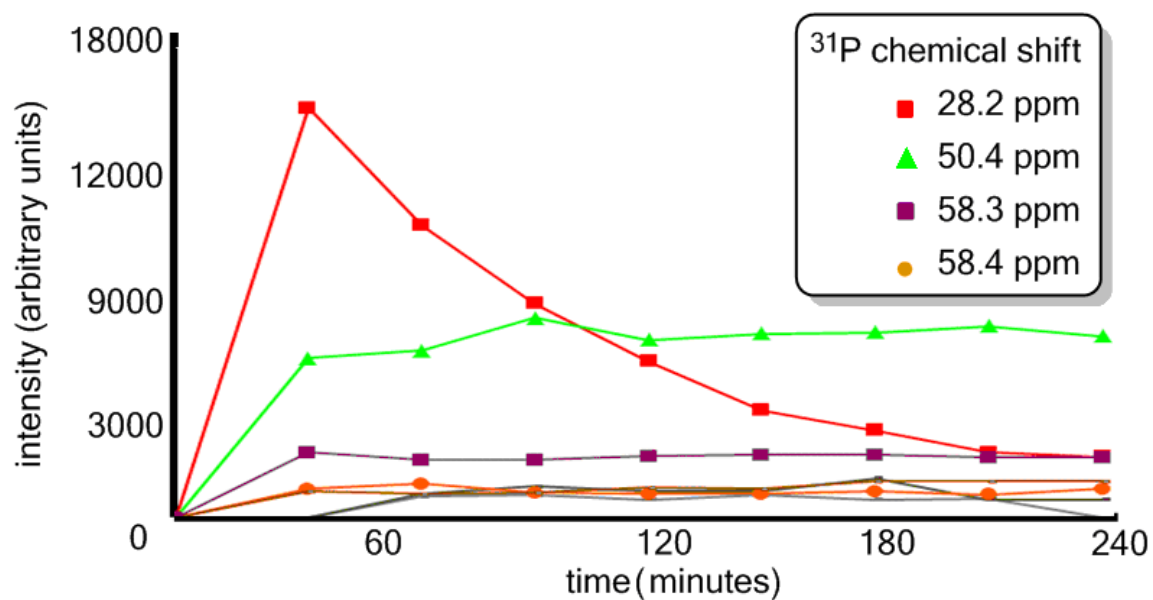


Figure 2.6. Intensity traces generated by quantitative ^{31}P NMR.

2.2.3 PSI-ESI-MS

To determine the identity of the numerous phosphonium species present in the mixture, PSI-ESI-MS was used, allowing continuous monitoring of a reaction solution. The presence of a phosphonium group implies a charged species, provided an anionic group is not also present. The time scale that ESI-MS works on is considerably faster than ^{31}P NMR; we collected a full spectrum every second. Five phosphonium species appeared at reasonable concentration over the first two hours (Figure 2.7), and the combination of m/z ratio and isotope pattern allowed their composition to be determined.

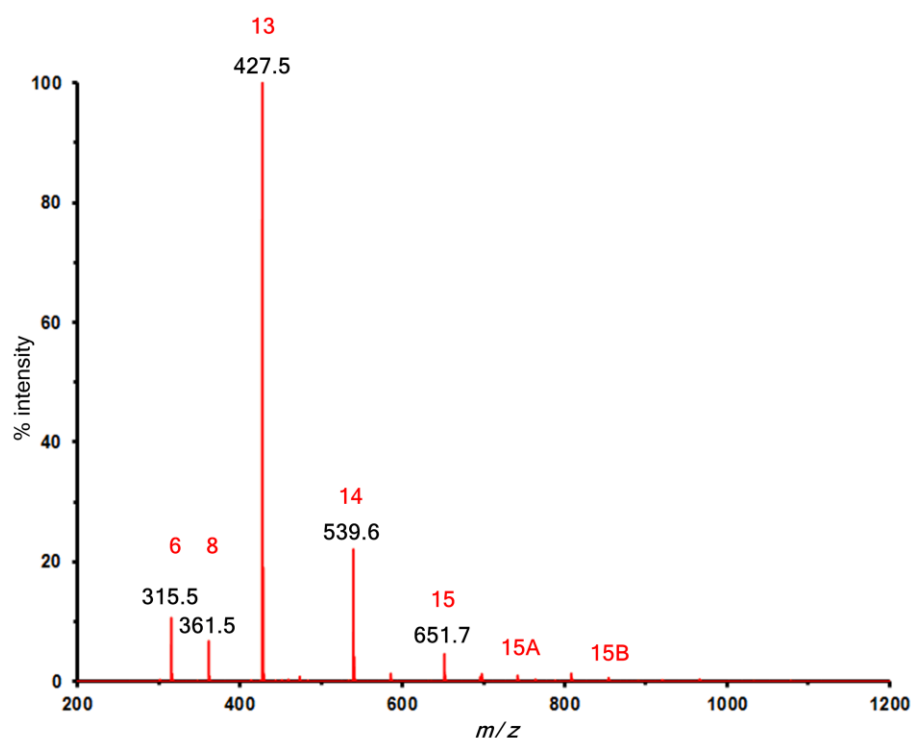


Figure 2.7 Positive ion mass spectrum 20 minutes after catalyst addition. Higher mass oligomers can also be observed at low (<1%) abundance.

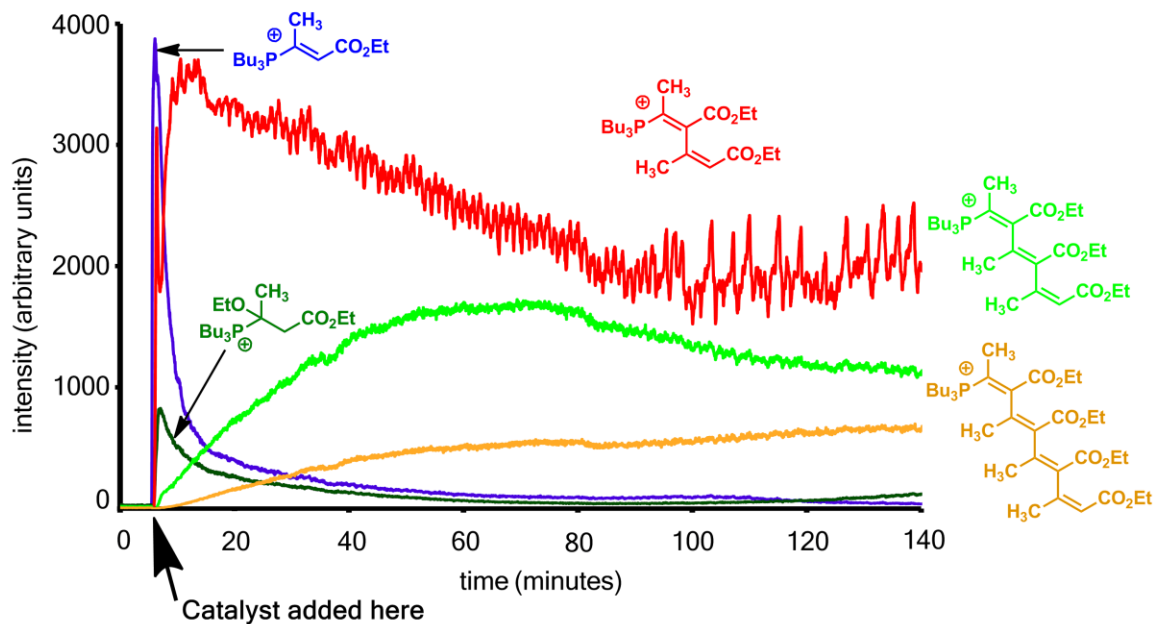


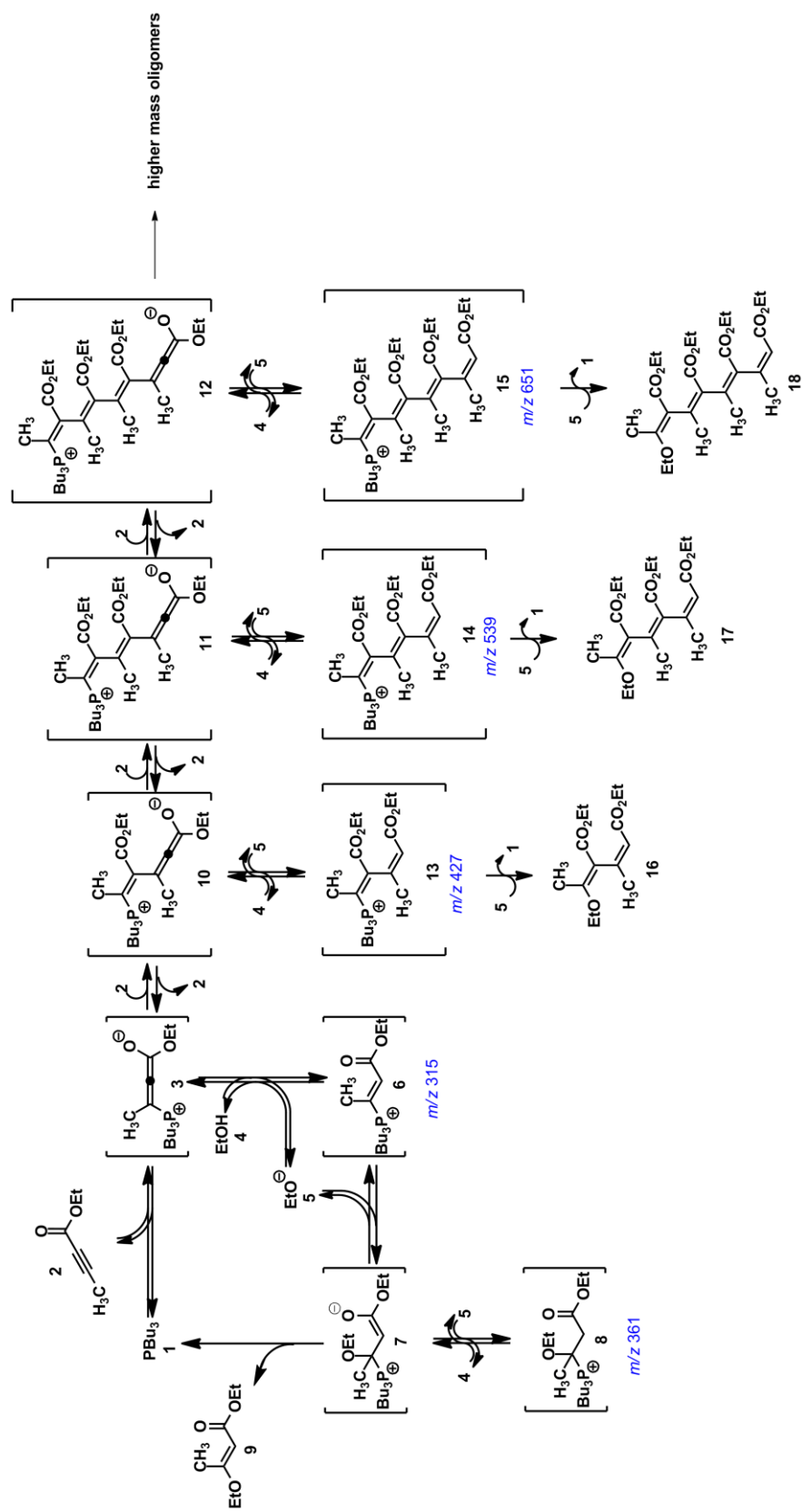
Figure 2.8. Reaction progress according to PSI-ESI-MS.

The first species to appear was at m/z 315, (Figure 2.8) which corresponds to $[\text{PBu}_3 + \mathbf{2} + \text{H}]^+$, i.e. addition of the phosphine to the alkyne followed by protonation (the assumption is made that protonation does not occur first, since the protonated alkyne is not observed in any significant concentration in an ethanol solution). This species spiked to a maximum intensity immediately after addition of the phosphine, then rapidly dropped to a low level (to about 15% of its original intensity within 10 minutes). The intensity of that species slowly decayed, dropping to almost 0 after 2 hours. We assume this ion is one of the low abundance phosphonium ions observed in the ^{31}P NMR; which one is not possible to determine.

An ion at m/z 361 also appeared immediately after phosphine introduction. It corresponds to $[\text{PBu}_3 + \mathbf{2} + \text{EtO}^- + \text{H}]^+$, and like the m/z 315 species, decays quickly and cannot be assigned with any confidence to one of the phosphonium ions in the ^{31}P NMR spectrum. The relative

intensity of this species is much lower, indicating that the phosphine quickly disengages generating the product.

A species at m/z 427 that is somewhat slower than either the m/z 315 or 361 ions to appear, but reaches a maximum intensity similar to that of the maximum level of m/z 315, is also prominent. It decays only slowly over time, and its behavior closely matches that of one of the phosphonium ions observed in the ^{31}P NMR spectrum, at 28.2 ppm. Its decay is compensated for by the appearance of at least two other products: species at m/z 539 and m/z 651. Collectively, these three compounds sum to approximately the same total ion intensity, suggesting that they are closely related. Their masses increment by 112 Da - the same mass as the alkyne starting material - from m/z 315, strongly suggesting that they are the result of multiple additions of alkyne. Because these species presumably go on to form oligomeric by-products, they will appear off the catalytic cycle and Scheme 7 has to be expanded in order to accommodate them (Scheme 8).



Scheme 8: Proposed mechanism suggested by ^1H NMR, ^{31}P NMR, and PSI-ESI-MS.

The allene zwitterions are not seen in the ESI data, and it is likely that they are being quickly consumed in the formation of the protonated olefins. This also explains why the forward rate of reaction to form **8** is substantially lower again, since when there is not much **6** present, not much **8** can form. The MS data shows that these two species are tied to each other in terms of relative concentration. For whatever concentration of **8** that is present, the rate that the phosphine disengages from the substrate is fast enough that **8** does not accumulate. Also of importance is the rate of release of catalyst from the multiple addition species forming **16**, **17**, and **18**. The rate of catalyst release from **13**, **14**, and **15** appears to be slow, as the MS data demonstrates that the intensity of the phosphonium multiple addition species does not decrease noticeably after 2 hours. This is corroborated by the ^{31}P data, which also shows that the catalyst is being tied up by the off-cycle species and is not available to form more product. By the time the phosphine is released, there is no longer much alkyne left to react, which also hinders product formation.

2.2.4. Numerical modeling

To test whether or not the pieces of the puzzle provided by ^1H NMR, ^{31}P NMR and PSI-ESI-MS made sense in light of the proposed mechanism, several numerical models were constructed iteratively and innumerable attempts were made to fit a set of rate constants that would regenerate the three sets of concentration vs. time plots. Initially, PowerSim Studio 9 Academic software was employed as it used simple icons and demonstrated the required ability to model fairly complex systems. It is usually used in business to model inventory projections. It was thought that it could be useful to model the kinetics of catalytic systems. For the simple system of A and B starting materials produce C and D products, a simple model could be constructed

and the corresponding abundance traces could be generated, merely by changing the rate constants until the traces matched the experimental data, Figure 2.9.

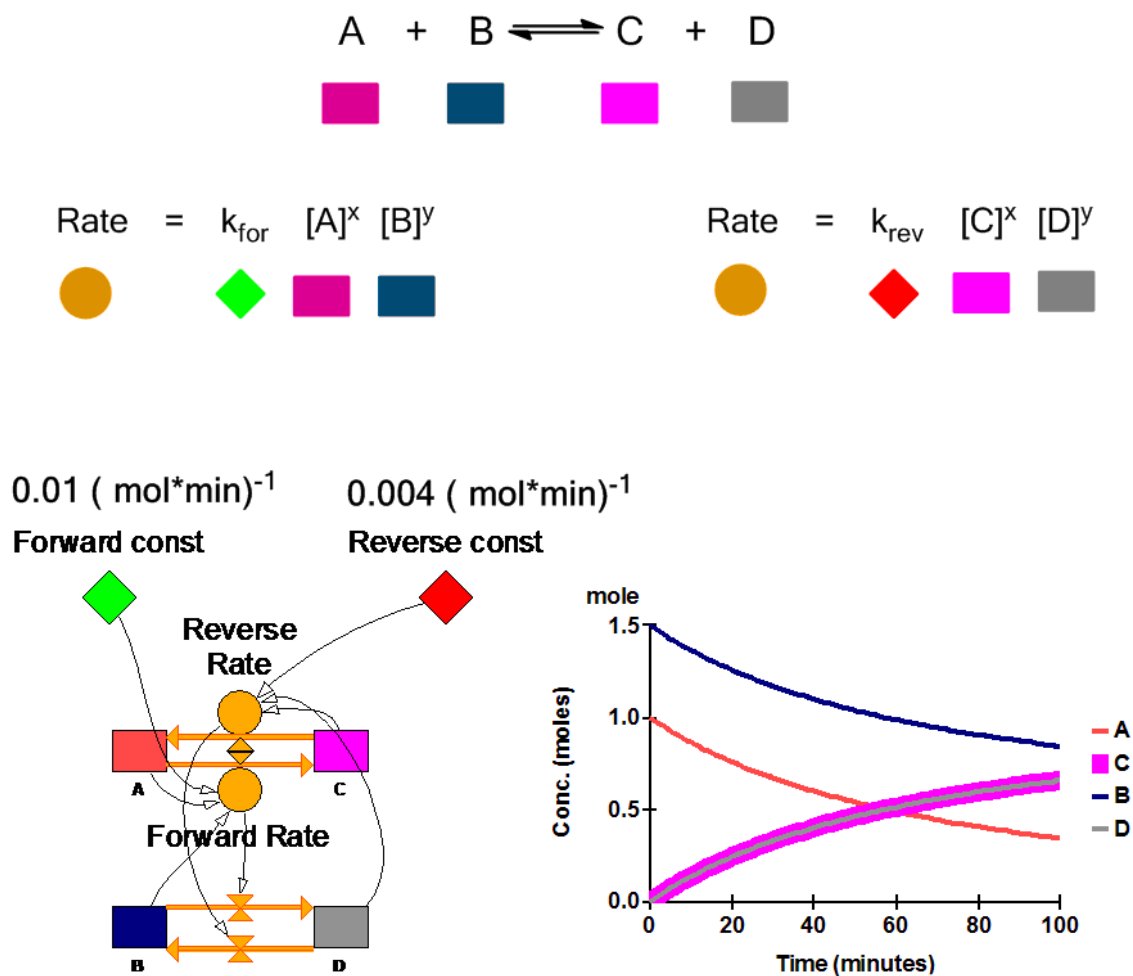


Figure 2.9. Simple example with PowerSim Studio 9 Academic software. Model for 2 starting materials generating 2 products (bottom left). Each rectangle represents one species in the catalytic cycle, each circle represents a rate and each diamond represents a rate constant. A and B have initial concentrations of 1.5 and 1.0 moles respectively. The abundance traces for the disappearance of A and B and appearance of C and D over 100 minutes (bottom right).

As more permutations of the model were constructed, and changes to the mechanism were required, the model became increasingly complex (Figure 2.10).

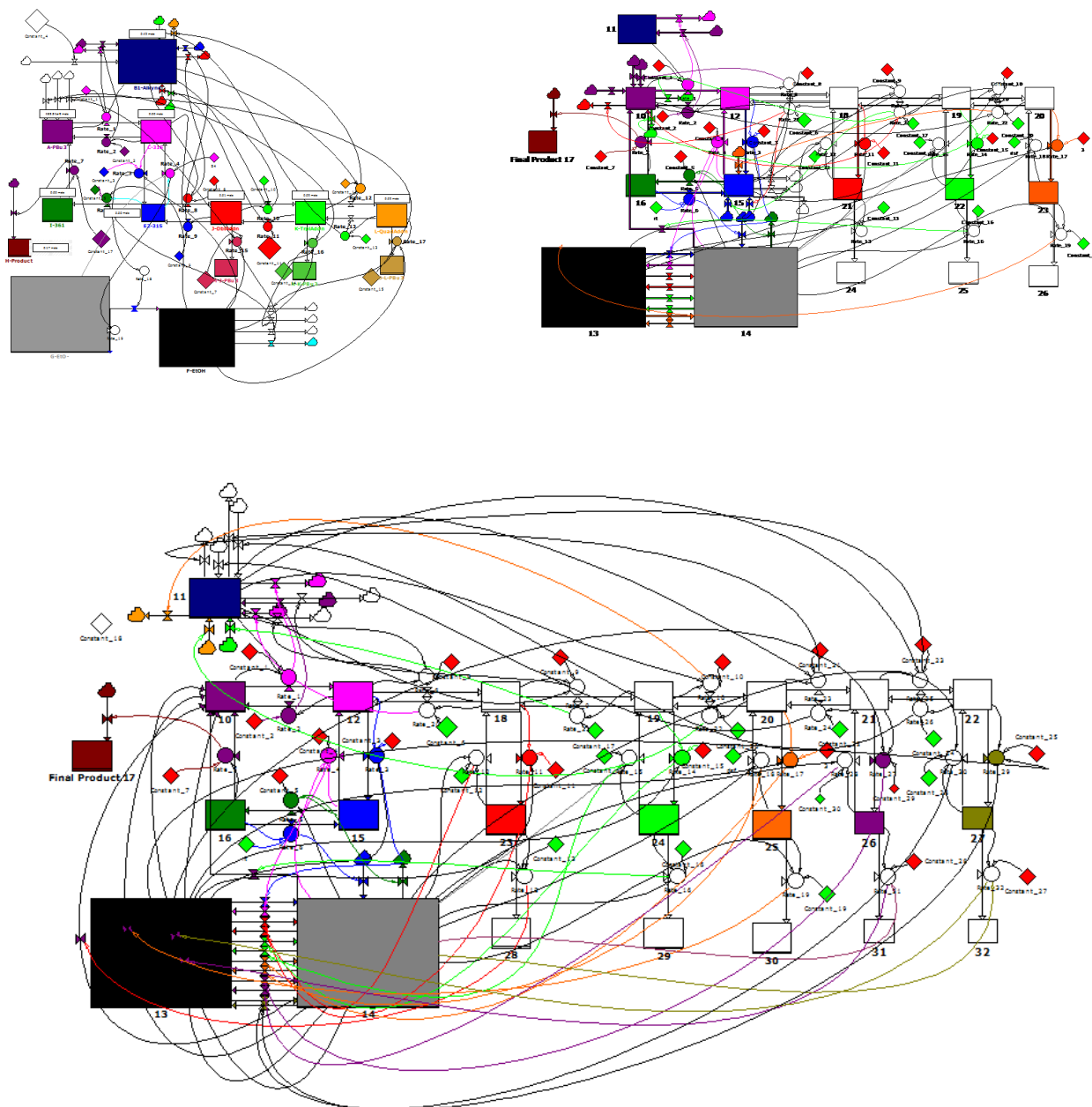


Figure 2.10. Top left: early PowerSim model for simpler mechanism; top right, model for advanced mechanism; expanded model for mechanism that includes higher oligomers, bottom.

As the mechanism evolved, increasing in complexity, so the model changed, becoming increasingly convoluted and requiring longer processing time. It became increasingly difficult to generate abundance traces with confidence in the correct construction of the model. Another, more simplistic modeling program was discovered and implemented immediately. The issues of

correct model construction were removed and modelling a very complex system became simplistic.

Copasi 4.11 (Build 64) freeware is a joint project between the Virginia Bioinformatics Institute, the University of Manchester (Mendes group) and the University of Heidelberg (Kummer group). It is an application that simulates dynamic biochemical networks and supports the Systems Biology Markup Language (www.sbml.org). Copasi utilizes ODEs (ordinary differential equations, Figure 2.14) and the deterministic LSODA method⁴⁴ which can select between stiff and non-stiff ODE solvers. The LSODA method dynamically monitors the data, and starts with non-stiff solvers, switching to stiff methodologies when approximation errors become large. The ODE solvers generate a time course simulation, based on the rate equations and the changing rate constants, and as the rate constants are varied iteratively, the time course simulation more closely approximates the experimental traces until plausible rate are obtained.

With Copasi, the reaction equations are entered as “A” + “B” = “C” + “D” as a mass action reversible rate law, and is read as “A and B are in reversible equilibrium with C and D”, where “A” and “B” are starting materials and “C” and “D” are products of that reaction. When a reaction is not reversible, the reaction equation is entered as “W” + “X” -> “Y” + “Z” as a mass action irreversible rate law, and is read as “W and X irreversibly produce Y and Z, where W and X are starting materials and Y and Z are products. A list of the reaction equations used to generate the traces for this project is detailed in Figure 2.11.

#	Name	Reaction	Rate Law	Flux (mmol/min)
1	1 to 3	"1" + "2" = "3"	Mass action (reversible)	0
2	3 to 10	"3" + "2" = "10"	Mass action (reversible)	0
3	10 to 11	"10" + "2" = "11"	Mass action (reversible)	0
4	11 to 12	"11" + "2" = "12"	Mass action (reversible)	0
5	12 to 12A	"12" + "2" = 12A	Mass action (reversible)	0
6	12A to 12B	12A + "2" = 12B	Mass action (reversible)	0
7	10 to 23	"10" + "4" = "5" + "13"	Mass action (reversible)	0
8	11 to 14	"11" + "4" = "5" + "14"	Mass action (reversible)	0
9	20 to 25	"12" + "4" = "5" + "15"	Mass action (reversible)	0
10	12A to 15A	12A + "4" = "5" + 15A	Mass action (reversible)	0
11	12B to 15B	12B + "4" = "5" + 15B	Mass action (reversible)	0
12	13 to 16	"13" + "5" -> "16" + "1"	Mass action (irreversible)	0
13	14 to 17	"14" + "5" -> "17" + "1"	Mass action (irreversible)	0
14	15 to 18	"15" + "5" -> "18" + "1"	Mass action (irreversible)	0
15	15A to 18A	15A + "5" -> 18A + "1"	Mass action (irreversible)	0
16	15B to 18B	15B + "5" -> 18B + "1"	Mass action (irreversible)	0
17	3 to 6	"3" + "4" = "5" + "6"	Mass action (reversible)	0
18	6 to 7	"6" + "5" = "7"	Mass action (reversible)	0
19	7 to 9	"7" -> "1" + "9"	Mass action (irreversible)	0
	New Reaction			

Figure 2.11. Screen shot of all the reaction equations used in Copasi to produce the traces for the starting alkyne (**2**) and the product (**9**) detected by ^1H NMR as well as intermediates and oligomers detected by ESI-MS and ^{31}P NMR.

The rate constants for each forward (k_1) and reverse (k_2) reaction are changed on the reaction tab. An example in which **1** and **2** react to form **3** is shown in Figure 2.12, where $k_1(\text{forward})$ is $750 \text{ mL}(\text{mmol} \cdot \text{min})^{-1}$, and $k_2(\text{reverse})$ is 80 min^{-1} .

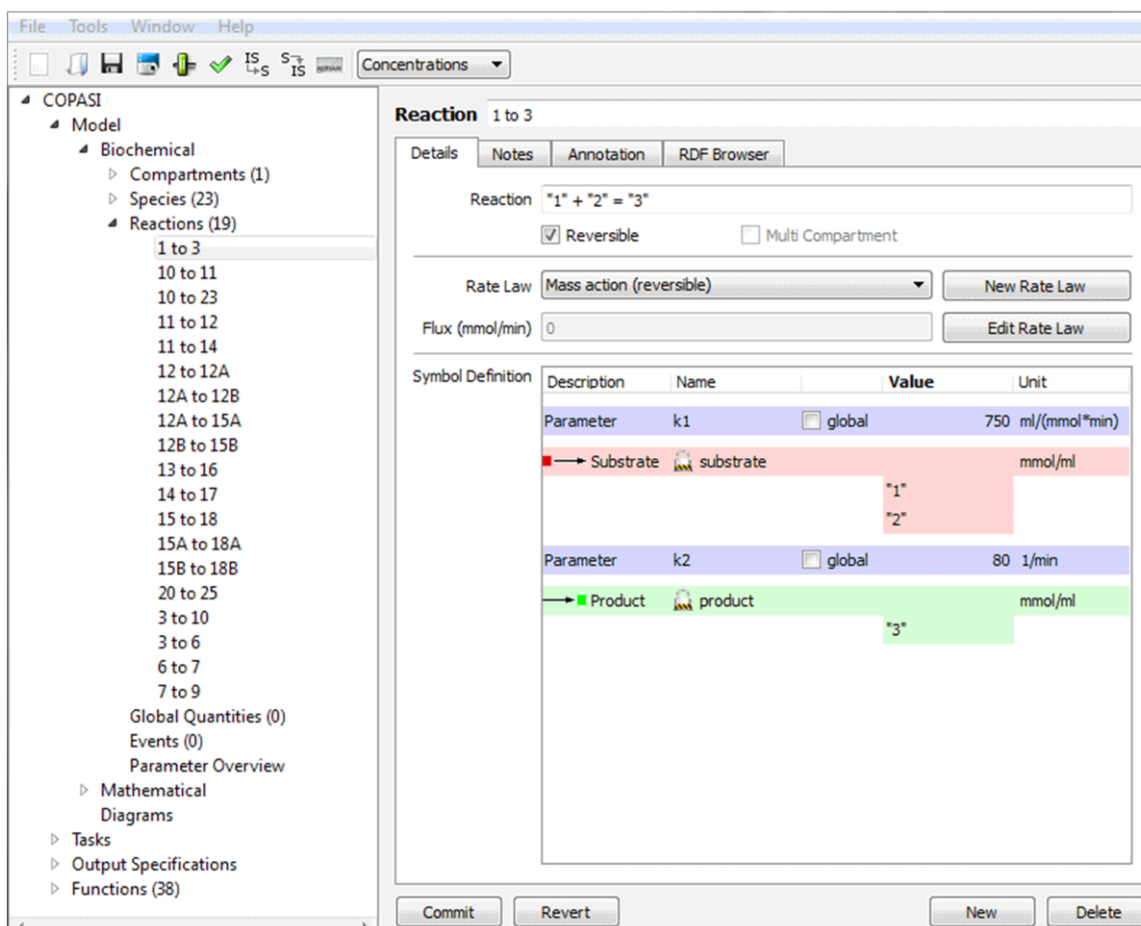


Figure 2.12. Screen shot for Copasi showing the reaction tab where the rate constants for k1 and k2 in each reaction can be changed.

Running the time course simulation is selected from the “Tasks” tab, and the time duration (240 minutes), the number of steps required (interval size), and the ODE solver method (Deterministic LSODA) may be selected in this tab, Figure 2.13.

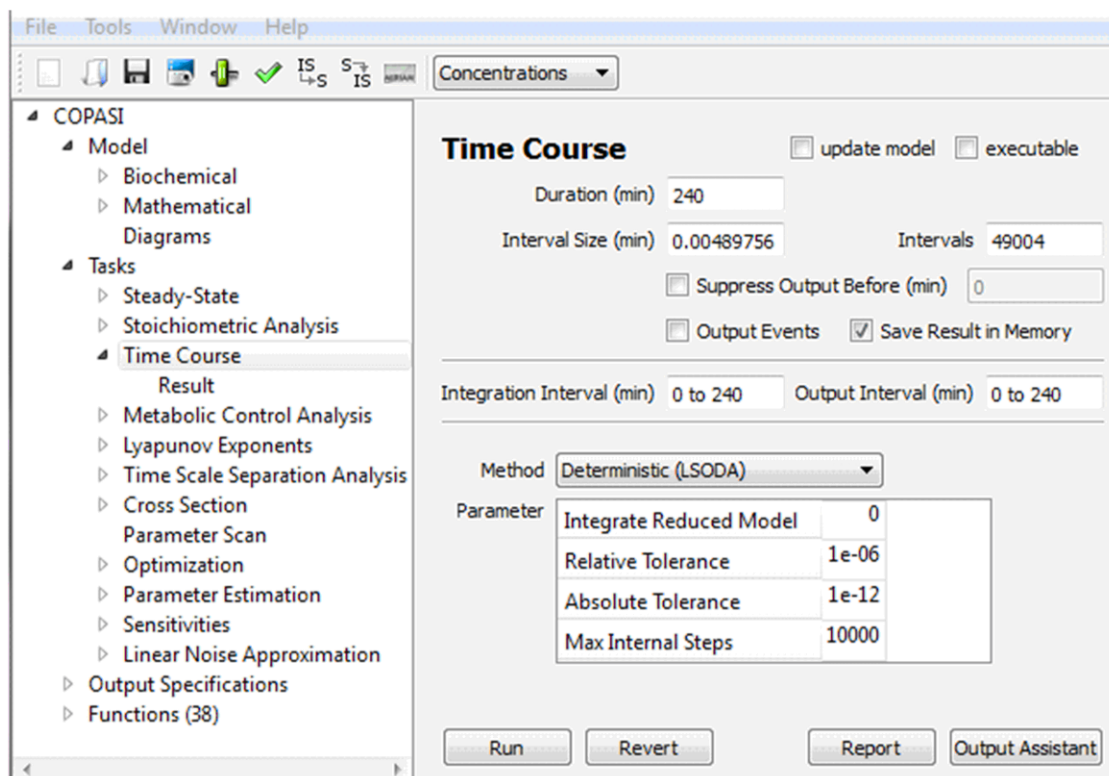


Figure 2.13. Copasi screen shot of the time course tab where the simulation duration (240 minutes), number of steps (interval size) and ODE solver method (deterministic LSODA) may be selected.

The simulation then generates a series of differential equations detailing the rate constants of each species in combination with every other species it reacts with over time, Figure 2.14.

$$\begin{aligned}
 \frac{d([1]\text{-}\nu\text{compartment})}{dt} &= -\nu\text{compartment} \cdot ((750 \cdot [1] \cdot [2] - 80 \cdot [3])) \\
 &\quad +\nu\text{compartment} \cdot (0.001 \cdot [13] \cdot [5]) \\
 &\quad +\nu\text{compartment} \cdot (0.001 \cdot [14] \cdot [5]) \\
 &\quad +\nu\text{compartment} \cdot (0.001 \cdot [15] \cdot [5]) \\
 &\quad +\nu\text{compartment} \cdot (0.001 \cdot [15A] \cdot [5]) \\
 &\quad +\nu\text{compartment} \cdot (0.001 \cdot [15B] \cdot [5]) \\
 &\quad +\nu\text{compartment} \cdot (0.8 \cdot [7]) \\
 \frac{d([2]\text{-}\nu\text{compartment})}{dt} &= -\nu\text{compartment} \cdot ((750 \cdot [1] \cdot [2] - 80 \cdot [3])) \\
 &\quad -\nu\text{compartment} \cdot ((400 \cdot [3] \cdot [2] - 20 \cdot [10])) \\
 &\quad -\nu\text{compartment} \cdot ((50 \cdot [10] \cdot [2] - 1 \cdot [11])) \\
 &\quad -\nu\text{compartment} \cdot ((40 \cdot [11] \cdot [2] - 0.5 \cdot [12])) \\
 &\quad -\nu\text{compartment} \cdot ((40 \cdot [12] \cdot [2] - 0.01 \cdot [12A])) \\
 &\quad -\nu\text{compartment} \cdot ((40 \cdot [12A] \cdot [2] - 0.01 \cdot [12B])) \\
 \frac{d([3]\text{-}\nu\text{compartment})}{dt} &= +\nu\text{compartment} \cdot ((750 \cdot [1] \cdot [2] - 80 \cdot [3])) \\
 &\quad -\nu\text{compartment} \cdot ((400 \cdot [3] \cdot [2] - 20 \cdot [10])) \\
 &\quad -\nu\text{compartment} \cdot ((50 \cdot [3] \cdot [4] - 5 \cdot [5] \cdot [6])) \\
 \frac{d([4]\text{-}\nu\text{compartment})}{dt} &= -\nu\text{compartment} \cdot ((1e-005 \cdot [12B] \cdot [4] - 0.001 \cdot [5] \cdot [15B])) \\
 &\quad -\nu\text{compartment} \cdot ((50 \cdot [3] \cdot [4] - 5 \cdot [5] \cdot [6])) \\
 &\quad -\nu\text{compartment} \cdot ((30 \cdot [10] \cdot [4] - 10 \cdot [5] \cdot [13])) \\
 &\quad -\nu\text{compartment} \cdot ((0.7 \cdot [11] \cdot [4] - 1e-005 \cdot [5] \cdot [14])) \\
 &\quad -\nu\text{compartment} \cdot ((0.5 \cdot [12] \cdot [4] - 0.006 \cdot [5] \cdot [15])) \\
 &\quad -\nu\text{compartment} \cdot ((0.05 \cdot [12A] \cdot [4] - 0.001 \cdot [5] \cdot [15A])) \\
 \frac{d([5]\text{-}\nu\text{compartment})}{dt} &= +\nu\text{compartment} \cdot ((1e-005 \cdot [12B] \cdot [4] - 0.001 \cdot [5] \cdot [15B])) \\
 &\quad +\nu\text{compartment} \cdot (0.001 \cdot [13] \cdot [5]) \\
 &\quad +\nu\text{compartment} \cdot (0.001 \cdot [14] \cdot [5]) \\
 &\quad +\nu\text{compartment} \cdot (0.001 \cdot [15] \cdot [5]) \\
 &\quad +\nu\text{compartment} \cdot (0.001 \cdot [15A] \cdot [5]) \\
 &\quad +\nu\text{compartment} \cdot (0.001 \cdot [15B] \cdot [5]) \\
 &\quad +\nu\text{compartment} \cdot ((50 \cdot [3] \cdot [4] - 5 \cdot [5] \cdot [6])) \\
 &\quad +\nu\text{compartment} \cdot ((35 \cdot [6] \cdot [5] - 0.4 \cdot [7])) \\
 &\quad +\nu\text{compartment} \cdot ((30 \cdot [10] \cdot [4] - 10 \cdot [5] \cdot [13])) \\
 &\quad +\nu\text{compartment} \cdot ((0.7 \cdot [11] \cdot [4] - 1e-005 \cdot [5] \cdot [14])) \\
 &\quad +\nu\text{compartment} \cdot ((0.5 \cdot [12] \cdot [4] - 0.006 \cdot [5] \cdot [15])) \\
 &\quad +\nu\text{compartment} \cdot ((0.05 \cdot [12A] \cdot [4] - 0.001 \cdot [5] \cdot [15A])) \\
 \frac{d([6]\text{-}\nu\text{compartment})}{dt} &= +\nu\text{compartment} \cdot ((50 \cdot [3] \cdot [4] - 5 \cdot [5] \cdot [6])) \\
 &\quad -\nu\text{compartment} \cdot ((35 \cdot [6] \cdot [5] - 0.4 \cdot [7])) \\
 \frac{d([7]\text{-}\nu\text{compartment})}{dt} &= +\nu\text{compartment} \cdot ((35 \cdot [6] \cdot [5] - 0.4 \cdot [7])) \\
 &\quad -\nu\text{compartment} \cdot (0.8 \cdot [7]) \\
 \frac{d([9]\text{-}\nu\text{compartment})}{dt} &= +\nu\text{compartment} \cdot (0.8 \cdot [7]) \\
 \frac{d([10]\text{-}\nu\text{compartment})}{dt} &= +\nu\text{compartment} \cdot ((400 \cdot [3] \cdot [2] - 20 \cdot [10])) \\
 &\quad -\nu\text{compartment} \cdot ((50 \cdot [10] \cdot [2] - 1 \cdot [11])) \\
 &\quad -\nu\text{compartment} \cdot ((30 \cdot [10] \cdot [4] - 10 \cdot [5] \cdot [13])) \\
 \frac{d([11]\text{-}\nu\text{compartment})}{dt} &= +\nu\text{compartment} \cdot ((50 \cdot [10] \cdot [2] - 1 \cdot [11])) \\
 &\quad -\nu\text{compartment} \cdot ((40 \cdot [11] \cdot [2] - 0.5 \cdot [12])) \\
 &\quad -\nu\text{compartment} \cdot ((0.7 \cdot [11] \cdot [4] - 1e-005 \cdot [5] \cdot [14])) \\
 \frac{d([12]\text{-}\nu\text{compartment})}{dt} &= +\nu\text{compartment} \cdot ((40 \cdot [11] \cdot [2] - 0.5 \cdot [12])) \\
 &\quad -\nu\text{compartment} \cdot ((40 \cdot [12] \cdot [2] - 0.01 \cdot [12A])) \\
 &\quad -\nu\text{compartment} \cdot ((0.5 \cdot [12] \cdot [4] - 0.006 \cdot [5] \cdot [15])) \\
 \frac{d([12A]\text{-}\nu\text{compartment})}{dt} &= +\nu\text{compartment} \cdot ((40 \cdot [12] \cdot [2] - 0.01 \cdot [12A])) \\
 &\quad -\nu\text{compartment} \cdot ((40 \cdot [12A] \cdot [2] - 0.01 \cdot [12B])) \\
 &\quad -\nu\text{compartment} \cdot ((0.05 \cdot [12A] \cdot [4] - 0.001 \cdot [5] \cdot [15A])) \\
 \frac{d([12B]\text{-}\nu\text{compartment})}{dt} &= -\nu\text{compartment} \cdot ((1e-005 \cdot [12B] \cdot [4] - 0.001 \cdot [5] \cdot [15B])) \\
 &\quad +\nu\text{compartment} \cdot ((40 \cdot [12A] \cdot [2] - 0.01 \cdot [12B])) \\
 \frac{d([13]\text{-}\nu\text{compartment})}{dt} &= -\nu\text{compartment} \cdot (0.001 \cdot [13] \cdot [5]) \\
 &\quad +\nu\text{compartment} \cdot ((30 \cdot [10] \cdot [4] - 10 \cdot [5] \cdot [13])) \\
 \frac{d([14]\text{-}\nu\text{compartment})}{dt} &= -\nu\text{compartment} \cdot (0.001 \cdot [14] \cdot [5]) \\
 &\quad +\nu\text{compartment} \cdot ((0.7 \cdot [11] \cdot [4] - 1e-005 \cdot [5] \cdot [14])) \\
 \frac{d([15]\text{-}\nu\text{compartment})}{dt} &= -\nu\text{compartment} \cdot (0.001 \cdot [15] \cdot [5]) \\
 &\quad +\nu\text{compartment} \cdot ((0.5 \cdot [12] \cdot [4] - 0.006 \cdot [5] \cdot [15])) \\
 \frac{d([15A]\text{-}\nu\text{compartment})}{dt} &= -\nu\text{compartment} \cdot (0.001 \cdot [15A] \cdot [5]) \\
 &\quad +\nu\text{compartment} \cdot ((0.05 \cdot [12A] \cdot [4] - 0.001 \cdot [5] \cdot [15A])) \\
 \frac{d([15B]\text{-}\nu\text{compartment})}{dt} &= +\nu\text{compartment} \cdot ((1e-005 \cdot [12B] \cdot [4] - 0.001 \cdot [5] \cdot [15B])) \\
 &\quad -\nu\text{compartment} \cdot (0.001 \cdot [15B] \cdot [5]) \\
 \frac{d([16]\text{-}\nu\text{compartment})}{dt} &= +\nu\text{compartment} \cdot (0.001 \cdot [13] \cdot [5]) \\
 \frac{d([17]\text{-}\nu\text{compartment})}{dt} &= +\nu\text{compartment} \cdot (0.001 \cdot [14] \cdot [5]) \\
 \frac{d([18A]\text{-}\nu\text{compartment})}{dt} &= +\nu\text{compartment} \cdot (0.001 \cdot [15A] \cdot [5]) \\
 \frac{d([18B]\text{-}\nu\text{compartment})}{dt} &= +\nu\text{compartment} \cdot (0.001 \cdot [15B] \cdot [5]) \\
 \frac{d([18]\text{-}\nu\text{compartment})}{dt} &= +\nu\text{compartment} \cdot (0.001 \cdot [15] \cdot [5])
 \end{aligned}$$

Figure 2.14. Differential equations as generated by Copasi for the entire proposed mechanism. Rate constants for each forward and reverse step are listed.

The assignment of the ^{31}P plot was made with the help of the PSI-ESI-MS data, so essentially the model needed to fit the overall rate, the overall yield, and the dynamic abundances of the observed intermediates and by-products. The mechanism cannot be proven but it can be shown that a set of plausible rate constants is capable of generating the traces observed based on the proposed mechanism. In this case, the rate constants shown on the catalytic cycle (Scheme 9) generate the numerically modelled plots shown in Figure 2.15.

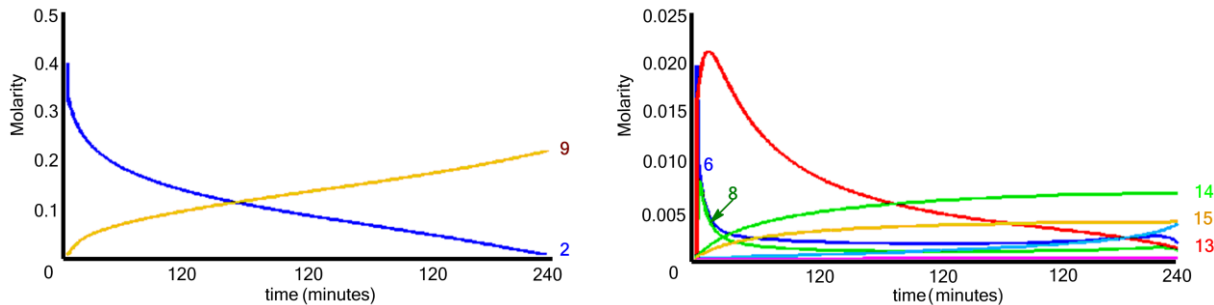


Figure 2.15. Numerical model output for the substrate **2** and product **9** (left), and for key phosphonium intermediates (**6**, **8**) and decomposition oligomers (**13**, **14**, **15** and other higher mass oligomers) observed by ESI-MS and ^{31}P NMR.

It is important to note that according to the numerical model, the set of rate constants playing the most influential roles are the set controlling the equilibrium of the forward and reverse reaction of the formation of the double addition product, and hence dictates the yield of the final product. It makes sense, since dropwise addition of the alkyne experimentally helps to hinder the formation of the off-cycle multiple addition species.

When the model was initially constructed without including the higher mass oligomers, the traces for the oligomers seemed to match well for the ESI-MS data, but did not match well with the ^1H or ^{31}P data. The MS spectrum did show higher mass oligomers in low concentration which were not added to the proposed mechanism as they were deemed unnecessary. However, when they were added to the numerical model, the starting alkyne trace dropped more intensely and quickly, as was seen in the ^1H NMR results. The rate constants for the formation of those highly conjugated allene zwitterions of higher mass are an order of magnitude slower than the rate constant for the generation of **10** but it brings the starting alkyne and product traces much closer to the ^1H NMR results (Figure 2.16). The formation of the higher oligomer allenes (**12A** and **12B**) as well as the higher phosphonium oligomers detected by ESI-MS likely form in the same manner as do allenes **10-12** and phosphoniums **13-15** (Scheme 8). The oligomer traces also

more closely match the ^{31}P NMR results. There is an increase in concentration for **6** near the end of the reaction when the catalyst is released. The model shows that release of **1** from **7** causes an increase the concentration of **6**. When the rate constants for the release of **1** from the oligomers are set to zero from $0.001\text{ (mol}^{-1}\text{min)}^{-1}$, the concentration of **6** still increases near the end. When the rate constant for the formation of **9** is increased, the concentration of **6** also increases earlier.

This closer, more compelling match enabled the construction of the final mechanism with the corresponding rate constants that included the higher mass oligomers. The rate constants for the allene zwitterions in the higher oligomers are lower, demonstrating that they appear to be more stable species, likely due to the increasing conjugation. Additionally, those conjugated phosphonium olefins (**13**, **14**, **15**) are detected by MS hours and even days after the reaction is complete, albeit with some decomposition occurring. This also lends credence to the proposal that the release of **1** from the oligomers is very slow.

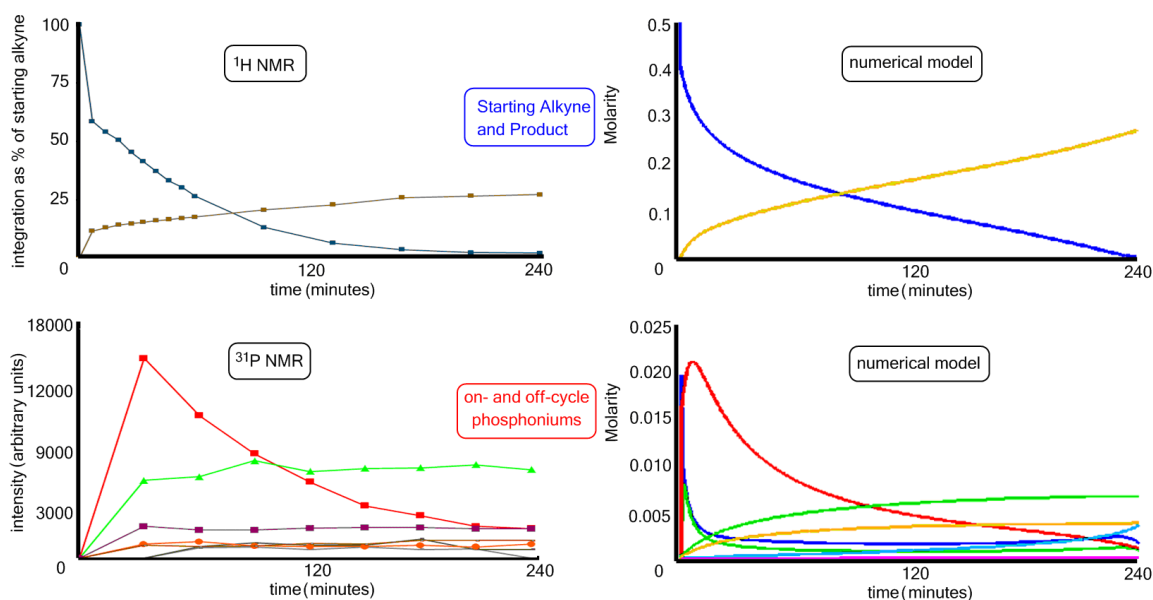


Figure 2.16. Experimental results for ^1H NMR (top left) are compared to the numerical model (top right) for the starting alkyne and product traces. The ^{31}P NMR results (bottom left) are compared with the oligomer traces for the numerical model (bottom right). The traces for higher mass oligomers are also included in this model.

2.2.5. Drop-wise addition of alkyne

When alkyne is added drop-wise over 80 minutes to the reaction solution, the concentration of off-cycle oligomers detected by ESI-MS is minimal, as seen in Figure 2.17. Two on-cycle species are detected: **6** and **8**. However, **8** is detected ~20 minutes after the initial addition of alkyne, instead of the two appearing simultaneously, and as before is present only in very low amounts, as it is likely that it is quickly consumed in the next step of the cycle which generates the product.

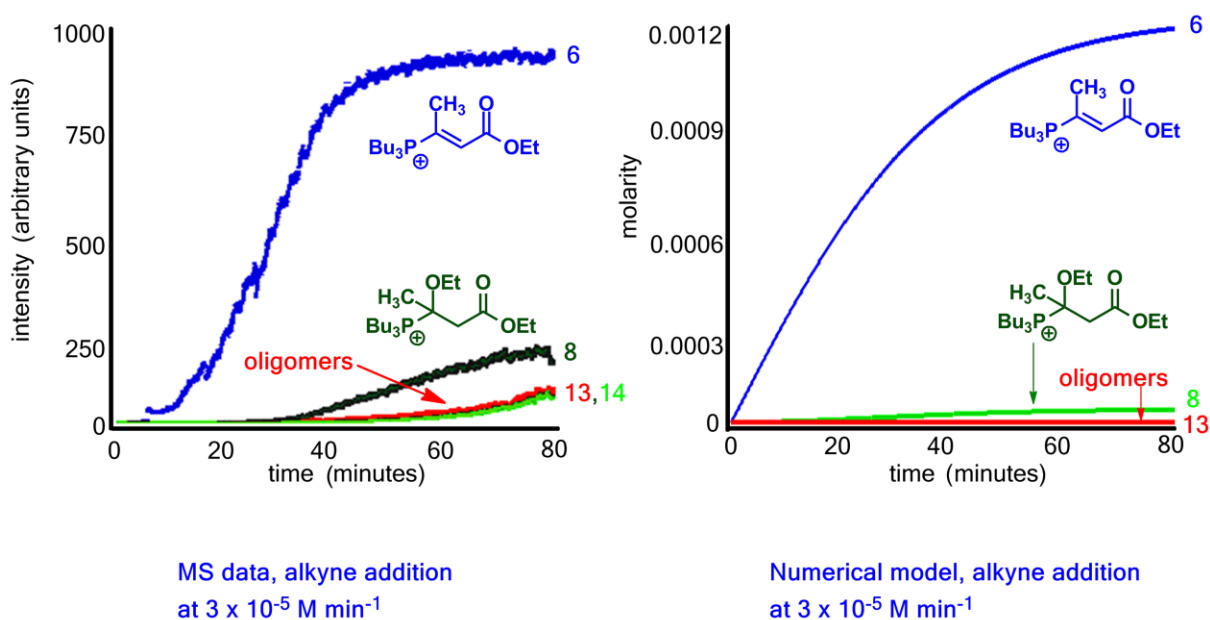


Figure 2.17. Drop-wise addition of alkyne to ethanol and tributylphosphine catalyst, at the rate of 0.00003 moles per minute, PSI-ESI-MS traces (left). Copasi numerical model, same rate of addition (right).

This is confirmed by the numerical model. As long as the rate of addition of alkyne remains slow, the concentration of the off-cycle oligomers remains low, while the yield of product approaches 100%. An addition rate of 0.00003 moles/minute was used for both the model, and for the experimental rate. As there are now fewer oligomers present, there is more catalyst available to react with the alkyne, and it does not get tied up in the stable oligomers. This was

confirmed experimentally by Natasha O'Rourke where dropwise addition of the alkyne over 30 minutes gave a greater than 90% yield of product after 4 hours.

2.2.6 Effect of a sterically hindered alcohol on product yield

When the sterically hindered neopentyl alcohol is used instead of ethanol, there is a dramatically lower concentration of off-cycle oligomers compared to the on-cycle species observed. This time the main product competitor was from an esterification-type reaction in which the ethoxide from the ester in the starting material could be replaced by the neopentyloxy generated upon deprotonation of the neopentyl alcohol. This mirrored-cycle competition outpaced the formation of oligomeric species that were observed with EtOH. This confirmed the findings made by Natasha O'Rourke⁴¹ when the same hindered alcohol was used. Throughout the reaction, charged species are observed, separated by 42 amu, which is the mass difference between ethoxide and neopentyloxy. According to the data, as illustrated in Figure 2.18, the formation of **6** and **6A** occurs nearly simultaneously meaning that the alkoxide switch likely occurred prior to that step. **19** is the next species to be detected, (analogous to **8** from the previous EtOH reaction) and it is the next species in the same catalytic cycle. **13** again is formed in the same time frame as for the reaction with EtOH, but the concentration increases much more slowly, and stays low over 30 minutes, which was not seen with the unhindered EtOH. Since **13** stays low, the concentration of **6** does not drop to nearly zero until after 25 minutes, where it took 10 minutes to completely deplete in the EtOH reaction. This confirms that the bulkier neopentyl alcohol hinders the formation of the off-cycle oligomers and explains why the % yield of the bulkier product was close to 99%, seen in the Wulff group compared to 30% with EtOH. **6A** and subsequently **19A**, in the competing cycle, are present at ~ 10% of the intensity of **6** and

19, which indicates that the di-neopentyloxyde product formation is disfavored, as is the formation of the **13A** off-cycle oligomer.

The more hindered alcohol does not slow down either the protonation step (**3** \rightarrow **6**) or the conjugate addition step (**6** \rightarrow **19**) since there is also an immediate and large jump in intensity upon catalyst addition, as was seen with ethanol. **6**, **6A** and **19** appear to behave with pseudo-first order kinetics, but due to the low concentration of the other species it is more challenging to make that claim. No triple addition oligomer (**14**) was detected, which indicates that the more hindered alcohol disfavors the formation of oligomers through off-cycle reactions, and the concentrations of on-cycle species remains higher leading to greater product formation. Since **19** and **19A** drop off quickly and are present in low intensity, this indicates that the formation of product in the next step is fast, likely the same rate as with ethanol. However, the much lower concentrations of **6A** and **19A** indicate that the hindered alcohol forestalls the formation of **20A**.

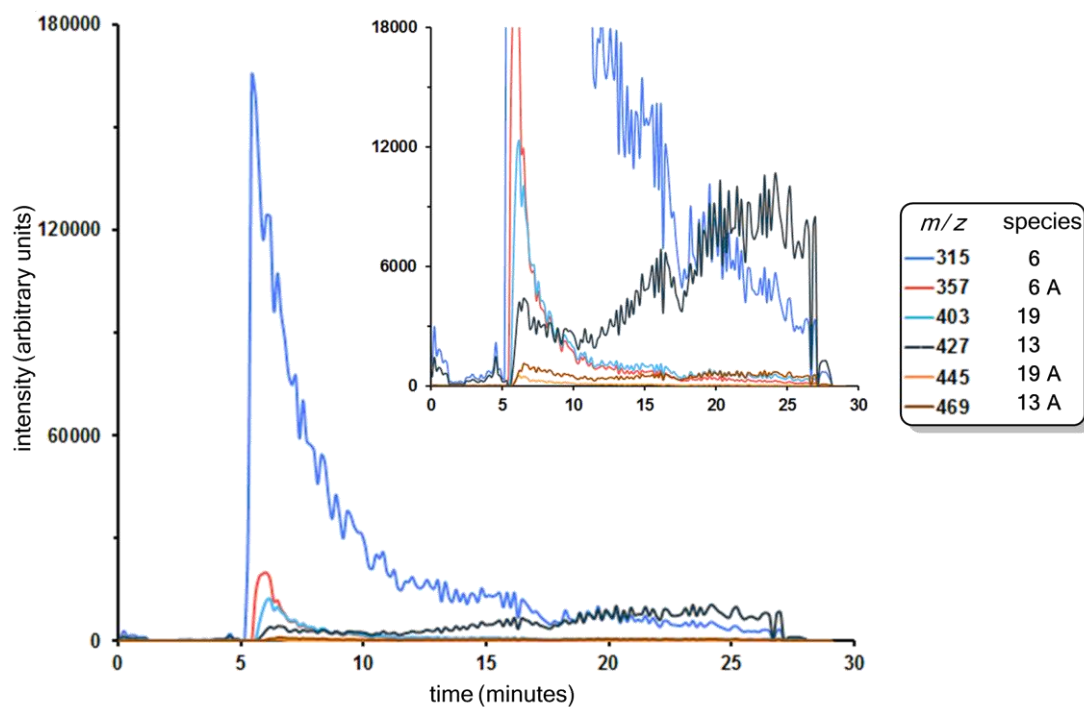
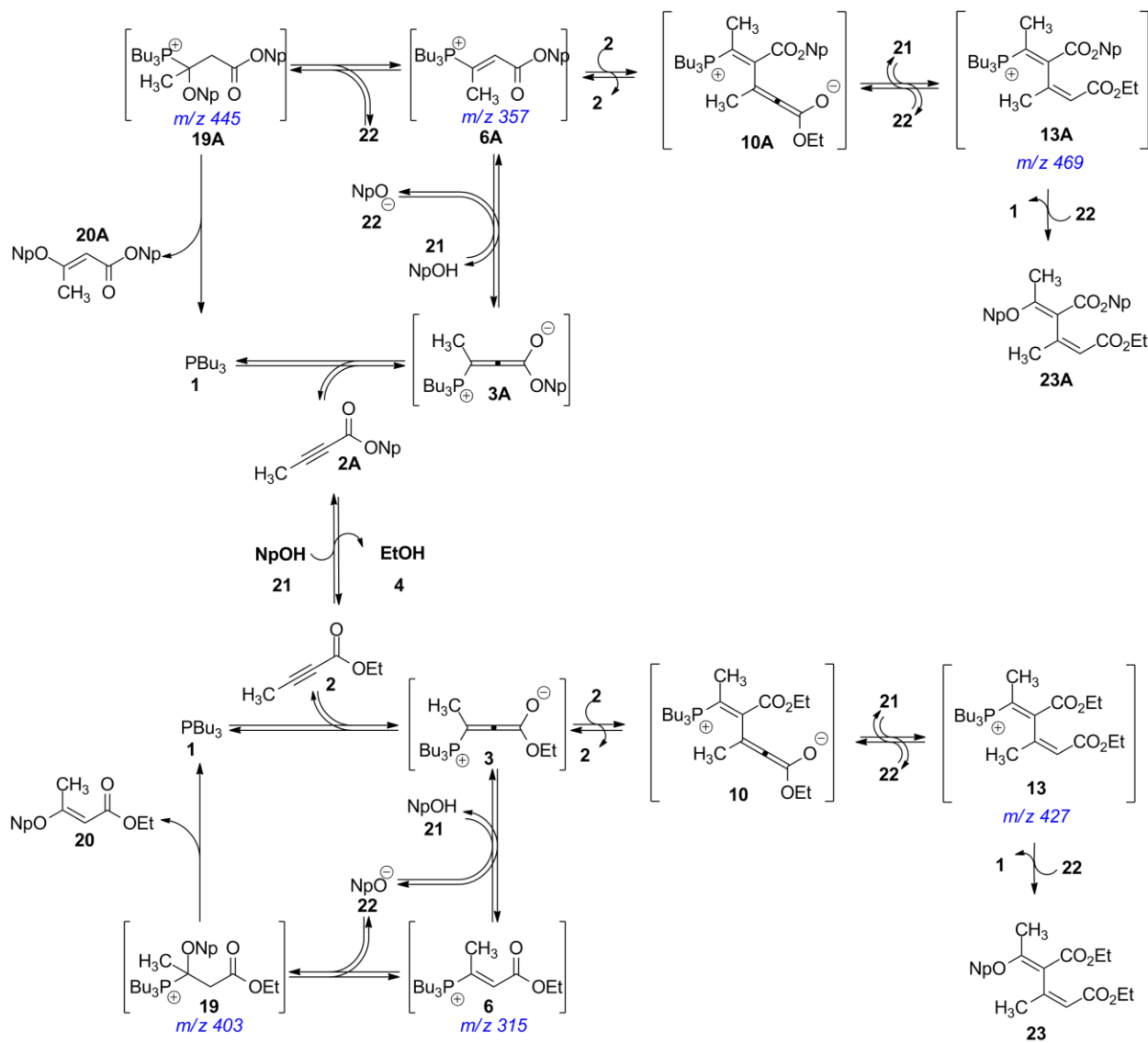


Figure 2.18. MS data for the reaction of ethyl-2-butyrate (0.4 M) with neopentyl alcohol (2.4 M) and $n\text{Bu}_3\text{P}$ catalyst (0.04M), and close-up (inset). Rate of data collection is 1 spectrum / 8 seconds.

The MS data suggest a condensed mechanism similar to that which was deduced for the EtOH reaction. The main differences lie in there being some competition between the 2 alkoxides, EtO⁻ and NpO⁻ to form another cycle, rather than the production of off-cycle oligomers, Scheme 10.



Scheme 10. Mechanism accounting for the exchange of the two alkoxides present in solution and the formation of the phosphonium intermediates detected by PSI-ESI-MS.

2.3 Conclusions

In examining phosphine catalysis through PSI-ESI-MS, NMR and numerical modelling, greater insight was gained into the mechanism of conjugate addition of ethanol to an alkynic acid ester. Each technique employed solved a piece of the puzzle and allowed the whole picture of the catalytic cycle to be viewed: ^1H NMR gave kinetic information about the disappearance of starting alkyne against the appearance of addition product; ^{31}P NMR showed that many phosphonium species were present, that the catalyst was in such low concentration that it could not be detected, and it supported the conclusions drawn from PSI-ESI. PSI-ESI provided the relative real time intensities of each phosphonium species over the first 2 hours revealing that the concentrations of the off-cycle species were much higher than originally anticipated, including data for a hindered alcohol which might not have been detected by a slower method. The PSI-ESI technique demonstrated that its strength lay in helping to interpret not only the species present in a complex mixture, but also in obtaining information about the kinetics of every species present in the mixture, using data points collected every second, which other techniques are not capable of doing. The numerical model combined the data from NMR and PSI-ESI to reveal the possible forward and reverse rate constants for each species in the mechanism. Each different method of analysis contributing to the whole picture served to emphasize the power of catalytic evaluation, and can reveal possible methods to improve catalysis.

2.4 Experimental

Solvents were HPLC grade and were purified on an MBraun solvent purification system. Ethyl-2-butynoate and *n*-tributylphosphine were obtained from Sigma-Aldrich and were

used without further purification. Anhydrous ethyl alcohol was HPLC grade and was obtained from Commercial Alcohols (Brampton, ON) and used without further purification. All mass spectra were collected on a Micromass Q-ToF *micro* mass spectrometer in positive mode, using electrospray ionization: capillary voltage, 2900 V; extraction voltage, 0.5 V; source temperature, 100 C; desolvation temperature, 200 C; cone gas flow, 100 L/h; desolvation gas flow, 100 L/h; collision voltage, 2 V for MS experiments and 2-25 V for MS/MS experiments; MCP voltage, 2700 V.

PSI-ESI-MS procedure: Ethyl-2-butynoate, (0.29 mL, 2.5 mmol) and ethanol, (0.73 mL, 12.5 mmol) were added to 5 mL of acetonitrile in a Schlenk flask equipped with a stir bar and a septum. PEEK tubing was then inserted into the reaction mixture solution, with the other end of connected to a T-junction. A syringe pump set at 15 μ L/minute pumped acetonitrile through the PEEK tubing to the T-junction where a third piece of tubing, connected to the mass spectrometer, took both solutions into the source. Argon gas was applied to the Schlenk flask at 3 psi and the extra pressure pushed the solution through the tubing to the spectrometer. Spectra were recorded once per second. The catalyst, n-tributylphosphine (0.73 mL, 0.25 mmol) was injected by syringe through the septum into the reaction mixture to initiate the reaction.

^1H NMR was conducted in CD_3CN . All reagents except ethanol were obtained from Sigma Aldrich and used without further purification. Ethanol was obtained from Commercial Alcohols. Ethyl-2-butynoate (0.5 mmol, 60 μ L), CD_3CN (500 μ L) and anhydrous ethanol (2.5 mmol, 145 μ L) were measured by syringe and injected into an NMR tube. A rubber NMR septum was used to cap the tube, which was sparged with nitrogen. $^n\text{Bu}_3\text{P}$ was added to a small flask capped with a septum which previously had been sparged with nitrogen. 285 μ L of CD_3CN was added to the flask containing $^n\text{Bu}_3\text{P}$. The solution of butynoate and ethanol was placed in the magnet and a

spectrum was obtained before the catalyst was added. Spectra were obtained on a 500 MHz Bruker magnet, with spectra collected every 7 minutes for the first hours, with 30 minute wait times between 7 minute scans afterwards, over a total of 4 hours. A 30 degree pulse program was used with a delay time of 20 seconds, since the T1 relaxation for all species was experimentally determined to be 9.4 seconds. This resulted in each ^1H spectrum to be collected every 6 minutes, 45 seconds, decreased line broadening and gave better shimming results. Before the addition of catalyst: δ 7.53-7.37 (10 H, dm), 4.14 (2H, q), 3.54 (2H, q), 3.44 (1H, br s), 1.96 (3H, s), 1.23 (3H, t), 1.11 (3H, t). After addition of catalyst: δ 7.54-7.38 (10H, dm), 4.99 (1H, s), 4.14 (2H, q, height decreases over reaction), 4.14 (2H, q, height increases over reaction), 4.06 (2H, q), 3.92 (2H, q), 3.88 (2H, q), 3.82 (2H, q), 3.54 (2H, q), 3.20 (1H, br s), 2.22 (3H, s), 1.96 (3H, s), 1.27 (3H, t), 1.23 (3H, t, height decreases over reaction), 1.23 (3H, t, height increases over reaction), 1.20 (3H, t), 1.11 (3H, t), 0.8- 0.9 (m).

^{31}P NMR experiments were conducted in an NMR tube using the same reagents and concentrations as were used for ^1H NMR. Spectra were obtained at 202 MHz in CD_3CN , and collected every 28 minutes with no wait times between over 4.5 hours. A 30 degree pulse program was used with a delay time of 65 seconds. The T1 relaxation for all species was experimentally determined to be 13 seconds. A delay time of five times T1 was used for a total delay time of 65 seconds.

Numerical modeling was conducted with PowerSim Studio 9 Academic software using 1st order Euler integration to generate the traces. Numerical modeling with Copasi 4.11 (Build 64) was generated with the biochemical network simulator, using the deterministic LSODA method.

Chapter 3: Olefin Metathesis

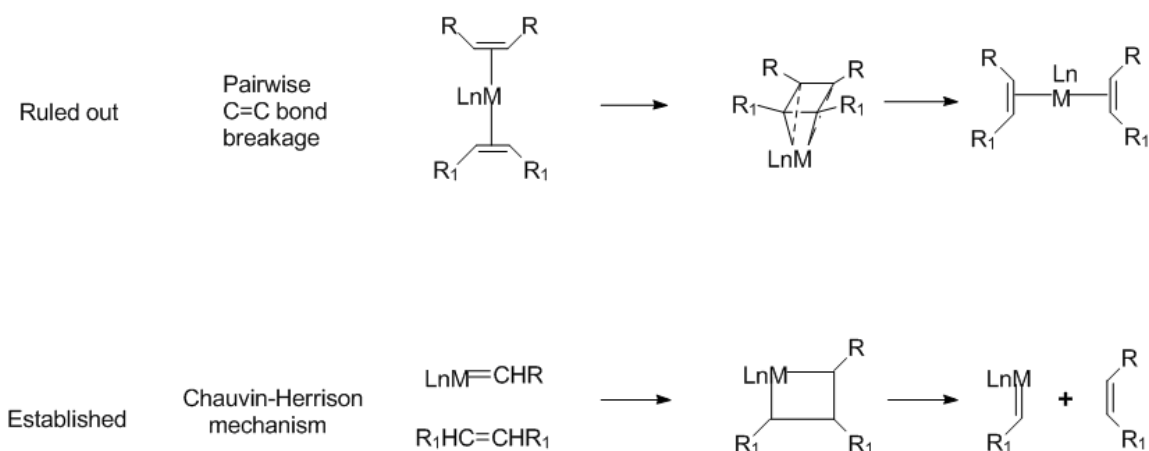
3.1 Overview of Olefin Metathesis

The process of olefin metathesis was discovered in the 1950's in petrochemical labs, and often named "olefin disproportionation" by researchers such as Edwin F. Peters, Alex Zletz, and Bernard L. Evering. Solid molybdates on activated alumina with triisobutyl aluminum as a catalyst were discovered, in 1957⁴⁵ to form ethylene polymers. Herbert S. Eleuterio patented the polymerization of cyclic olefins in 1963⁴⁶ using the same catalyst at atmospheric pressure in the presence of hydrogen gas. When studying monocyclic rings, he found that linear polymers formed; with bi- and tri-cyclic rings, polymers formed in which repeating cyclic units were present containing one less ring than the starting monomer. Also in 1963, Zeigler published a patent detailing the polymerization of ethylene to low-molecular weight polymers using trialkylaluminums.⁴⁷

In 1964, Banks and Bailey⁴⁸ studied linear olefins using molybdenum hexacarbonyl on alumina under high pressure but generating high yields of linear polymer. Also in 1964, Natta, Dall'Asta and Mazzanti published the results of their studies with cyclopentene using $\text{MoCl}_5/\text{Al}(\text{Et})_3$ and $\text{WCl}_6/\text{Al}(\text{Et})_3$, which gave *cis*- and *trans*- polymers, respectively, in much higher yields than $\text{TiCl}_4/\text{AlR}_3$ or $\text{VCl}_3/\text{AlR}_3$.⁴⁹ The mechanism through which metathesis proceeded was at that time unknown, and much speculation and discussion occurred as to the details of the process. In 1964, Bradshaw, Howman and Turner⁵⁰ and separately, Calderon, Chen and Scott⁵¹ at Goodyear Tire in 1966 theorized that a "quasicyclobutane" intermediate was present in the olefin metathesis of 1-butene and of 2-pentene respectively. This came to be

known as the “pairwise” mechanism. Calderon’s results with 2-pentene gave 3 products by mass spectral analysis: 2-butene, 2-pentene, and 3-hexene in a ratio of 1:2:1.

In 1971, Yves Chauvin proposed a new metallacyclic mechanism to account for the ratios of products formed. This new proposal was important because it stated that metathesis was initiated by a metal carbene,⁵² a two-coordinate carbon with two non-bonding electrons and no formal charge on the carbon,⁵³ and could be thought of as carbon(II). The carbene reacts with an olefin in a [2 + 2] cycloaddition reaction to form the metallacycle transition state (Scheme 11.), the “non-pairwise” mechanism.



Scheme 11. Top depicts the proposed “pairwise” breakage of C=C bonds to form a metal coordinated cyclobutene followed by construction of new C=C bonds. Bottom depicts the now established [2 + 2] cycloaddition to form the metallacycle followed by cycloreversion to form the new olefin and metal carbene.

This is the presently accepted mechanism of olefin metathesis.⁵⁴ Chauvin won the 2005 Nobel Prize for this contribution to “the development of the metathesis method in organic synthesis” and shared the prize with Robert Grubbs⁵⁵ and Richard Schrock.⁵⁶

3.2 Living polymerization and polydispersity index

“Living polymers”, as described in 1956 by Swarc⁵⁷ “are born in an initiation process, grow by a propagation process, and finally ‘die’ in a termination process”. He stated that growth occurs when “food” is present, i.e. the monomer, and that conceivably as long as monomer is present the chain will grow. He proved this to be correct through the addition of monomer after the propagation step had ceased and that termination occurred via addition of termination agents, often oxygen-containing species.

A living polymer requires that the rate of initiation be expeditious and at least as fast as, or faster than, the rate of propagation and that each polymer chain begin growth at the same time, since the initiator is consumed right away. Obviously, for the chain to propagate, the reverse reaction must be highly unfavorable. In order to qualify as “living”, the chain cannot undergo decomposition, make off-cycle products, or have the chain terminated or transferred. The molecular weight of the polymer can be controlled by the monomer/catalyst ratio, which is a linear relationship in the case of homopolymers. The number averaged MW (M_n) on the y-axis increases linearly with monomer/catalyst ratio increasing on the x-axis; additionally there is a linear dependence on the weighted average molecular weight of polymers to the number averaged molecular weight.

In terms of polymer formation there is a distribution of polymer masses,⁵⁸ often Gaussian shaped, with the number average molecular weight, M_n , at the center of the distribution of the number of molecules. The weight average molecular weight, M_w , is the value at which there are equal masses of molecules on either side, and as higher mass polymers contribute more to the weighted average, M_w is higher in the Gaussian distribution, Figure 3.1.

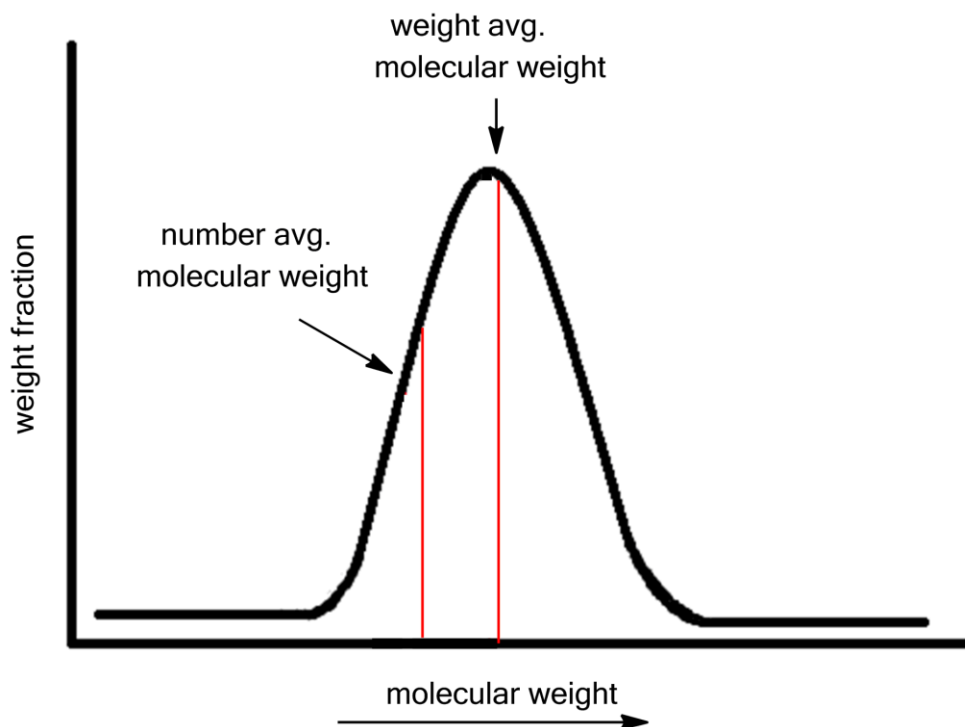


Figure 3.1. Example of molecular weight distribution for polymer chains

In measuring the distribution of molecular weight of a polymer, the polydispersity index, or PDI is applied. It is defined as the weighted average molecular weight divided by the number average molecular weight. The PDI is always greater than or equal to 1. As the chain lengths get more similar, the PDI approaches unity. Gel Permeation Chromatography (GPC) is an analytical technique that characterizes the weight distribution of a polymer and determines M_n and M_w . This is accomplished by physically separating the molecules in solution according to size by flowing the dissolved polymer with solvent (mobile phase) through a tightly-packed column containing porous, rigid particles (stationary phase). The smaller molecules are retained within the small pores longer and hence elute later than the larger molecules, thus they have a longer

retention time. A wide molecular weight distribution will show a bell-shaped curve over a longer period of time and a high weight distribution of polymers will shift the distribution according to the shorter retention time.

3.3 Ring Opening Metathesis Polymerization

Ring opening metathesis polymerization (ROMP) is a metal-catalyzed 1,2-insertion reaction with a strained cyclic olefin, and is considered to be a living polymerization. The alkylidene on the metal forms a metallacycle with the incoming olefin, thus breaking the double bond of the olefin and relieving strain. Olefin metathesis reactions are reversible, and hence under thermodynamic control, however relief of strain and breaking the double bond serve to drive the equilibrium in the forward direction toward polymer formation. When a strained cyclic olefin is introduced, an unsaturated polymer forms which has one less ring than the original starting material (i.e. the norbornene monomer has two strained 5-membered rings (sharing as they do two edges), whereas each polymer unit has one unstrained 5-membered ring). This simple reaction has been utilized with a large number of starting monomers, with or without added functionality, including, but not limited to cyclobutenes, norbornenes, and *trans*-cyclooctenes, which are considered to have greater strain and more easily consume all the monomer and can utilize a less active catalyst. Cyclopentenes, *cis*-cyclooctenes, and cyclooctadienes are less strained, requiring a more active catalyst to consume all the monomer. ROMP is considered to be a living polymerization technique, meaning that if more monomer were added, the reaction could continue, elongating each chain. Termination of the chain can occur via intramolecular chain transfer (backbiting), or by intermolecular chain transfer. High catalyst efficiency and control over the length of each chain for a narrow PDI are characteristics of successful

ROMP. When initiation is slow, broad molecular weight distributions of polymer chain lengths are common and cannot be considered to be “living” polymerizations.⁵⁹

3.4 Development of ROMP catalysts

3.4.1 Ill-defined ruthenium metathesis catalysts for ROMP

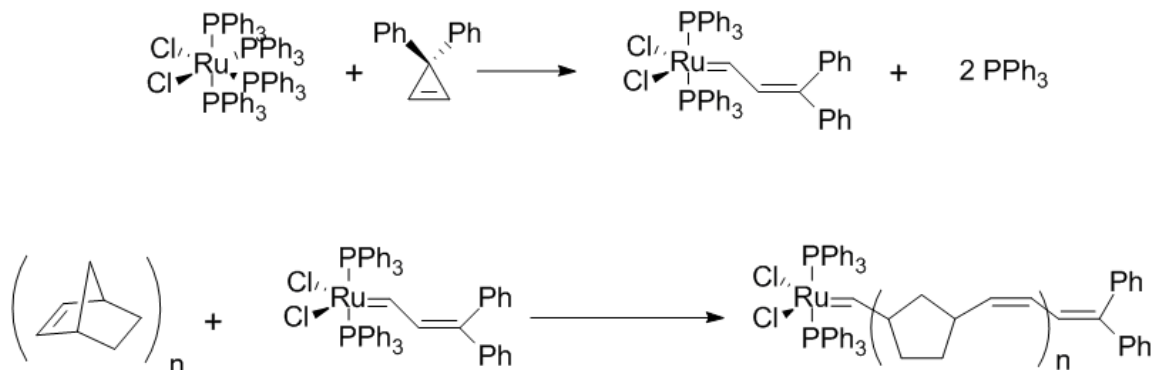
In 1988, Novak and Grubbs published 2 papers⁶⁰ in which the ROMP of 7-oxanorbornene was accomplished using the ill-defined catalysts, RuCl_3 , $\text{Ru}(1,5\text{-cyclooctadiene})\text{Cl}_3$, and OsCl_3 and tungsten catalysts, for which the former were the most successful, although initiation times were long. Water in the solvent, acting as a co-catalyst, greatly reduced the initiation time to 30 minutes, but the Ru catalysts still produced broad MW distributions for polymers,⁶¹ Ru catalysts were nevertheless robust, making them the best candidates for further ROMP investigations and ligand tuning.

3.4.2 Well-defined ruthenium catalysts for ROMP

Since the early 1980s, ROMP with norbornene analogues have been investigated with catalysts based on Mo, W, Re, Os, Ru and Ir compounds,⁶² including Schrock’s seminal work with well-defined tungsten and molybdenum catalysts (Figure 3.2).⁶³ Although they are more active in olefin metathesis, the catalysts are air- and water- sensitive and decompose quickly, in addition to their sensitivity to other functional groups such as alcohols, amides, aldehydes, and carboxylic acids.

Grubbs started to develop ruthenium catalysts in 1992 that were highly selective for alkenes and remained unaffected by such functional groups. The earliest well-defined ruthenium

alkylidene catalyst to successfully perform metathesis with a strained cyclic olefin was $(\text{PPh}_3)_2\text{Cl}_2\text{Ru}=\text{CH}-\text{CH}=\text{CPh}_2$;⁶⁴ a 16 electron, 5-coordinate alkylidene with an open coordination site for olefins. ROMP of norbornene was easily accomplished and included functionalization of the growing polymer chain by the diphenyl olefin (Scheme 12).



Scheme 12. Synthesis (top) of the first well-defined ruthenium (II) metathesis catalyst, and (bottom) reaction with the norbornene monomer and functionalization of the growing polynorbornene.

It would not, however metathesize acyclic olefins. A more strongly electron donating ancillary ligand was required, and PCy_3 was substituted as PPh_3 was less electron donating, and ring closing metathesis of acyclic dienes was achieved in good to excellent yields, but with long reaction times⁶⁵ of between 1 and 40 hours. This became known as Grubbs' first generation catalyst, Figure 3.2. Grubbs and co-workers found that their new catalysts had increased activity toward olefin metathesis but were subject to decomposition.⁶⁶

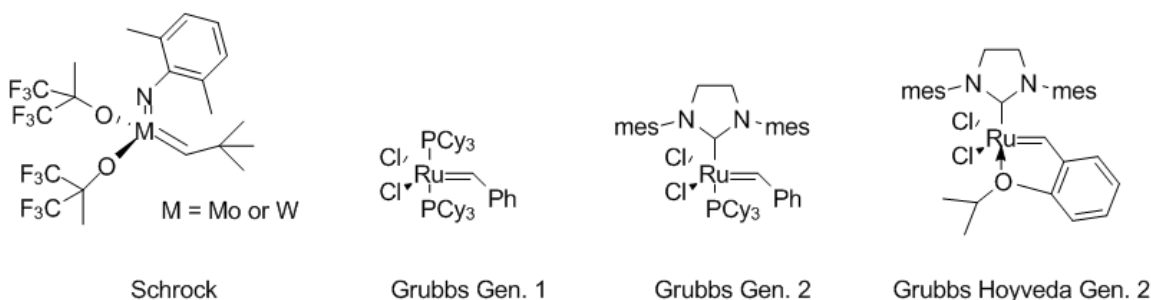


Figure 3.2. Example of a Schrock metathesis catalyst, Grubbs' first and second generation metathesis catalysts, and Hoyveda-Grubbs second generation metathesis catalyst.

The inherent reactivity of the Grubbs 1st generation catalyst, $(\text{PCy}_3)_2\text{Cl}_2\text{Ru}=\text{CHPh}$, was affected by the halogen and the phosphine used. The *trans* influence of the halogen decreases up the series for $\text{I} > \text{Br} > \text{Cl}$, with the incoming olefin bound *trans* to a halogen and bound more tightly with Cl. The influence of the *cis* halogen is largely steric; a smaller halogen serves to favor olefin binding. The effect of the phosphine is seen both in the cone angle and in the electron-donating ability. A larger cone angle leads to a greater willingness of the phosphine to dissociate, opening up a coordination site, creating the reactive catalyst species. A more electron-donating phosphine will stabilize the newly open position *trans* to it, which also encourages olefin binding.⁶⁷

Grubbs 1st generation catalyst was studied in Peter Chen's group in 2000, in conjunction with ESI-MS, to investigate the reactivity and mechanism of ROMP with norbornene and a small amount of charge-tagged norbornene as a "fishhook".⁶⁸ They discerned the resting state of the catalyst as being the dissociation of a phosphine with the polymer chain bound to Ru via an intramolecular π -bond. They also saw the Cl-bridged Ru dimer, which is known in Grubbs' work to be a decomposition product.

Grubbs 2nd generation Ru catalyst (Figure 3.2) proved to be more active toward olefin metathesis. An *N*-heterocyclic carbene (NHC) ligand replaced one of the more labile phosphines,

which upon dissociation of the phosphine, an open co-ordination site would allow faster initiation for metathesis. Since the NHC is a stronger σ -donor, and is therefore less labile than its phosphine counterpart, this could encourage the phosphine to dissociate at a faster rate, enhancing initiation. The NHC is also a bulkier ligand with a large cone angle, in addition to being strongly electron donating, and would better stabilize the metathesis active 16-electron ruthenium complex, thus increasing activity and thermal stability.⁶⁹

Hoyveda-Grubbs catalysts (Figure 3.2) contain a further modification that was originally designed to make the catalyst recoverable and recyclable, in that the styrenyl alkoxide is a bidentate ligand which does not fully dissociate, and could be fully recovered in high yield along with the desired product.⁷⁰ One of its greater values lay in the absence of the nucleophilic phosphine moiety which, when dissociated from the metal complex, can attack an intermediate methylene complex and create decomposition by-products. This catalyst also showed greater thermal stability than Grubbs 1st and 2nd generation metathesis catalysts and were better suited to higher temperature catalysis, although the greater thermal stability also decreased the rate of initiation.

3.4.3 Ruthenium Catalyst Decomposition

Since ruthenium olefin metathesis catalysts have consistently demonstrated high activity and specificity for functional groups, there has been much interest in studying their lifetime, efficiency and decomposition.⁷¹ Decomposition limits the lifetime of the catalyst and can be caused by the increased temperatures required for phosphine dissociation to occur, leading to the reactive species. Unfortunately, it can also limit catalyst turnover numbers and contribute to unwanted side reactions including olefin isomerization (migration of the double bond along the

alkyl chain)⁷² and catalyst dimerization. The mechanism of olefin and catalyst decomposition is not known, but it is possible that metal-based hydride, and π -allyl pathways may be contributors,⁷³ or activation by solvent or by the phosphine may promote decomposition. When Ulman and Grubbs looked at decomposition of one of the 1st generation Grubbs' catalysts (with a propylidene) by ³¹P NMR, they found mostly free PCy₃, but a number of other unknown phosphorus signals grew in over time. ¹H NMR showed that the major decomposition products were *trans*-3-hexene, (from dimerization of the propylidene fragment), a mixture of unidentified ruthenium species and free PCy₃. When more free PCy₃ was added, decomposition was slowed, indicating that dissociation is required for decomposition to happen. Unfortunately, the activity of the catalyst is dependent upon dissociation of the phosphine ligand, so decomposition and reactivity of the catalyst were both slowed.^{71d} When Grubbs' 2nd generation catalyst was investigated it was noted that co-ordinating solvents could compete with the olefin for the open co-ordination site.⁷⁴ The presence of the mesityl group on the NHC ancillary ligand provided another decomposition pathway that was characterized by Grubbs and Hong.^{71b} Methylphosphonium salts and C-H insertion products were found and characterized. Methylphosphonium salts formed as a result of dissociation of the phosphine, followed by nucleophilic attack of the phosphine on the methylidene carbon. Ruthenium (and rhodium) has been known to insert into the C-H bond of the methyl on the mesityl group.⁷⁵ Some proposed decomposition species for Grubbs' 2nd generation are in Figure 3. 3.

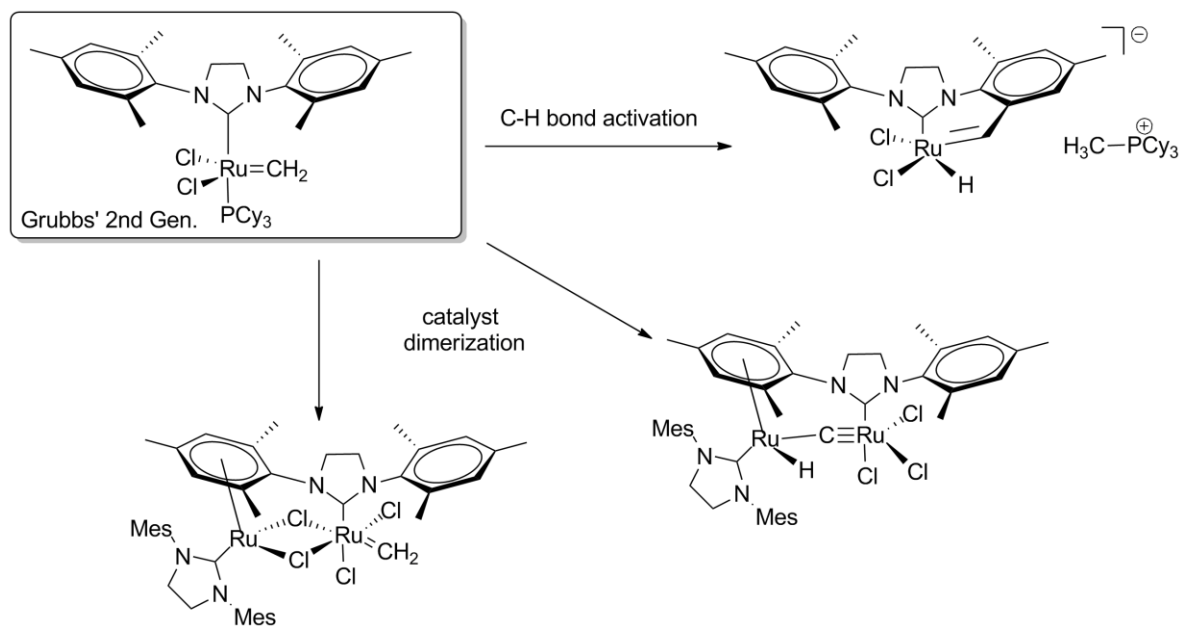


Figure 3. 3. Grubbs' 2nd generation catalysts characterized by X-ray crystallography, and ¹H and ³¹P NMR.

3.5 Piers' Catalyst for ROMP

Piers' catalyst is a fast initiating derivative of Grubbs' 2nd generation catalyst, first reported in 2004. The reason for this fast initiation is likely due to the innate, reactive 14-electron catalyst which does not require dissociation of a phosphine to become reactive, unlike the Grubbs' catalysts. Piers made a modification to Grubbs' 2nd generation catalyst in which the phosphine was now bound directly to the carbene, creating a phosphonium moiety.⁷⁶ This analogue was designed to prevent competition between the incoming olefin and the dissociating phosphine for the open site on the metal center. It was found to be as reactive as the Schrock alkylidenes and still held the tolerance for other functional groups that Grubbs' catalysts employed, while displaying stability in the presence of air and water. Initiation times were found to be faster than for the Schrock alkylidenes, and with rapid initiation came polymer products with narrower M_w

distributions.⁷⁷ It was proposed that all the ruthenium could act as a catalyst, barring decomposition or attack by the nucleophilic phosphine to the metal center, thus relegating an inactive 16-electron complex. An additional perk with the reactivity of Piers' catalyst was that it could accomplish low temperature metathesis.⁷⁸ It was through this discovery about low temperature catalysis that the ruthenacycle was isolated and characterized in 2005 (Figure 3. 4). Until this time the metallacycle was thought to be a transition state but was instead shown to be an intermediate.

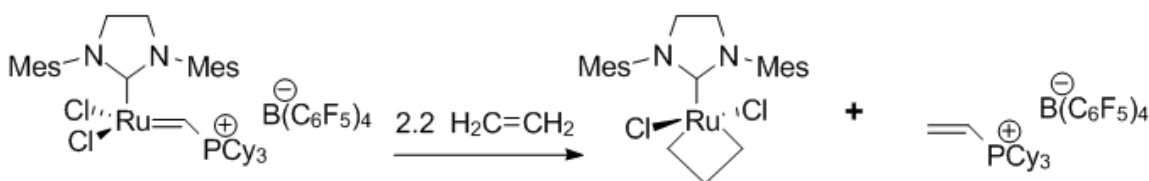
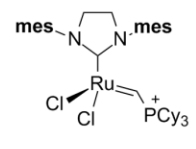
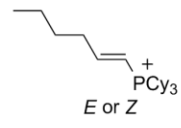
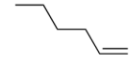
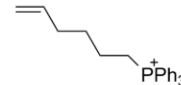
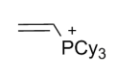
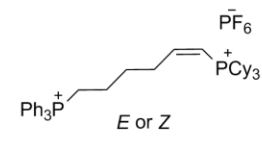

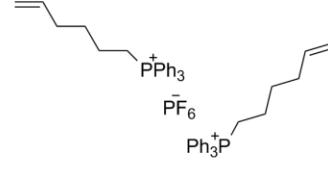
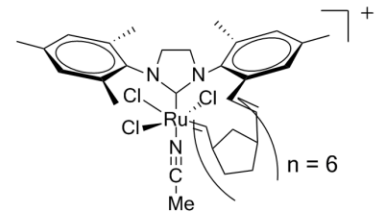
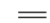
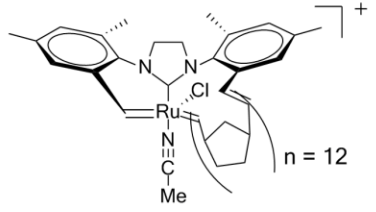
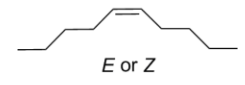


Figure 3. 4. Reaction of Piers' catalyst with ethylene at -50°C generating the vinylphosphonium salt and parent ruthenacycle in high yield.

As Piers' catalyst is a fast initiating ROMP catalyst, this reaction occurred quickly at low temperature, generating the ruthenacycle quantitatively without showing the appearance of decomposition by-products.

3.6 Results and Discussion for ROMP

Table 2. List of numbered species for ROMP and CM.

Species #	Species	<i>m/z</i>	Species #	Species	<i>m/z</i>
1		<i>m/z</i> 771	8		<i>m/z</i> 363
2	H-PCy_3^+	<i>m/z</i> 281	9		
3	Me-PCy_3^+	<i>m/z</i> 295	10		<i>m/z</i> 345
4		<i>m/z</i> 307	11		<i>m/z</i> 769
5			12		<i>m/z</i> 835
6		<i>m/z</i> 1116	13		
7		<i>m/z</i> 1607	14		

3.6.1 ESI-MS

Piers' catalyst was chosen for this project since in the literature it has proven to be fast initiating and contains a phosphonium group which is easily distinguishable by MS.

Additionally, ruthenium catalysts have been demonstrated to have good ionization efficiencies. Norbornene was used for this project since it is a strained, cyclic olefin that has been well studied in ROMP and known to react efficiently. In monitoring the ROMP reaction of norbornene and Piers' catalyst, it was learned that the variation in norbornene concentration had to be small out of necessity. Since a sticky polymer was produced in this reaction which was being fed through a piece of PEEK tubing with an inner diameter of 0.0125 cm, and subsequently fed through a metal capillary with an even smaller inner diameter, clogging occurred with great regularity. Over time it was learned that using fused silica tubing instead of PEEK for sample infusion gave better results with less clogging.

When the reaction was observed by PSI-ESI-MS, using 0.04 M norbornene monomer and a 1% catalyst loading in acetonitrile solvent at reflux, there was a high concentration of unreacted catalyst (**1**, m/z 771) observed for the first 20 minutes, which then began to decompose. Three species, **2**, **3**, **4** (m/z 281, 295, and 307) which appeared immediately, remain fairly constant throughout, Figure 3.6. It is assumed these species denote decomposition of the catalyst. The corresponding ruthenium partner is not detected by ESI indicating that it carries no charge, overall. The species in Figure 3.5 have been proposed in the thermal decomposition of Piers' catalyst in the 2008 paper by Leitao et al⁷⁹.

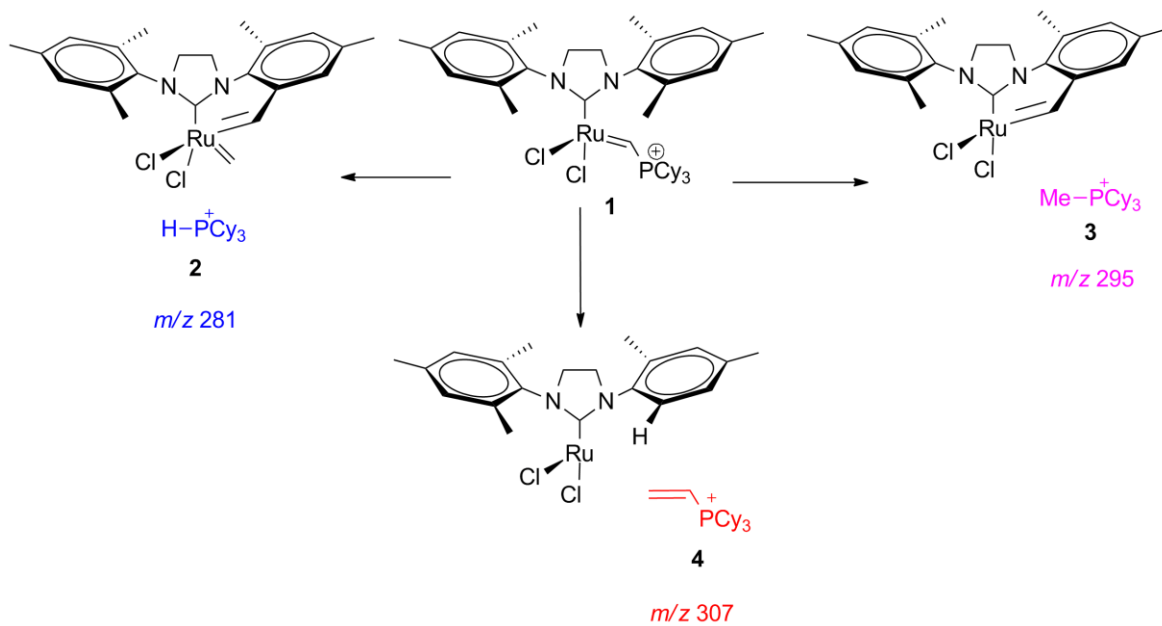


Figure 3.5. Depiction of possible ruthenium decomposition partners

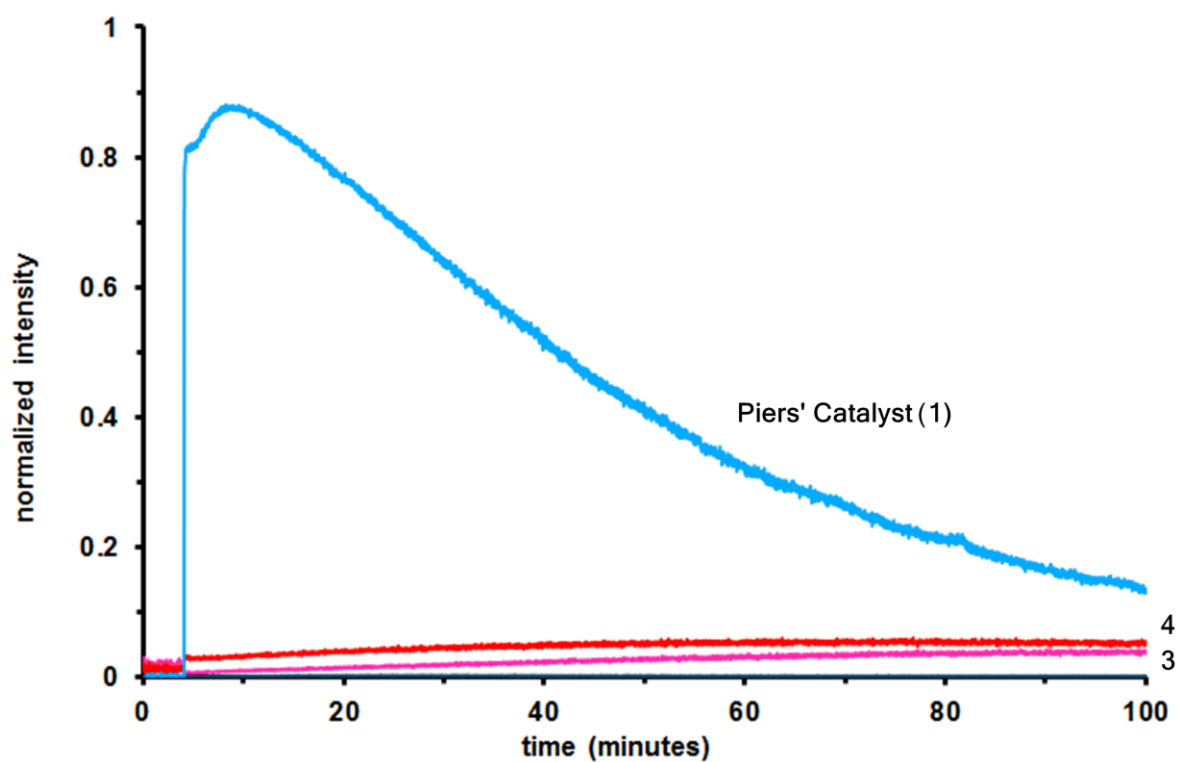


Figure 3.6. Normalized plot showing the decomposition of Piers' catalyst with heat in acetonitrile solvent, and m/z 307, 295 remain at a constant low intensity over 100 minutes.

Additionally, small concentrations of charged oligomer were seen to form and were observed because they carried the cyclohexylphosphonium moiety, Figure 3.7.

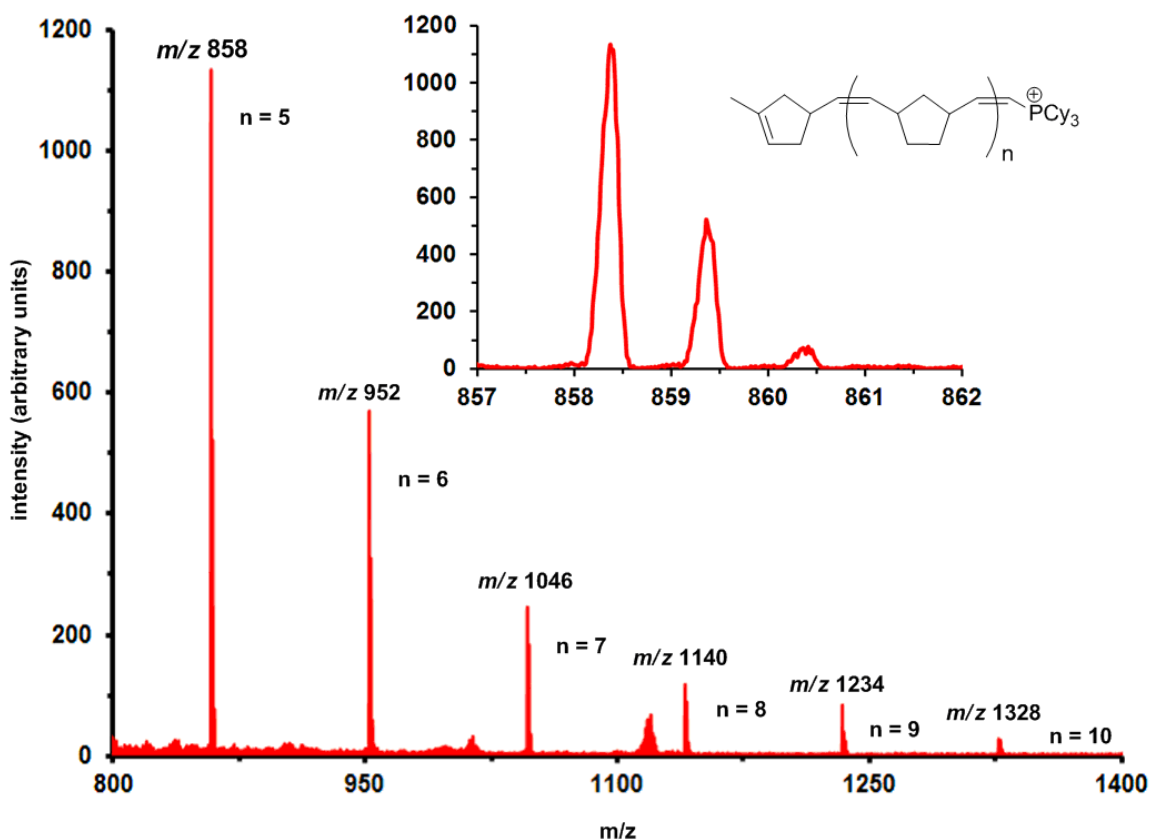


Figure 3.7. 1800 combined spectra of oligomers for $n = 5$ to $n = 10$. The greatest relative intensity is ~ 1200 a.u. This is in comparison with the relative intensity of the catalyst at ~ 80000 a.u. Inset: Isotope pattern for m/z 858, $n = 5$.

One of the oligomers, the first norbornene monomer-phosphonium, forms immediately which reinforces the fast initiation of the catalyst (Figure 3.8).

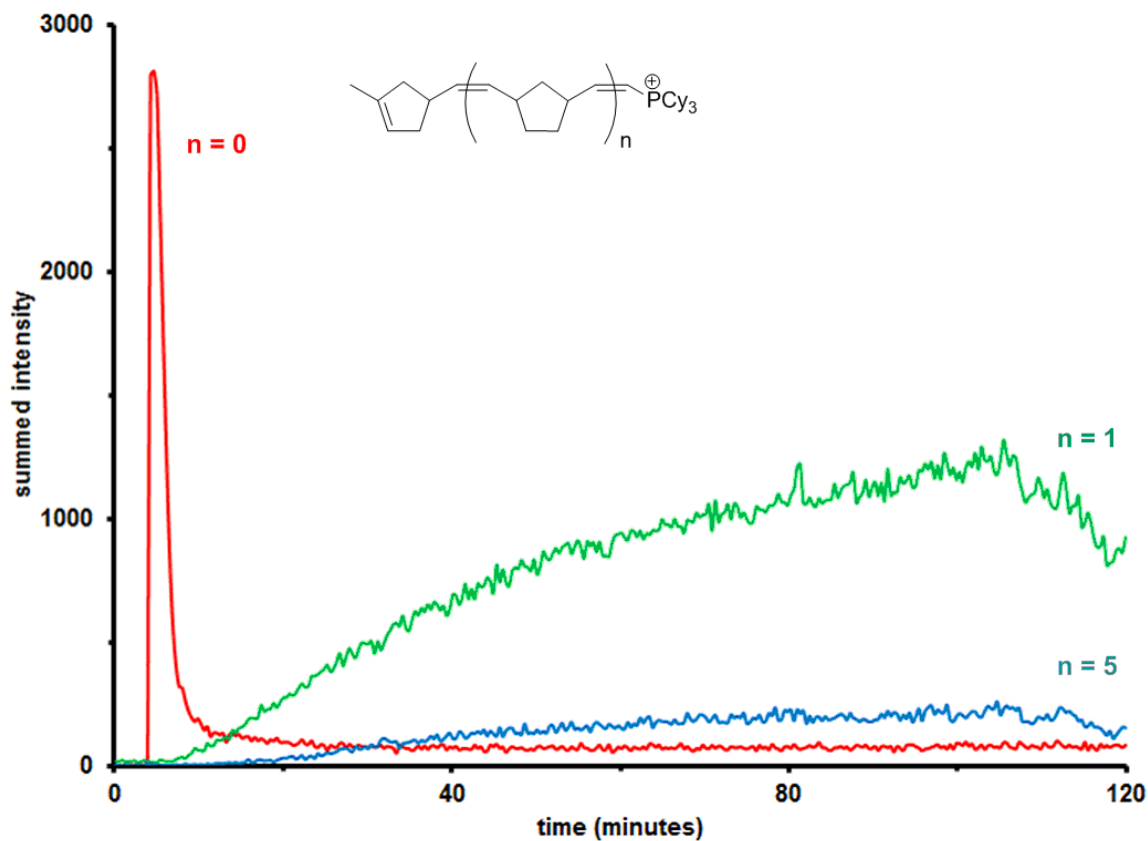


Figure 3.8. 1% catalyst loading with Piers' catalyst and norbornene in MeCN solvent at reflux temperature. Abundance traces for $n = 0$ (red), $n = 1$ (green), and $n = 5$ (blue). The traces were generated and smoothed by summing 20 data points.

Since the intensity of the phosphonium species increase gradually, there are also some ruthenium intermediates present at low relative concentration which start to form as the concentration of catalyst starts to decrease (Figure 3.9).

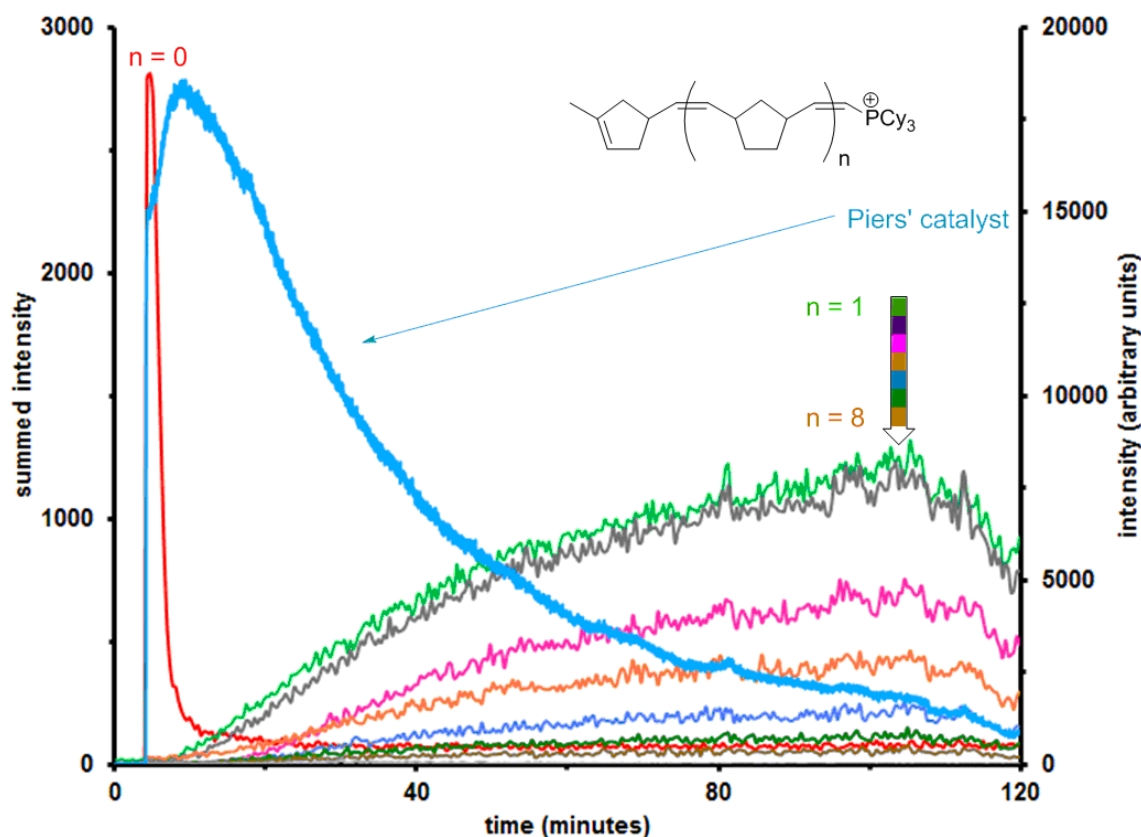


Figure 3.9. 1% catalyst loading with Piers' catalyst and norbornene in MeCN solvent at reflux temperature. Piers' catalyst (aquamarine trace) has a relative maximum intensity of 20,000; formation of oligomers (red, $n = 0$, to brown, $n = 8$) shown with relative maximum intensities of 2900 for $n = 0$, to 10 for $n = 8$. The oligomer traces were generated and smoothed by summing 20 data points, while the catalyst trace was untouched.

Next, we wanted to compare the differences in the rate of disappearance of catalyst by changing the solvent and the temperature. A non-coordinating solvent, dichloromethane, was used at room temperature and was compared to the co-ordinating solvent, MeCN at room temperature and at reflux, the rate of disappearance of the catalyst under these three conditions could be probed (Figure 3.10). All species in the reaction solution are uncharged and only upon addition of the catalyst by syringe can any ion intensity be discerned. In CH_2Cl_2 at RT over 30 minutes, the relative concentration of the catalyst barely decreases. The three decomposition

species, **2**, **3**, **4** appear immediately upon addition of the catalyst but their relative concentrations do not change much over time. Some charged ruthenium species also appear in very low concentrations which also do not grow in much over time. The same can be said for **2**, **3**, and **4** in a coordinating solvent, but cannot be said of the catalyst. At both RT and at reflux in MeCN, the concentration of the catalyst decreases noticeably over 30 minutes with approximately zero order kinetics. In coordinating solvent, charged oligomers are produced, but are not detected in non-coordinating solvent. Since the concentration of charged oligomers could not entirely account for the decrease in catalyst concentration, the production of decomposition species, (charged and uncharged) were the likely culprits.

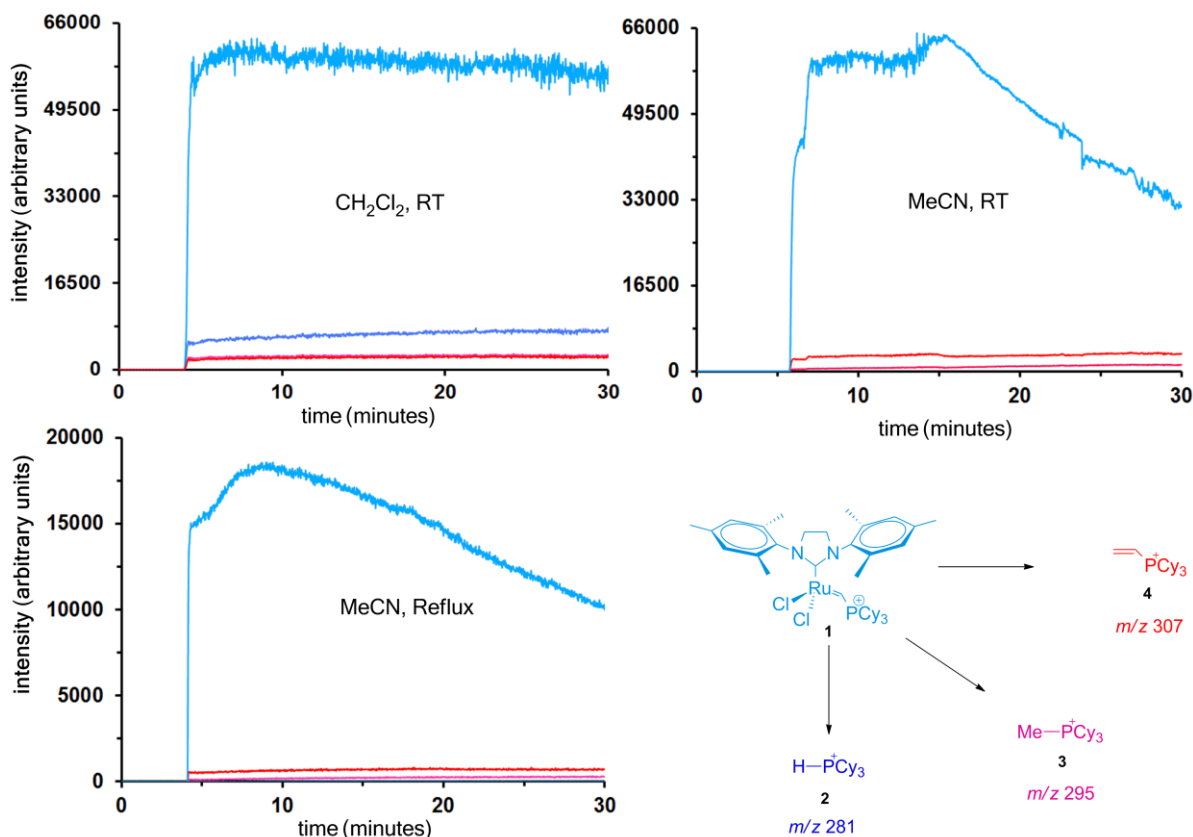


Figure 3.10. Catalyst loading is 1% for the three reactions above. Catalyst is added to 0.02g norbornene at ~ 5 minutes for all 3 reactions, at the point when the ion intensity increases dramatically. Catalyst trace is light blue, *m/z* 281 (medium blue), *m/z* 295 (pink) and *m/z* 307 (red).

The presence of several thermally decomposed ruthenium species were detected with various masses, depending on starting concentrations, catalyst loadings and solvent conditions. No attempts were made to isolate or characterize any of these ruthenium species using other methods; however their m/z ratio and isotope patterns could be used to discern what species they could plausibly be. Two examples, **6** and **7** (m/z 1116 and 1607), were consistent with C-H activation of the mesityl group on the NHC ligand. This was consistent with studies conducted on the decomposition of ruthenium catalysts with the same mesityl groups on the NHC ligands. Both species were singly charged and the isotope patterns of both indicate that they each contain one ruthenium and one (**6**) or three (**7**) chlorides. The isotope modelling feature on the Mass Lynx software and ChemCalc⁸⁰ were used to determine this (Figure 3.11). MS/MS was attempted on **6** and **7**, but their intensity was too low before the collision energy was increased, and no species were detected above the baseline, so this technique did not yield any useable results. Since no species were isolated or characterized beyond this method, it can only be stated that these species are plausible, based on previous studies conducted in the literature, and that the limits of isotope matching and the use of CID did not yield further results.

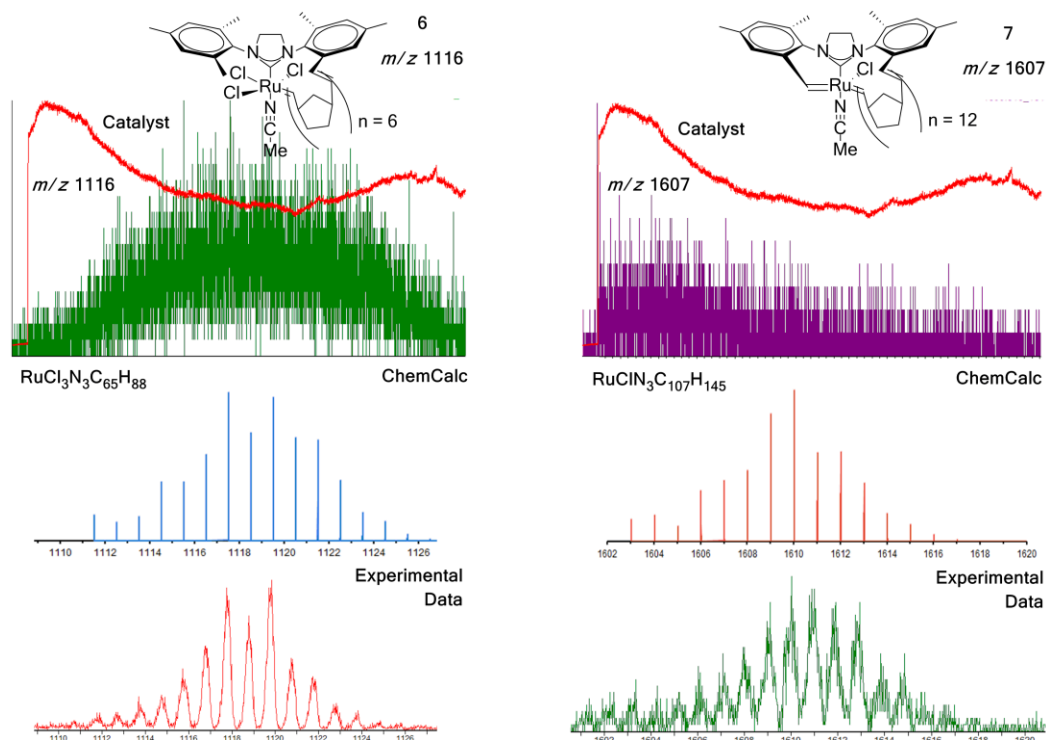
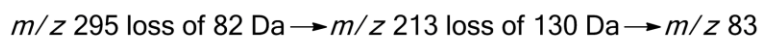
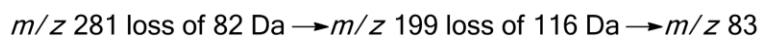


Figure 3.11. Top: 0.02g Norbornene with 1% Piers' catalyst in MeCN at 85°C Abundance traces for the catalyst over 120 minutes (red traces) and Ru intermediates (green and violet traces, generated by combining ~3600 spectra); Middle: ChemCalc isotope models for the proposed intermediates; Bottom: Experimental data for thermally decomposed Ru intermediates.

When Piers' catalyst (0.8% loading) was reacted with norbornene (0.01 M) in dichloromethane at room temperature, the intensity of the catalyst stayed fairly constant over time, as did the phosphonium decomposition species, but at a much lower intensity. However this was necessary to facilitate the transfer of solution to the mass spec without clogging and degrading the signal. While no desired distribution of oligomers was detected, a few decomposition species were. Analysis of these species by MS/MS showed that when increasing the collision voltage to 35 volts, **2**, **3** and **4** show losses of cyclohexane:



When norbornene is added slowly, the catalyst signal decreases slowly and **3** increases immediately, indicating that more thermal decomposition is occurring while more polymer is being formed. The formation of more polymer is indicative of a “living” system.

Two possible mechanisms for decomposition could occur: exchange with the solvent methylenes or insertion of ruthenium into the C-H bond of the NHC ligand. In order to test whether any methylenes were exchanging with the solvent, the reaction was done in deuterated dichloromethane, with an expected increase in m/z of 2, however no such species were detected (Figure 3.12) in either the catalyst or in the 3 decomposition species, **2** (H-PCy_3)⁺, **3** (Me-PCy_3)⁺, **4** ($\text{H}_2\text{C-CH-PCy}_3$)⁺. This confirmed the C-H activation and insertion mechanism of decomposition.

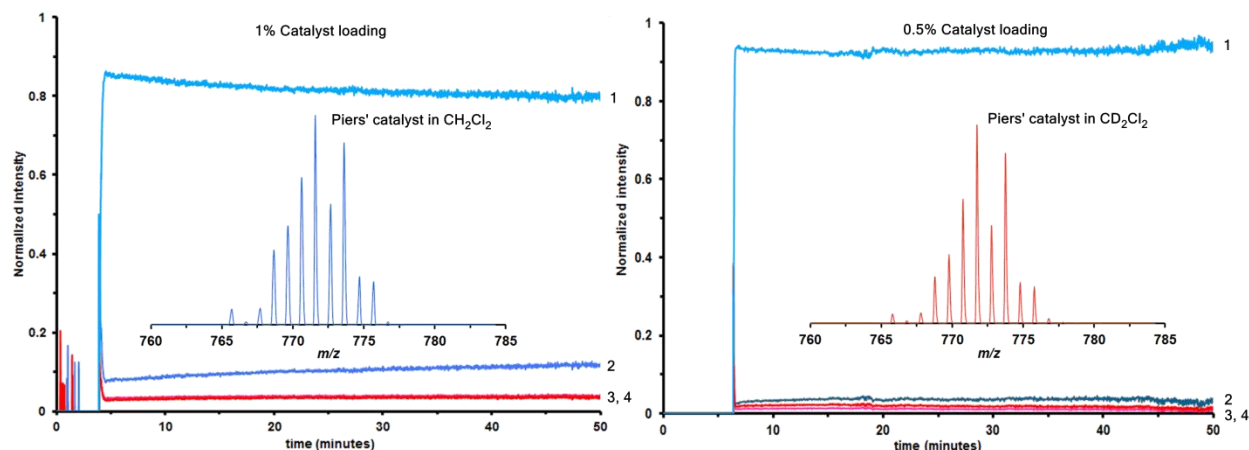


Figure 3.12. Normalized plots showing the constant intensity of Piers' catalyst (1% loading at left, 0.5% loading at right) at RT. Insets: Isotope pattern for Piers' catalyst in CH_2Cl_2 solvent, left and in CD_2Cl_2 solvent, right. Traces for decomposition species m/z 307 (red), 295 (pink), and 281 (medium blue) shown at low constant intensity in both plots.

3.6.2 ^1H NMR

When the ROMP reaction was monitored by ^1H NMR over time, a fair amount of unreacted catalyst was still detected after the reaction was completed. Figure 3.13 shows that some unreacted catalyst is still present after the reaction has finished. No norbornene monomer is

present, only the polymeric form, as seen by the change in chemical shift and by the broadening of peaks denoting the formation of polymer. Since Piers' catalyst is such a fast initiator, a visual inspection of an NMR tube containing too much norbornene monomer showed the instantaneous formation of solid polymer in the NMR tube once the catalyst was added, so another reaction with a lower concentration of monomer was undertaken so as to detect the reaction in the liquid phase. A scan of the catalyst was obtained before addition of the dissolved monomer, and then 5 minutes after, and every 10 -30 minutes thereafter for 2.5 hours. An observation of change in NMR chemical shift after the monomer was added over time was unlikely, due to the instantaneous activation of the catalyst, and this was found to be true.

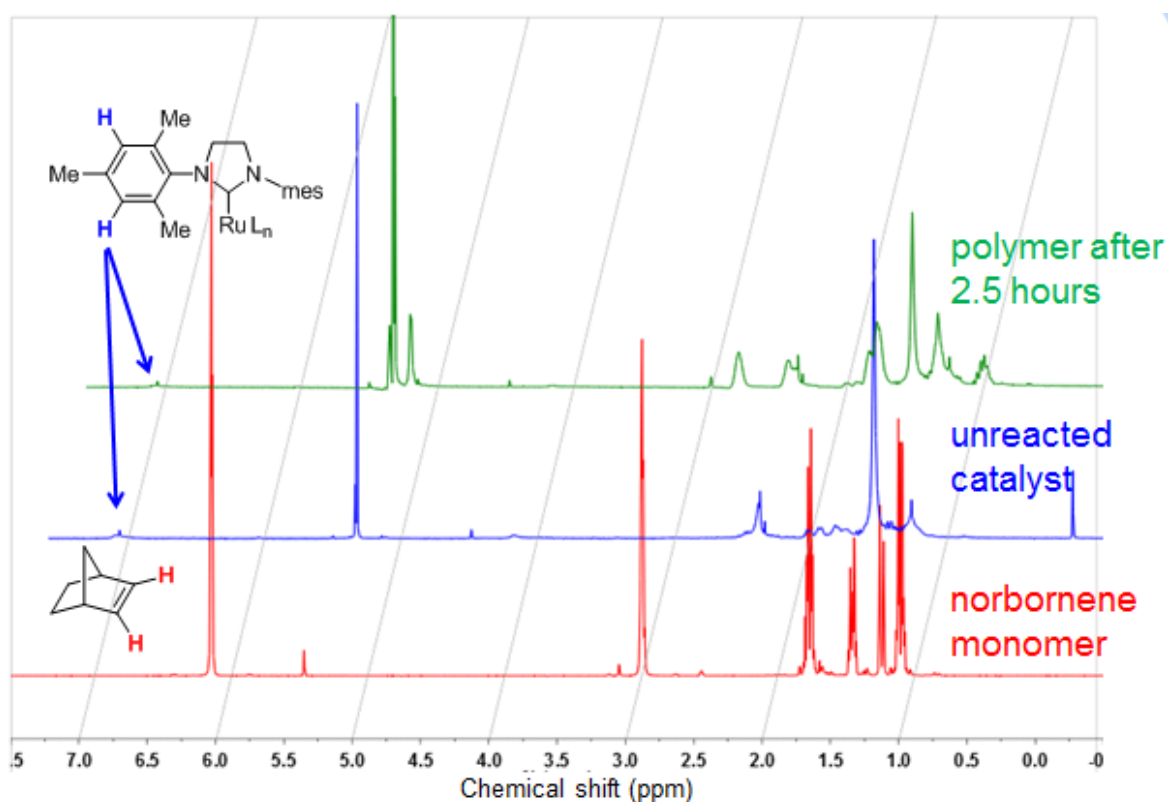


Figure 3.13. Stacked ^1H NMR plot for ROMP with norbornene and Piers' catalyst, unpurified. The bottom red trace shows unreacted norbornene monomer in CDCl_3 solvent, the middle green trace is unreacted Piers' catalyst in CDCl_3 , and the top blue trace is 2.5 hours after norbornene was added to Piers' catalyst in an NMR tube.

3.6.3 Polydispersity Index by Gel Permeation Chromatography

While the mass spectrometer revealed that the catalyst concentration was barely changing using a non-coordinating solvent at room temperature, a solid polymer could be visually confirmed. The Piers' group had previously determined that their catalyst was fast-initiating. They studied a precursor of the catalyst in the photo induced ROMP of COD under UV light and found that the M_n and M_w values were much higher than they expected (160 kDa and 447 kDa respectively). It was therefore possible that incomplete catalyst activation was occurring with this catalyst. Normally, it is expected that all of the catalyst reacts until either all of the monomer has been consumed or the catalyst decomposes and catalysis shuts down. Since ESI-MS results showed that much of the unreacted catalyst was still present after the monomer was consumed, and polymer formation could be visually confirmed, it then became necessary to determine what the polymer distribution might be. Gel permeation chromatography (GPC) using low-angle light scattering (LALS) allowed for the determination of the MW polymer distribution. M_n was 60,464 Da and M_w was 79,584 Da, with a PDI of 1.3, which is similar to most common synthetic polymers with a medium width distribution between 1.2 and 3. Since a 1% catalyst loading was used, and since M_n was 60 kDa, and each monomer unit had a mass of 94 g/ mol, that indicated that there was an average of ~600 monomer units in the polymer. If 1% of the catalyst was used for each 60 kDa of polymer, then only 1/6 of the total concentration of catalyst was being activated (Figure 3.14).

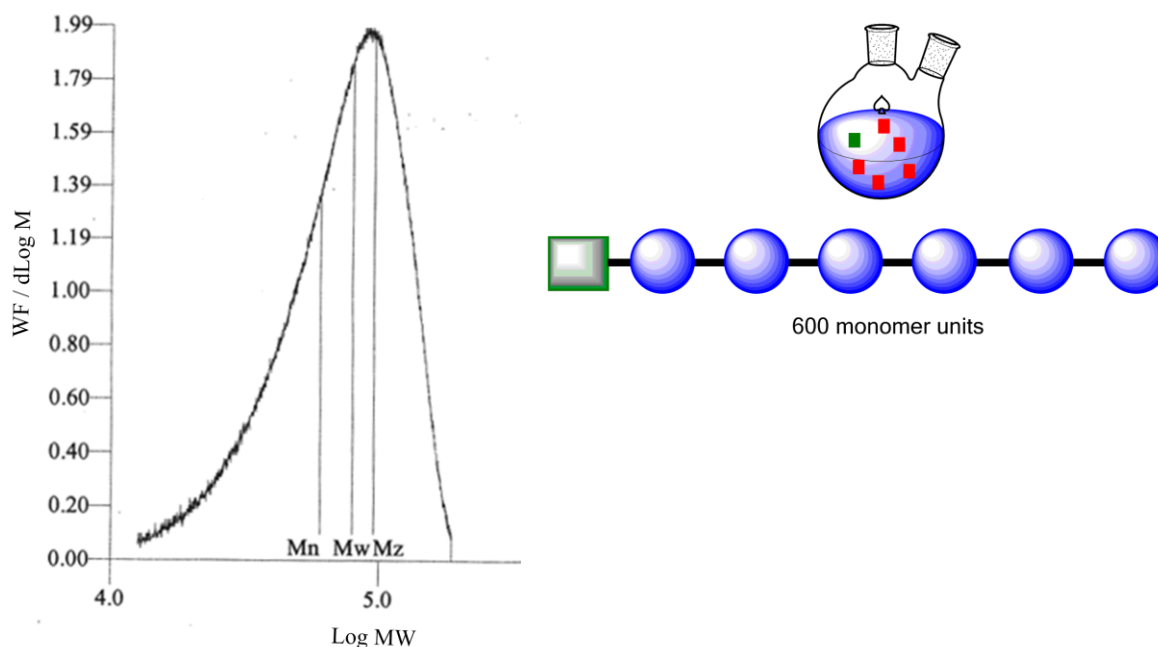


Figure 3.14. Left: LALS GPC plot for the ROMP of Piers' catalyst and norbornene, generating polynorbornene. M_n was found to be 60,464 Da; M_w was 79,584 Da; PDI was calculated to be 1.3. Right: Depiction of incomplete activation of catalyst and chain propagation as determined by GPC. Active catalyst (green) generates the polymer chain and comprises 1/6 of the total catalyst in the reacting solution.

3.7 Conclusions

In our investigation of ROMP with Piers' catalyst, we determined that while the catalyst was visually determined to be fast-initiating, propagation was much faster than was catalyst activation. This was determined by GPC which determined that the M_n and M_w were ~ 60 kDa and 80 kDa respectively indicating a high level of propagation at 1% catalyst loading. While NMR was unhelpful in this investigation, results from PSI-ESI-MS demonstrated that high concentrations of unreacted catalyst were present over 90 minutes, and did not decrease much even though polymer formation was visually observed. The detected decomposed species remained diminutive over 90 minutes at RT and in the presence of a non-coordinating solvent. When heat or coordinating solvent was present, the rate of catalyst decomposition was seen to

hasten greatly and charged polynorbornene phosphonium oligomers were detected. Piers' catalyst meets the requirement for a "living" metathesis catalyst since more polymer formed as more monomer was added.

3.8 Cross Metathesis

3.8.1 Introduction

Olefin cross metathesis (CM) involves the formation of new C=C bonds in the same manner as ROMP, in which the olefins are the reactive functional groups and they are coupled via a transition metal catalyst. A strained cyclic olefin is not required, as with ROMP; CM is an intermolecular reaction and merely requires an acyclic olefin. The alkylidene reacts with the incoming olefin; a metallacycle intermediate is quickly generated, followed by C-C bond breakage and formation, forming a new alkylidene with ethylene as the usual by-product. This ethylene elimination is the thermodynamic driving force that pushes the equilibrium in the forward direction. CM is tolerant of a wide range of functional groups, and rarely are protecting groups required; the starting materials can be inexpensive and simple to prepare. The products can be highly chemo-, regio- and stereoselective, provided the right conditions are met. Nevertheless, selectivity remains the largest challenge in CM applications.⁸¹

If two different olefin substrates are used with 1:1 starting stoichiometry and each reacts with the catalyst at similar rates, then each will react with the catalyst 50% of the time. This leads to an inefficient statistical distribution of products. In order to increase selectivity, it becomes necessary to utilize two different types of olefins: type I, which will undergo rapid homodimerization, is sterically unhindered, and is an electron-rich olefin (terminal olefins, 1°

allylic alcohols, allyl phosphonates, etc.); and type II which undergoes slow or no homodimerization, is more hindered, and is a less electron-rich olefin (styrenes, 2° allylic alcohols, 1,1-disubstituted olefins, etc.) Attempting to minimize undesirable side products is key in CM (Figure 3.15).⁸²

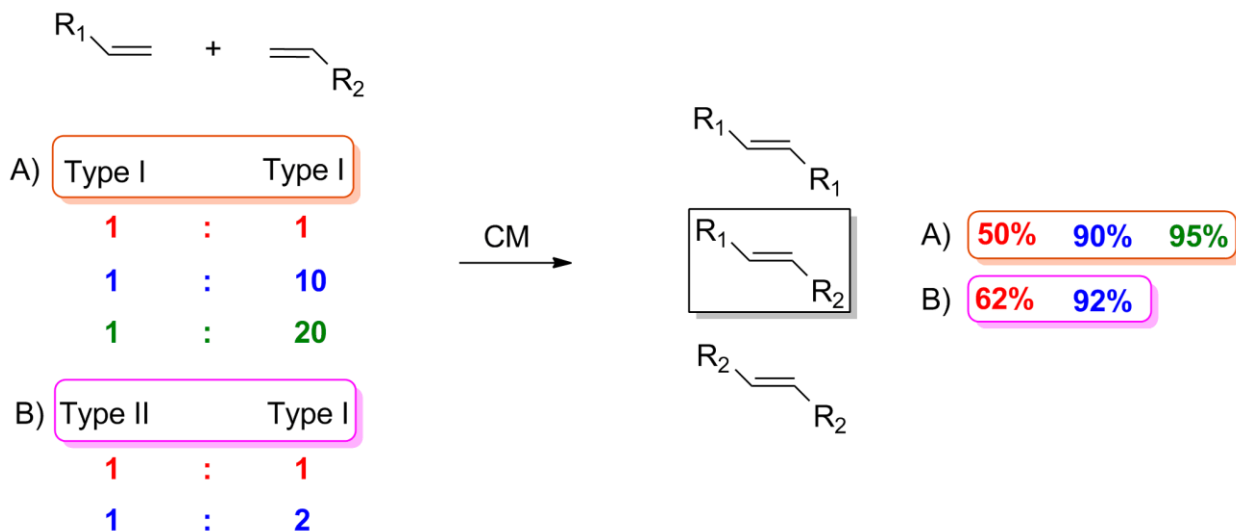


Figure 3.15. Optimization of statistical isomers by design, through careful choice of starting olefin partners.

3.8.2 Results and Discussion for CM

We next desired to study how Piers' catalyst functioned with cross metathesis (CM), and we chose a simple, Type I, acyclic olefin, 1-hexene (**9**), and used a 0.05% catalyst loading for this investigation. A different behavior was observed with CM compared with the ROMP results. When the hexene was added at 12 minutes, there was an immediate formation of the by-product, **4**, which continued to grow in pseudo-first order fashion. Likewise, the catalyst **1** disappeared with pseudo-first order kinetics. The charged cross-metathesis product, **8** (m/z 363) grew in

more slowly at a constant pace, while **2** (H-PCy_3)⁺ and **3** (Me-PCy_3)⁺ appeared when the catalyst was added and remained at low concentration over the 13 minute reaction (Figure 3.16).

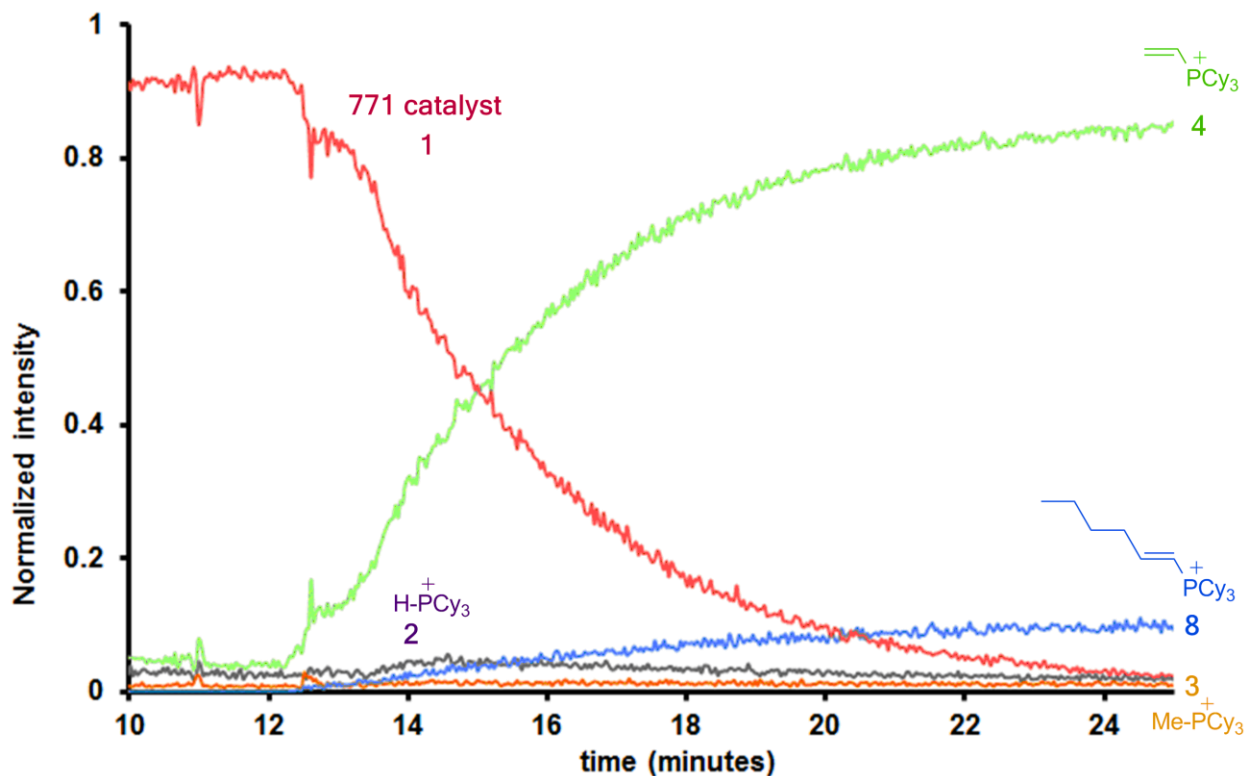


Figure 3.16. Appearance of charged product and by-product with disappearance of catalyst. 0.05% catalyst loading and 0.04M 1-hexene were used.

Species **4** and **8** were detected because of the charge due to the phosphonium, and while it is possible that some uncharged cross-metathesis product formed, it could not be detected by this method.

Following this experiment, the catalyst loading was increased 10-fold, and the production of **4** decreased by a third, as did the generation of **8**. No **2** was detected this time and the intensity of **3** also remained low (Figure 3.17). This indicates that the generation of the two phosphoniums

appears to be dependent on catalyst loading as the concentration of starting olefin was held constant.

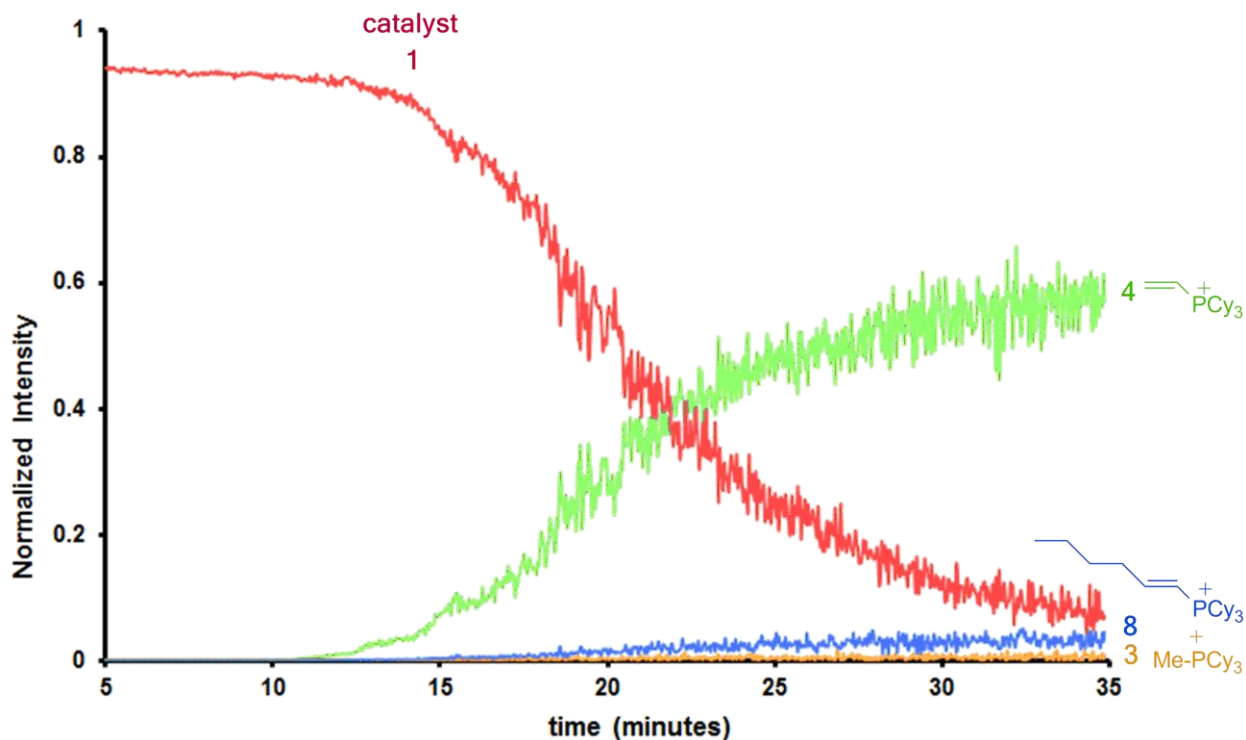


Figure 3.17. Piers' catalyst at 0.5% loading with 0.04 M 1-hexene in CH_2Cl_2 observed by ESI-MS.

Next, we desired to see the effect of using a charge-tagged phosphonium olefin, 1-hexene-6-triphenylphosphonium hexafluorophosphate (**10**), which is similar to 1-hexene in its steric properties, and with the tag far away from the reactive sight of the olefin. Some odd results were observed. We would have expected to see the generation of a 10-C olefin or even a product analogous to **8** with the untagged substrate. Instead, we saw regeneration of the charge-tagged olefin, as well as the production of a singly-charged 12-C olefin species, **12** (m/z 835). The apparent increase in the trace for **10** is due to the decrease in the Total Ion Count (TIC) (Figure

3.18). Miniscule amounts of **3** and **4** were detected, and no doubly-charged species were detected.

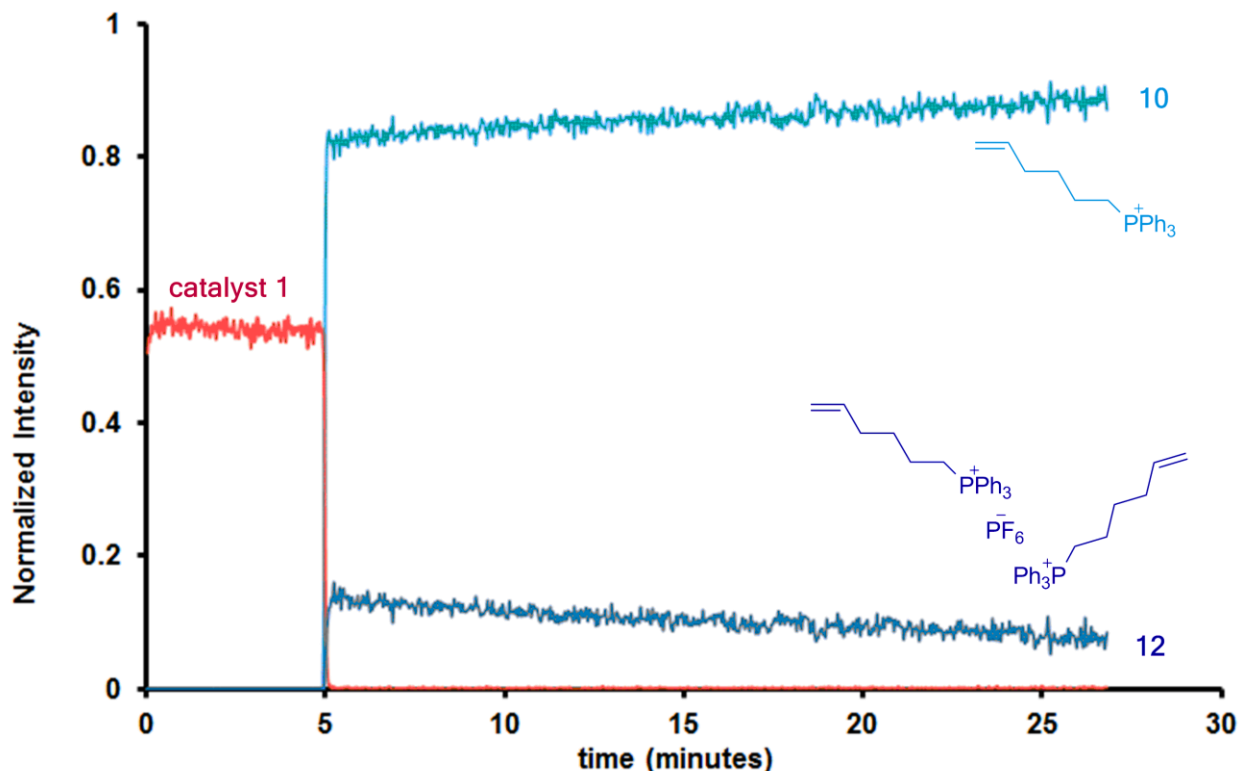
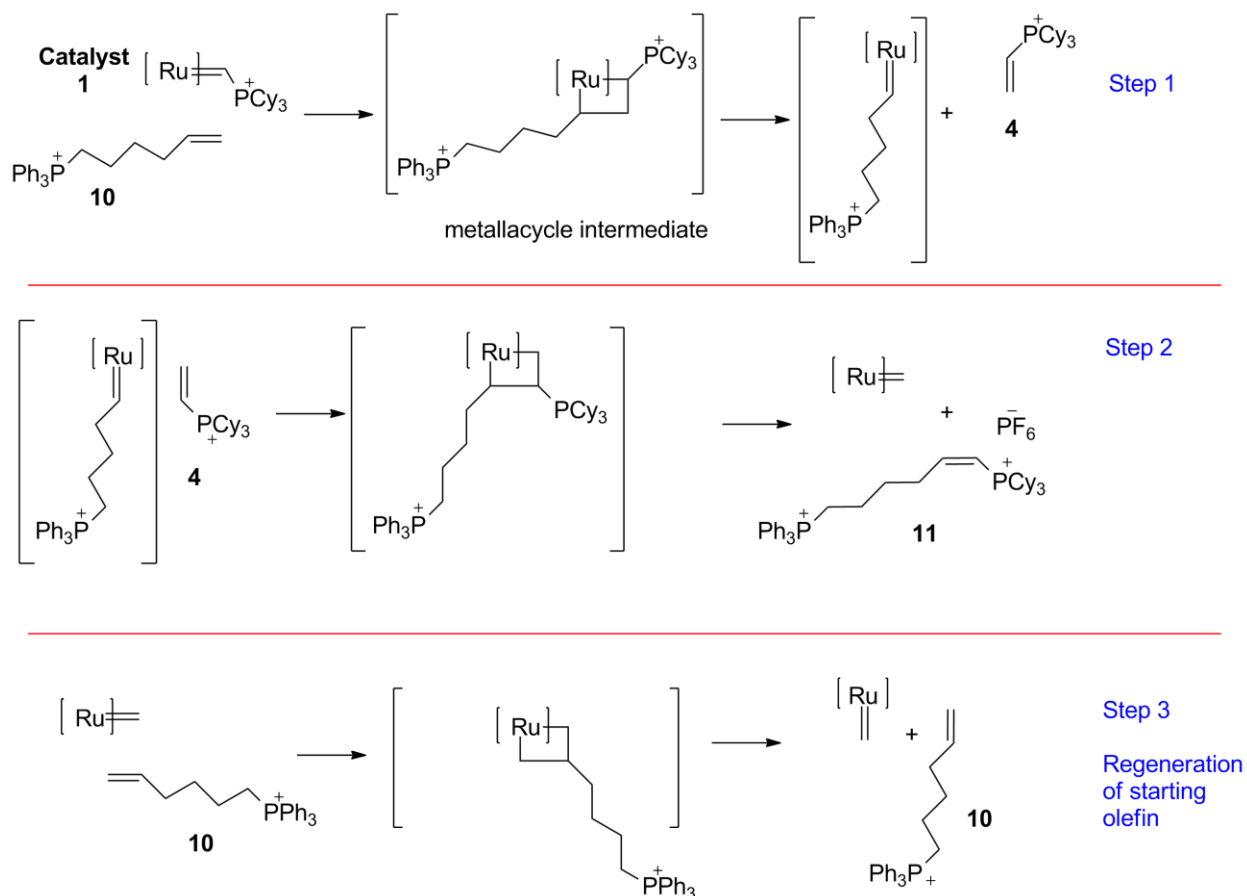


Figure 3.18. Reaction of Piers' catalyst (0.86% loading) with 1-hexene-6-triphenylphosphonium hexafluorophosphate (0.002 M in CH_2Cl_2).

There was only one way to explain the observed results. For the catalyst to disappear and for the observed regeneration of the starting phosphonium olefin to occur, it would have to react with the catalyst **1**, generating **4**, which was detected in miniscule amounts, forming a ruthenium-5-C chain phosphonium which could then react again with **4** in a different conformation to generate an uncharged, reactive Ru alkylidene and **11** (m/z 769, detected in miniscule amounts). The Ru

alkylidene would next react with the starting phosphonium olefin, **10** only to again form more starting phosphonium **10** (Scheme 13).



Scheme 13. Regeneration of the starting phosphonium olefin.

The formation of **12** was much simpler to explain. It was merely an aggregate of two starting olefins weakly associated with PF_6^- , singly charged. This reaction was done a second time with a 100% catalyst loading, thus eliminating excess starting olefin and **12** disappeared (Figure 3.19), confirming that strong ion pairing was the result of the high concentration of tagged-hexene **10**. Once the tagged hexene was added, catalyst intensity dropped by 60%, but was only depleted by

a further 10% over 80 minutes, lending credence to the claim that some uncharged, reactive alkylidene was formed and was then able to undergo CM to regenerate the starting olefin.

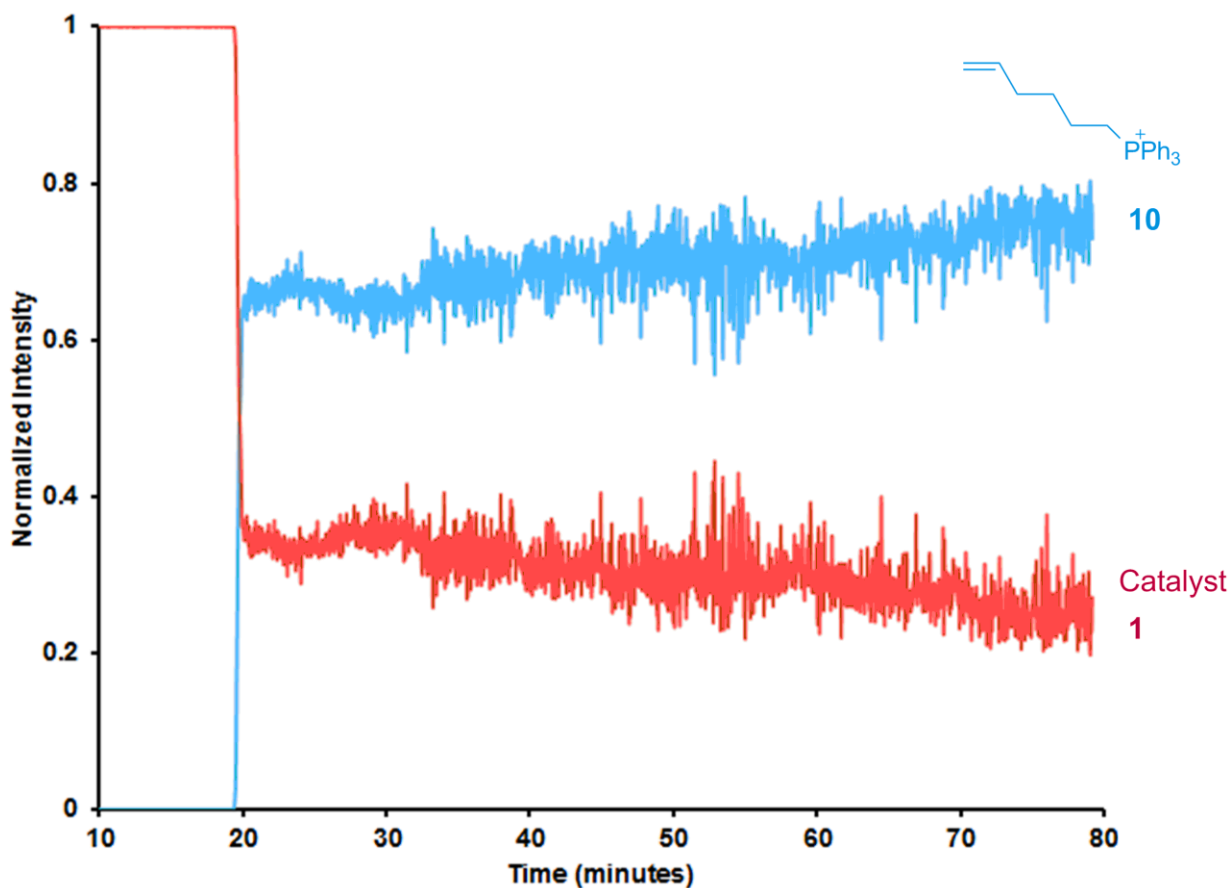


Figure 3.19. 100% catalyst loading with charge-tagged 1-hexene shows depletion of the charged catalyst and regeneration of the tagged hexene over 80 minutes at RT.

3.8.3 ^1H NMR with 1-hexene

^1H NMR was next used to detect the formation of any uncharged products in the reaction with 1-hexene. A spectrum of 1-hexene in CDCl_3 was obtained before the addition of catalyst, 0.1% catalyst loading (Figure 3.20) and the 6 peaks due to 1-hexene were visible at 0.90, 1.34, 2.04,

4.92, 4.98 and 5.81 ppm. Water (1.54 ppm), dichloromethane (5.30 ppm) and residual solvent (7.26 ppm) were also detected. Additional spectra were obtained after the addition of Piers' catalyst starting at 9 minutes, with spectra taken every minute for the first 8 minutes after catalyst addition. The remaining spectra were then taken every 5 or 10 minutes up until 45 minutes after catalyst addition. Figure 3.21, Figure 3.22 and Figure 3.23 show the ^1H NMR spectra 9, 10 and 45 minutes after the addition of catalyst.

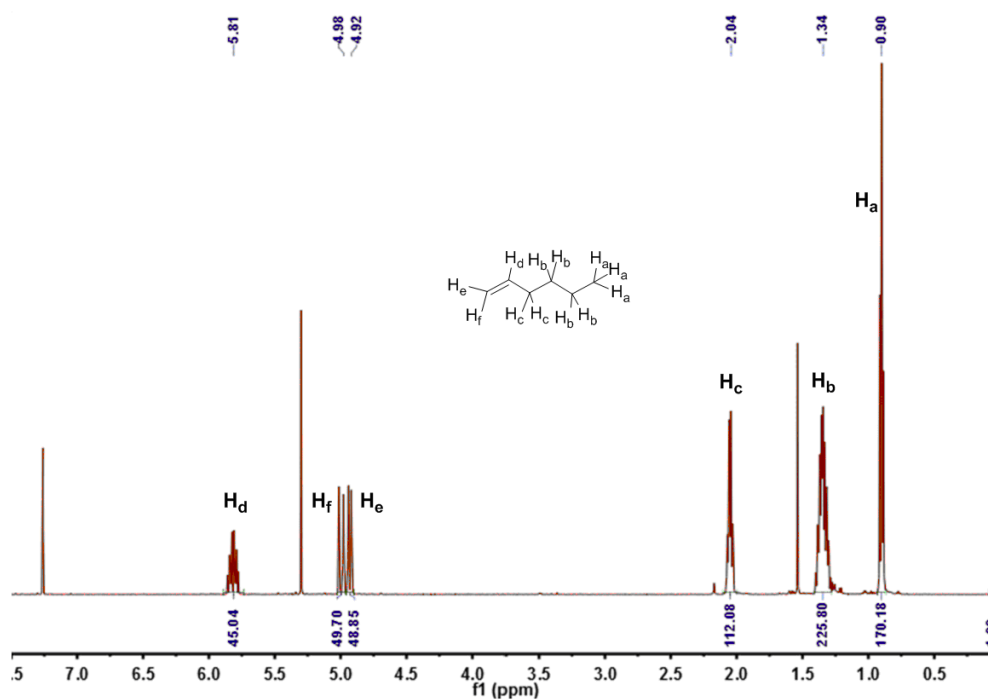


Figure 3.20. 1-hexene in CDCl_3 , before catalyst addition.

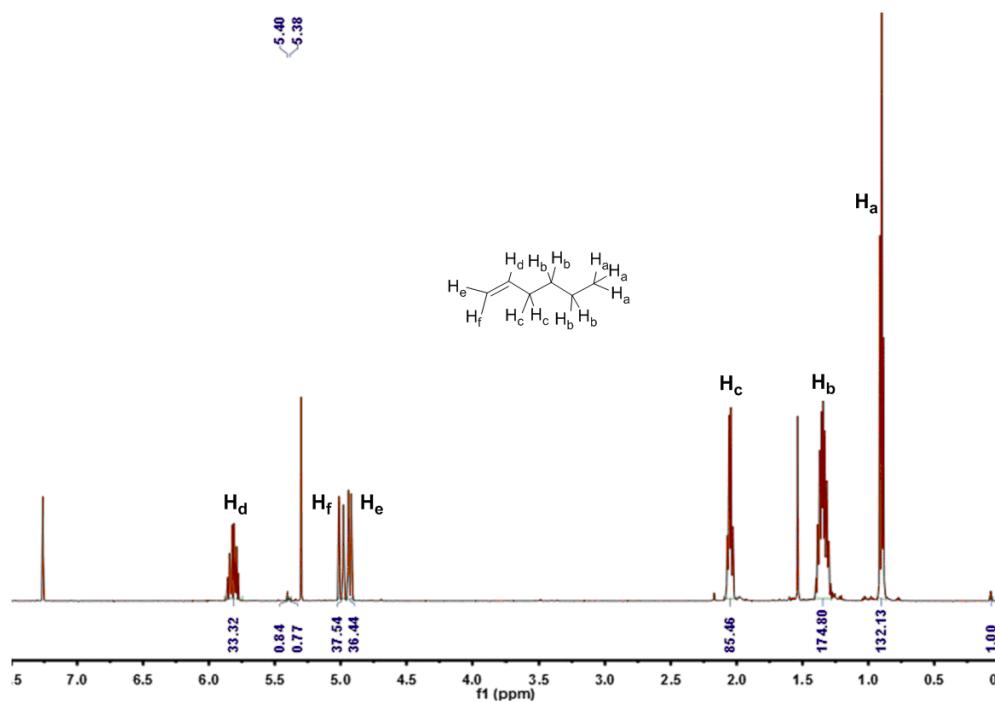


Figure 3.21. 9 minutes after catalyst addition.

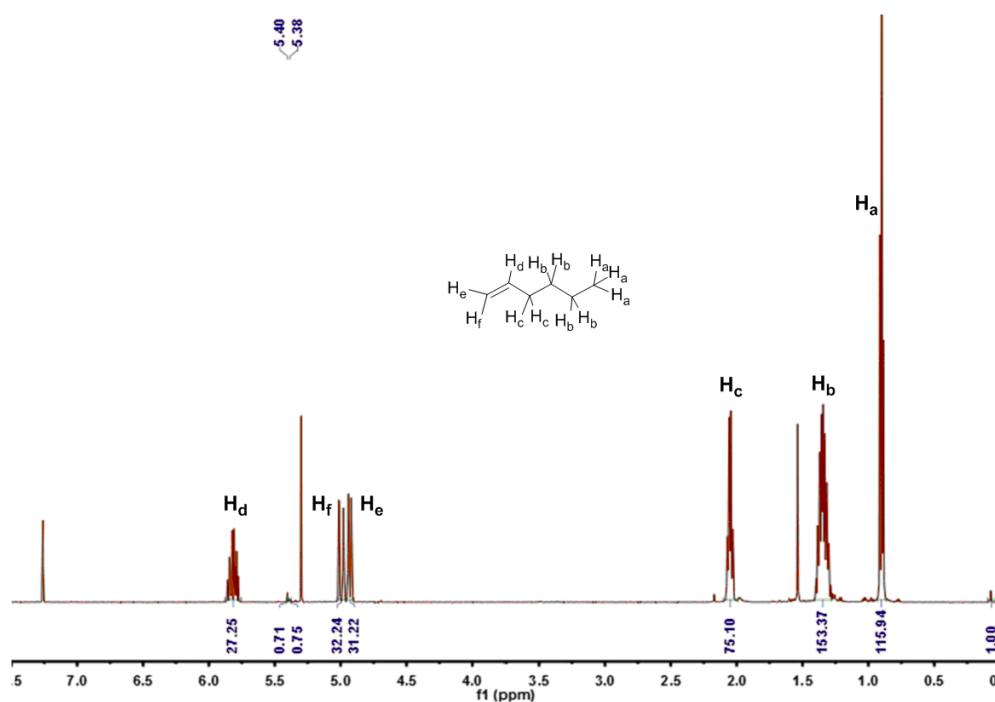


Figure 3.22. 10 minutes after catalyst addition.

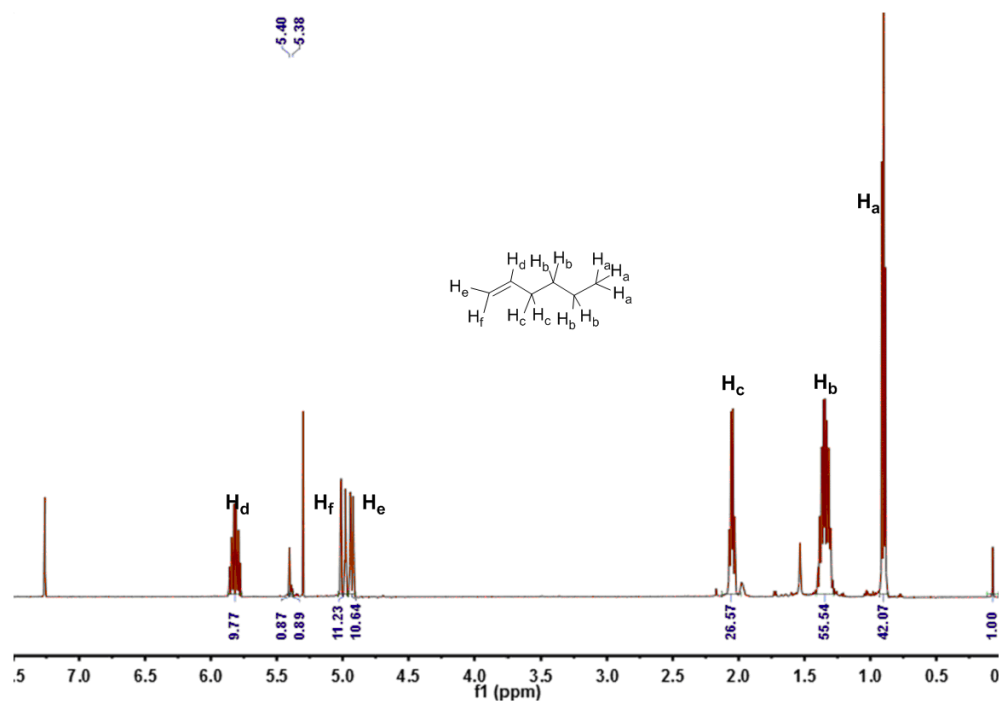


Figure 3.23. 45 minutes after catalyst addition.

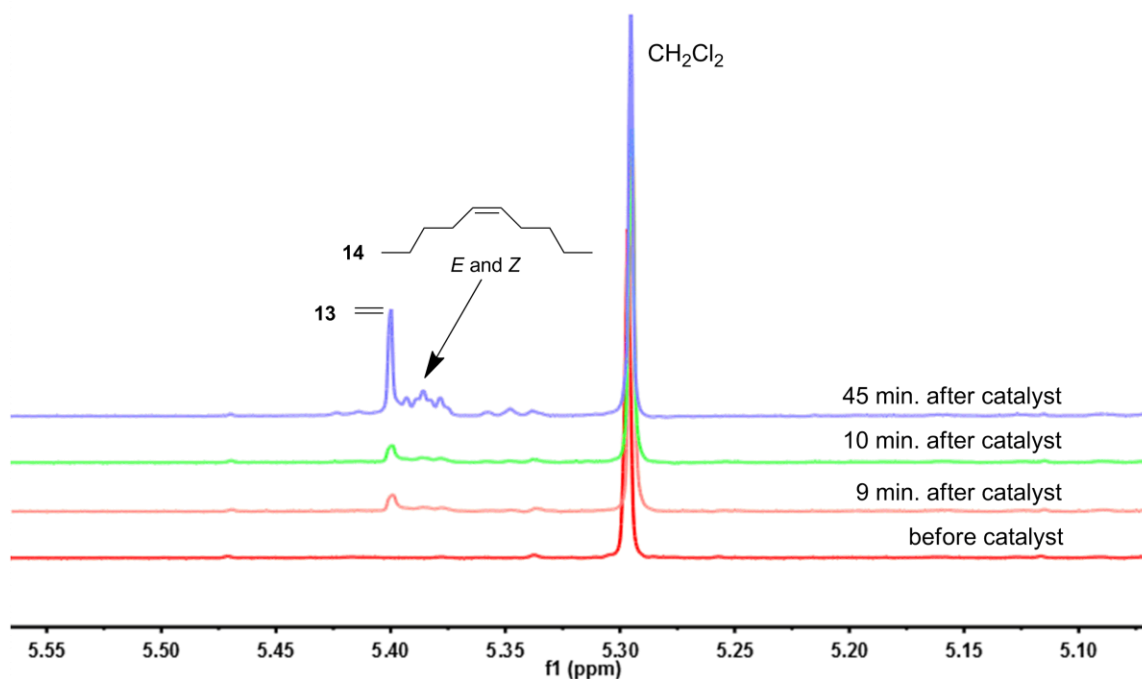
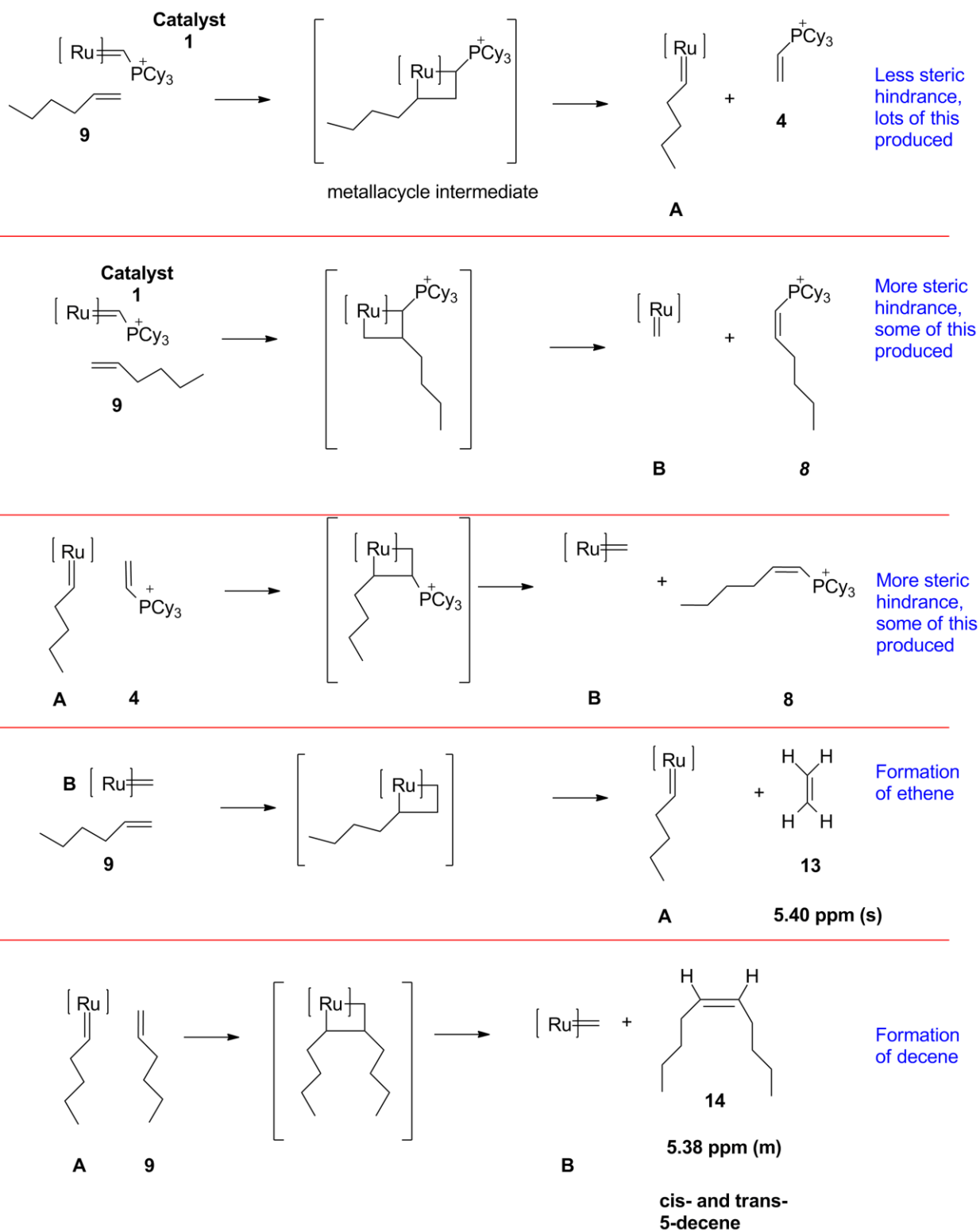


Figure 3.24. Expansion showing the appearance of ethene (s, 5.40 ppm) and of cis- and trans- decene (m, 5.38 ppm). Dichloromethane is also shown at 5.30 ppm.

Figure 3.24 shows the appearance of a singlet and multiplet over 45 minutes. The singlet corresponds to the proton chemical shift for ethene and the multiplet corresponds to the chemical shift for the olefin protons of *cis*- and *trans*-5-decene (**14**). There is likely a mixture of *cis* and *trans*, although it can be said that as hardly any CM product formed, it was deemed unnecessary to determine the ratios of each. The methylene protons were also detected, although they are partially obscured by the other peaks for 1-hexene.

In contrast with the results obtained in the ESI-MS reaction with 1-hexene and those from ^1H NMR, this reaction appears to reach an equilibrium state 12 minutes after the addition of catalyst, in which 2 charged species appear while the charged catalyst concentration is depleted. In the CM reaction, **4** ($\text{C}_2\text{H}_3\text{PCy}_3$)⁺ appears rapidly and with high intensity whereas in the ROMP reaction, it appears at low intensity which does not change noticeably over 30-120 minutes. This indicates that more **4** is forming due to the reaction with hexene, in which the alkyl chain on hexene is oriented away from the phosphonium group, forming proposed species **A**, which is not charged. This is reasonable, considering that there is less steric hindrance when hexene orients itself in this manner. **4** may also be formed in the CM of the charged catalyst and reaction with another **4**. However, in addition to being sterically disfavored, this would regenerate both species, which is not seen by ESI-MS, so that is not happening. The catalyst may also be regenerated by the reaction of **A** with **4**, but that is not seen either. The other charged species that is detected is **8**, which occurs when the alkyl chain on the hexene is oriented towards the phosphonium group. Since **8** appears more slowly and at a lower intensity, this tells us that sterics are a greater factor in slowing down this reaction. **8** may also be formed by reacting with **A** and with **4**, but that is not happening because we don't see the depletion of **4** with increased formation of **8**.

In looking at the ^1H NMR data, we can see that most of the 1-hexene remains after 45 minutes. We do, however detect the formation of ethene (**13**) and of *cis*- and *trans*-5-decene (**14**), albeit in small quantity at 5.40 and 5.38 ppm, respectively. This indicates that proposed species **B** is reacting with hexene to form small amounts of ethene, and also that **A** reacts with hexene to form small amounts of **14**. The summary of reactions occurring can be seen in Scheme 14.



Scheme 14. List of reactions detected by ESI-MS and by ^1H NMR

There are also a number of peaks forming in both the alkene and alkyl chemical shift ranges which may correspond to the phosphonium salts, **4** and **8**, but we cannot say with any confidence which they are, as they are overlain by the hexene and solvent peaks.

3.9 Conclusions

In monitoring this series of CM reactions, we found that the PSI-ESI-MS technique allowed us to observe the charged species and we ascertained that in the reaction with 1-hexene, equilibrium for the reaction was reached within 12 minutes after the olefin was added, and that the relative concentrations of the phosphonium species depended on the catalyst concentration, which was not found for ROMP. In our examination of the reactions with charge-tagged olefins, the catalyst disappeared immediately and regeneration of the starting material occurred but not the anticipated 10-C olefin.

In observing the ^1H NMR results, it was noted that even by working as quickly and efficiently as possible, it took 9 minutes to obtain the first NMR spectrum, thus losing the important first 9 minutes of the reaction. Very little ethene or decene product was formed in the reaction with the uncharged starting olefin, while no CM product formed for the charge-tagged reaction. We gained insight into the nature and orientation of the charged coupling partners forming the metallacycle as well as kinetic information about their formation and the disappearance of the charged catalyst. We know that the charged catalyst is not being regenerated, nor are $\text{C}_2\text{H}_3\text{PCy}_3^+$

(4) or $C_6H_{11}PCy_3^+$ (8) being depleted. Piers' catalyst does not appear to generate much CM product using a facile Type I olefin.

3.10 Future work

One large disadvantage for the investigation of catalytic systems for this thesis was in needing to utilize two different instruments to analyze one reaction, and the distance that lay between them. The largest issue lay in the variance of concentration when two different solutions needed to be made, one for ESI-MS and one for NMR. The MS studies were conducted in a Schlenk flask with a greater volume, while the NMR studies were conducted in an NMR tube with a much smaller volume. Every effort was made to most closely approximate the concentrations for both reactions, but of course they could not exactly match. Therefore, while the rates of reaction will be the same, the rate constants will be different. These investigations would have been rendered more exact if they were studied with an online NMR-MS system using the same reacting solution. Fortunately, that will not be an issue for future investigators in our group.

3.11 Experimental

Solvents were HPLC grade and were purified on an MBraun solvent purification system. Piers' catalyst and norbornene were obtained from Sigma-Aldrich and were used without further purification. MeCN and CH_2Cl_2 were obtained from the solvent purification system (SPS) and used without further purification. All mass spectra were collected on a Micromass Q-ToF *micro* mass spectrometer in positive mode, using electrospray

ionization: capillary voltage, 2900 V; extraction voltage, 0.5 V; source temperature, 100 C; desolvation temperature, 200 C; cone gas flow, 100 L/h; desolvation gas flow, 150 L/h; collision voltage, 2 V for MS experiments and 2-25 V for MS/MS experiments; MCP voltage, 2400 V.

PSI-ESI-MS procedure for ROMP with norbornene: norbornene, (0.02g, 0.21 mmol) and MeCN or CH₂Cl₂, (10 mL) were added to a Schlenk flask equipped with a stir bar and a septum. Fused silica tubing was inserted into the reaction mixture solution, and was sparged with argon for 20 minutes. The silica tubing was connected to the mass spectrometer and argon gas was applied to the Schlenk flask at 3 psi, the extra pressure pushing the solution through the tubing to the spectrometer. Spectra were recorded once per second. Piers' catalyst (0.0018 g, 0.0021 mmol) was diluted in CH₂Cl₂, prepared in a glovebox, and injected by air-tight syringe through the septum into the reaction mixture to initiate the reaction.

PSI-ESI-MS procedure for CM with 1-hexene and 1-hexene-6-triphenylphosphonium hexafluorophosphate: 1-hexene, (26μL, 0.21 mmol) and CH₂Cl₂, (5 mL) were added to a Schlenk flask equipped with a stir bar and a septum. Fused silica tubing was inserted into the reaction mixture solution, and was sparged with argon for 20 minutes. The silica tubing was connected to the mass spectrometer and argon gas was applied to the Schlenk flask at 3 psi, the extra pressure pushing the solution through the tubing to the spectrometer. Spectra were recorded once per second. Piers' catalyst (0.0018 g, 0.0021 mmol) was diluted in CH₂Cl₂, prepared in a glovebox, and injected by air-tight syringe through the septum into the reaction mixture to initiate the reaction.

¹H NMR for ROMP with norbornene was conducted in CD₂Cl₂, obtained from Sigma Aldrich and used without further purification. Norbornene (0.055g, 0.058 mmol), CD₂Cl₂ (720 μL) were

measured by airtight syringe and injected into an NMR tube equipped with a rubber NMR septum, and was sparged with nitrogen. Piers' catalyst (0.0005 g, 0.0006 mmol) was weighed and dissolved in 30 μL of CH_2Cl_2 in a glovebox and removed by airtight syringe. Once the spectrum of norbornene was obtained, the catalyst solution was added via syringe through the septum. Spectra were obtained on a 500 MHz Bruker magnet. Before the addition of catalyst: δ 6.03 (2 H, s), 2.88 (2H, s), 1.66 (2H, m), 1.34 (1H, dp), 1.11 (1H, m), 0.99 (2H, m). After catalyst addition: δ 6.98 (s), 5.28 (br. s), 5.25 (d), 5.12 (br. s), 4.40 (s), 2.93 (s), 2.73, (br. s), 2.25-2.41, (br, m), 1.65-1.9. (br. m), 1.46 (s), 1.11-1.35 (br. m), 0.85-1.00 (br. m).

^1H NMR for CM with 1-hexene was conducted in CD_2Cl_2 , obtained from Sigma Aldrich and used without further purification. 1-hexene (26 μL , 0.042 mmol), CD_2Cl_2 (720 μL) were measured by airtight syringe and injected into an NMR tube equipped with a rubber NMR septum, and was sparged with nitrogen. Piers' catalyst (0.0005 g, 0.0006 mmol) was weighed and dissolved in 30 μL of CH_2Cl_2 in a glovebox and removed by airtight syringe. Once the spectrum of 1-hexene was obtained, the catalyst solution was added via syringe through the septum. Spectra were obtained on a 500 MHz Bruker magnet. Before the addition of catalyst: δ 5.81 (1H, m), 4.98 (1H, dd), 4.92 (1H, dd), 2.04 (2H, q), (1.34 (4H, m), 0.90 (3H, t). After catalyst addition: δ 5.81 (1H, m), 5.40 (s), 5.38 (m) 4.98 (1H, dd), 4.92 (1H, dd), 2.04 (2H, q), 1.98 (br. m), 1.34 (4H, m), 0.90 (3H, t).

Chapter 4: The Colour-Changing Sports Drink

4.1 Introduction

Anthocyanins, which are counted among a class of compounds known as flavinoids, are believed to have health benefits, can be used as sunscreens, and are known antioxidants.⁸³ They are present in the leaves and petals of plants and are highly conjugated, instilling those leaves and flowers with brilliant colors.⁸⁴ Anthocyanins also contain hydroxyl groups, which hydrogen bond to other colourless flavinoids present in the plant, serving to modify their colors.⁸⁵ Red cabbage contains anthocyanins such as cyanidin, which readily changes colour over a wide pH range as its hydroxyl groups are protonated and deprotonated⁸⁶ while dissolved in water. The four different forms of cyanidin produce a range of colours that change with a change in pH. These assets not only make red cabbage useful as an acid/base indicator for pH demonstrations in the classroom, but can also be made into a visually dynamic, color-changing, hypotonic “sports drink” that is safe to consume at the end of the experiment. A solution containing anthocyanins is green at high pH and changes to blue then purple then pink then red as the pH decreases (Figure 4.1).

This inexpensive drink is easily made with kitchen ingredients, is visually compelling and easily scaled up to allow for classroom participation.

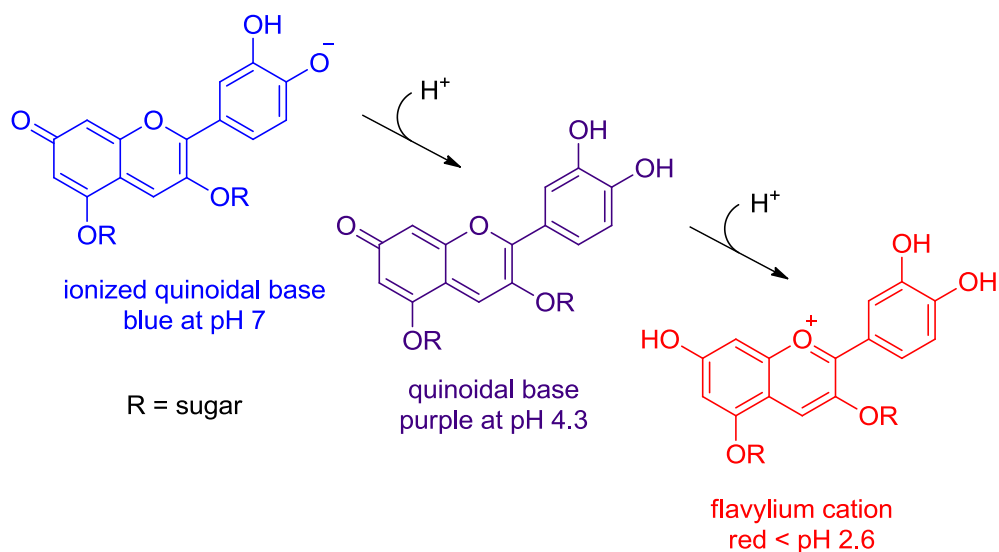


Figure 4.1. pH-causing transitional forms of cyanidin in red cabbage.

The properties of red cabbage as acid-base indicator have been employed in many educational demonstrations over the years,⁸⁷ including painting environmentally friendly artwork,⁸⁸ making natural dyes,⁸⁹ generating colorful patterns,⁹⁰ visualizing the electrolysis of water⁹¹ or the production of noxious gases.⁹² This particular version relies on the fact that all the chemicals used are commonly found in the kitchen, and so the experiment – like the result of all good recipes – can be safely consumed once complete. When green or red, cabbage solutions are too basic or acidic to consume, respectively, but the middle of the range is quite drinkable. A pinch of baking soda makes the solution a vivid blue, carbonic acid is enough to turn it back to purple, and citric acid will make it pink. A colorless soft drink is used as the source of the carbonic acid, and the end result is a faintly salty, sweet drink with an unusual flavor and a slight acid bite. It has similar ingredients to that of a hypotonic sports drink, and at the end of the experiment, it's perfectly safe to drink as such (Figure 4.2).

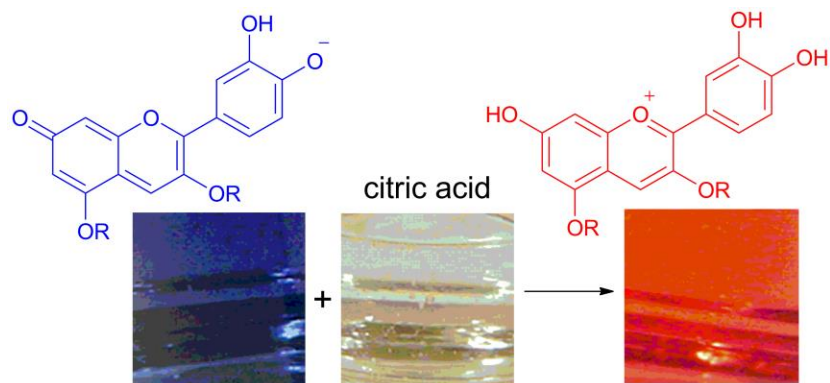


Figure 4.2. Changing pH causing protonation and rearrangement of the π -bonds in the anthocyanins from red cabbage change the colour in the sports drink.

The experiment can be extended by using other plant extracts as the indicator. Mebane and Rybolt have published a very useful table detailing the colour changes with pH of 15 natural indicators, including beets, blueberries, cherries, grapes, onions, tomatoes and the skins of apples, peaches, pears, radishes, rhubarb and turnip.⁹³ Herbal teas have been similarly documented.⁹⁴

The pK_a of citric acid is 3.09,⁹⁵ and the pK_b of sodium bicarbonate is 7.65. The anthocyanins in red cabbage are pink at $3.5 < \text{pH} < 4$, and blue at $6 < \text{pH} < 7$. Another good candidate for a colour-change using kitchen ingredients is blueberries (green to purple at $\sim \text{pH} 5.5$), which also perhaps provide a more appropriate flavour for a hypotonic sports drink.

4.2 Results and Discussion

This experiment was tested with some elementary school students and with a group of high-school teachers who made and sampled their own mixture of citric acid, baking soda (sodium

bicarbonate), 7-Up, and indicator. Either red cabbage or blueberry juice was used as an indicator. Two glasses were used, one containing a basic solution and the other an acidic solution; the order of mixing is not important to the experiment but a dramatic colour change is easily observed in the sports drink, indicating that a pH change transpired. The indicator may be added to the basic solution in the first glass, while the acidic solution in the other glass remains clear, (or vice versa). The students then mix the solutions together and witness the various colours emerging, demonstrating the properties of acid/base mixtures. The students are told that they may consume their newly-made beverage. The buffering effect of the citric acid and sodium bicarbonate will prevent the mixture from tasting unbearably tart.

4.3 Experimental

4.3.1 Red Cabbage

The colour was extracted from the red cabbage by chopping up a leaf and adding hot water, or by heating both in the microwave for 2 minutes, giving a violet solution. 5-20 mL of the indicator were added to one of the glasses and then made up to 1/3 full of water. A pinch of sodium bicarbonate was added, changing the violet solution bright blue. The other glass was half-filled with the clear soft drink, with ~0.5g of citric acid added, Figure 4.3. The two glasses were then mixed in random order and speed by the experimenters.

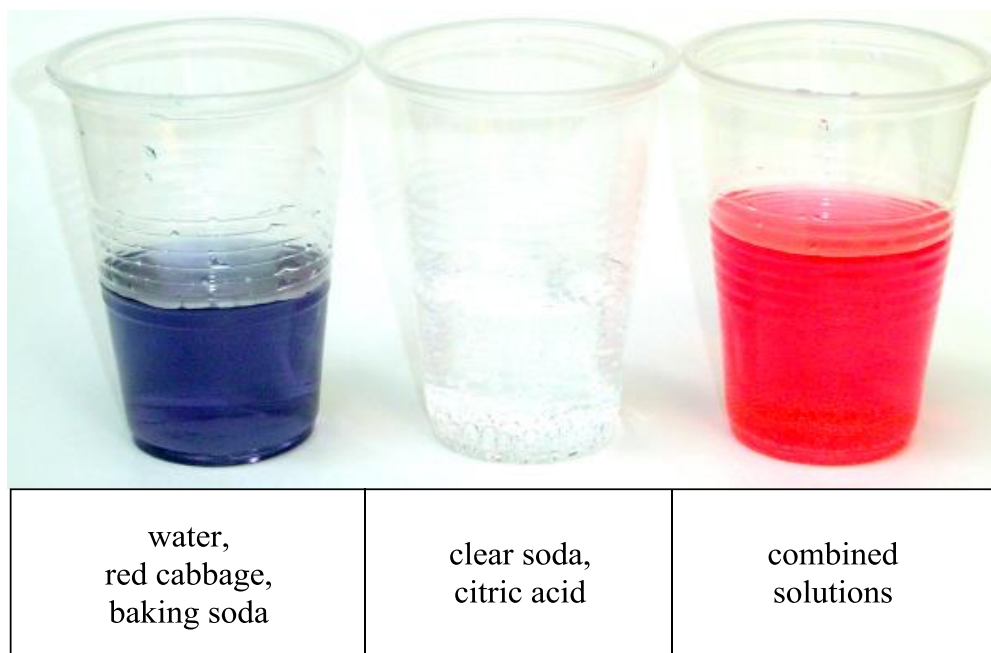


Figure 4.3. The three solutions used in the red cabbage experiment: blue + clear = pink.

4.3.2 Blueberries

Hot water was added to frozen blueberries in a blender and the mixture was then filtered through a coffee filter giving a violet indicator. The slightly acidic drinking soda was not added, and the contents of one glass were blueberry juice and water, while the other contained water, sugar and baking soda (Figure 4.4). Much more baking soda is required with blueberry indicator than is needed for red cabbage. The solutions were combined as previously discussed, and the colour of the juice changed from violet to green. In addition to cyanidin, blueberries also possess peonidin, delphinidin, petunidin and malvidin, all of which share the 3-ring backbone, and with various sugars attached, the majority are water-soluble.⁹⁶

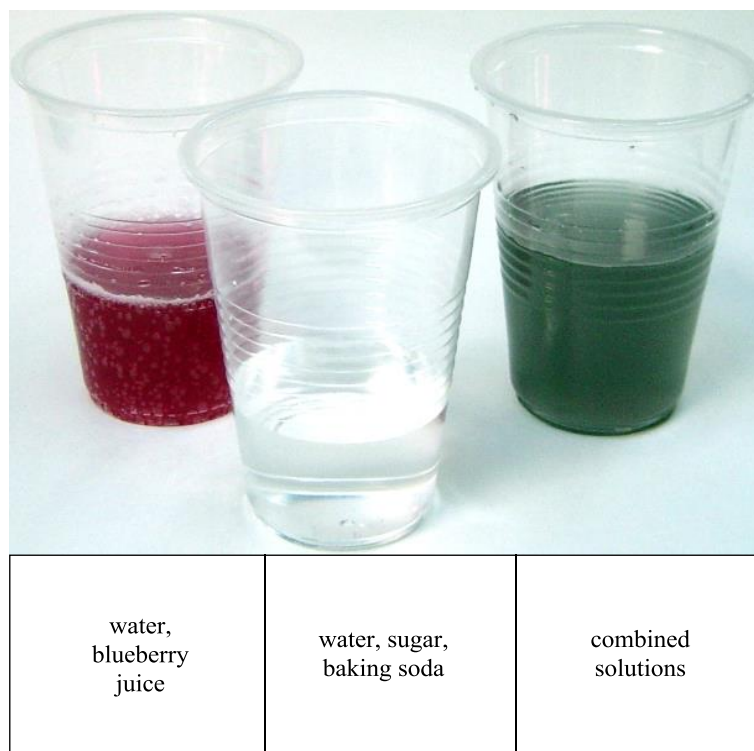


Figure 4.4. The three solutions used in the blueberry experiment: purple + clear = green.

4.4 Conclusions

This colourful and tasteful experiment is useful in demonstrating how indicators function in acid/base chemistry. The indicator is a simple and inexpensive to make, can come from a variety of coloured fruits and vegetables, and the change in pH is visually intriguing. This simple experiment is an attention-grabbing introduction for elementary through to high school students using easily obtained ingestible ingredients.

1 Bibliography

- (1) Fenn, J. B.; Mann, M.; Meng, C. K.; Wong, S. F.; Whitehouse, C. M. *Science*, **1989**, *246*, 64-71.
- (2) Yarwood, J.; Douthwaite, R.; Duckett, S. B., *Spectroscopic Properties of Inorganic and Organometallic Compounds: Techniques, Materials and Applications*. Royal Society of Chemistry: Cambridge, UK., 2010; Vol. 41, p 324.
- (3) Ashcroft, A. E., *Ionization Methods in Organic Mass Spectrometry*. Royal Society of Chemistry: Cambridge, UK, (1997); p 176.
- (4) Plattner, D. A. *Int. J. Mass Spectrom.*, **2001**, *207*, 125-144.
- (5) Aliprantis, A. O.; Canary, J. W. *J. Am. Chem. Soc.*, **1994**, *116*, 6985-6986.
- (6) Bruins, A. P. *J. Chromatogr. A*, **1998**, *794*, 345-357.
- (7) Price, W. D.; Schnier, P. D.; Williams, E. R. *Anal. Chem.*, **1996**, 859-866.
- (8) Vikse, K. L.; Ahmadi, Z.; Luo, J. W.; van der Wal, N.; Daze, K.; Taylor, N.; McIndoe, J. S. *Int. J. Mass Spectrom.*, **2012**, *323*, 8-13.
- (9) Jennings, K. R. *Int. J. Mass Spectrom.*, **2000**, *200*, 479-493.
- (10) Shukla, A. K.; Futrell, J. H. *J. Mass Spectrom.*, **2000**, *35*, 1069-1090.
- (11) (a) Marquez, C.; Metzger, J. O. *Chem. Commun.*, **2006**, 1539-1541; (b) Santos, L. S. *Eur. J. Org. Chem.*, **2008**, 235-253; (c) Schroder, D. *Acc. Chem. Res.*, **2012**, *45*, 1521-1532.
- (12) (a) Bakhtiar, R.; Hop, C. E. C. A. *J. Phys. Org. Chem.*, **1999**, *12*, 511-527; (b) Enquist, P. A.; Nilsson, P.; Sjoberg, P.; Larhed, M. *J. Org. Chem.*, **2006**, *71*, 8779-8786; (c) Pelagatti, P.; Carcelli, M.; Calbiani, F.; Cassi, C.; Elviri, L.; Pelizzi, C.; Rizzotti, U.; Rogolino, D. *Organometallics*, **2005**, *24*, 5836-5844; (d) Qian, R.; Guo, H.; Liao, Y. X.; Guo, Y. L.; Ma, S. M. *Angew. Chem. Int. Ed.*, **2005**, *44*, 4771-4774.
- (13) Santos, L. S., Ed., *Reactive Intermediates. MS Investigations in Solution*. Wiley-VCH: Weinheim, Germany, **2010**.
- (14) (a) Hinderling, C.; Feichtinger, D.; Plattner, D. A.; Chen, P. *J. Am. Chem. Soc.*, **1997**, *119*, 10793-10804; (b) Hinderling, C.; Plattner, D. A.; Chen, P. *Angew. Chem. Int. Ed.*, **1997**, *36*, 243-244.
- (15) Yunker, L. P. E.; Stoddard, R. L.; McIndoe, J. S. *J. Mass Spectrom.*, **2014**, *49*, 1-8.
- (16) Wager, P. A.; Lang, D. J.; Wittmer, D.; Bleischwitz, R.; Hagelucken, C. *Gaia*, **2012**, *21*, 300-309.
- (17) Spivey, A. C.; Arseniyadis, S. *Top. Curr. Chem.*, **2010**, *291*, 233-280.
- (18) Web of Science. Citation report for "phosphine catalysis" 2014.
http://apps.webofknowledge.com/CitationReport.do?product=WOS&search_mode=CitationReport&SID=1EduzeZDnzAQGrLsKy7&page=1&cr_pqid=7&viewType=summary&colName=WOS.
- (19) Aroyan, C. E.; Dermenci, A.; Miller, S. J. *Tetrahedron*, **2009**, *65*, 4069-4084.
- (20) (a) Ye, L. W.; Zhou, J.; Tang, Y. *Chem Soc Rev*, **2008**, *37*, 1140-1152; (b) Tran, Y. S.; Kwon, O. *Org. Lett.*, **2005**, *7*, 4289-4291.
- (21) Morita, K.; Suzuki, Z.; Hirose, H. *B. Chem. Soc. Jpn.*, **1968**, *41*, 2815-2816.
- (22) Baizer, M. M.; Anderson, J. D. *J. Org. Chem.*, **1965**, *30*, 1357-1358.
- (23) Declerck, V.; Martinez, J.; Lamaty, F. *Chem. Rev.*, **2009**, *109*, 1-48.
- (24) Lu, X. Y.; Lu, Z.; Zhang, X. M. *Tetrahedron*, **2006**, *62*, 457-460.

- (25) Dudding, T.; Kwon, O.; Mercier, E. *Org. Lett.*, **2006**, *8*, 3643-3646.
- (26) Liang, Y.; Liu, S.; Xia, Y. Z.; Li, Y. H.; Lu, Z. X. *Chem. Eur. J.*, **2008**, *14*, 4361-4373.
- (27) Marinetti, A.; Voituriez, A. *Synlett*, **2010**, 174-194.
- (28) (a) Cowen, B. J.; Miller, S. J. *Chem Soc Rev*, **2009**, *38*, 3102-3116; (b) Lu, X. Y.; Zhang, C. M.; Xu, Z. R. *Acc. Chem. Res.*, **2001**, *34*, 535-544.
- (29) (a) Voituriez, A.; Panossian, A.; Fleury-Bregeot, N.; Retailleau, P.; Marinetti, A. *J. Am. Chem. Soc.*, **2008**, *130*, 14030-14031; (b) Zhang, C. M.; Lu, X. Y. *J. Org. Chem.*, **1995**, *60*, 2906-2908; (c) Zhu, G. X.; Chen, Z. G.; Jiang, Q. Z.; Xiao, D. M.; Cao, P.; Zhang, X. M. *J. Am. Chem. Soc.*, **1997**, *119*, 3836-3837.
- (30) (a) Gao, L.; Ye, S.; Ding, Q.; Chena, Z.; Wu, J. *Tetrahedron*, **2012**, *68*, 2765-2769; (b) Guan, X. Y.; Shi, M. *ACS Catal.*, **2011**, *1*, 1154-1157; (c) Ma, R.; Xu, S.; Tang, X.; Wu, G.; He, Z. *Tetrahedron*, **2011**, *67*, 1053-1061; (d) Szeto, J.; Sriramurthy, V.; Kwon, O. *Org. Lett.*, **2011**, *13*, 5420-5423.
- (31) (a) Chiao, F. Y.; Kwon, O. *Molecules*, **2011**, *16*, 3802-3825; (b) Han, X. Y.; Wang, Y. Q.; Zhong, F. R.; Lu, Y. X. *J. Am. Chem. Soc.*, **2011**, *133*, 1726-1729; (c) Wilson, J. E.; Fu, G. C. *Angew. Chem. Int. Ed.*, **2006**, *45*, 1426-1429; (d) Xiao, D.; Zhang, Z.; Jiang, Q.; Zhang, X. *Tetrahedron Lett.*, **1998**, *39*, 5331-5334.
- (32) Khong, S.; Kwon, O. *J. Org. Chem.*, **2012**, *77*, 8257-8267.
- (33) (a) Na, R.; Jing, C.; Xu, Q.; Jiang, H.; Wu, X.; Shi, J.; Zhong, J.; Wang, M.; Benitez, D.; Tkatchouk, E.; Goddard, W. A.; Guo, H.; Kwon, O. *J. Am. Chem. Soc.*, **2011**, *133*, 13337-13348; (b) Zhu, X. F.; Lan, J.; Kwon, O. *J. Am. Chem. Soc.*, **2003**, *125*, 4716-4717.
- (34) Tran, Y. S.; Kwon, O. *J. Am. Chem. Soc.*, **2007**, *129*, 12632-12633.
- (35) (a) Andrews, I. P.; Kwon, O. *Chem. Sci.*, **2012**, *3*, 2510-2514; (b) Villa, R. A.; Xu, Q. H.; Kwon, O. *Org. Lett.*, **2012**, *14*, 4634-4637.
- (36) Martin, T. J.; Vakhshori, V. G.; Tran, Y. S.; Kwon, O. *Org. Lett.*, **2011**, *13*, 2586-2589.
- (37) Inanaga, J.; Baba, Y.; Hanamoto, T. *Chem. Lett.*, **1993**, *22*, 241-244.
- (38) Trost, B. M.; Li, C. J. *J. Am. Chem. Soc.*, **1994**, *116*, 3167-3168.
- (39) Zhang, C.; Lu, X. *J. Org. Chem.*, **1995**, *60*, 2906-2908.
- (40) Davies, K. A.; Wulff, J. E. *Org. Lett.*, **2011**, *13*, 5552-5555.
- (41) O'Rourke, N. F.; Davies, K. A.; Wulff, J. E. *J. Org. Chem.*, **2012**, *77*, 8634-8647.
- (42) (a) Ahmadi, Z.; McIndoe, J. S. *Chem. Commun.*, **2013**, *49*, 11488-11490; (b) Ahmadi, Z.; Oliver, A. G.; McIndoe, J. S. *Chempluschem*, **2013**, *78*, 632-635; (c) Henderson, M. A.; Luo, J. W.; Oliver, A.; McIndoe, J. S. *Organometallics*, **2011**, *30*, 5471-5479; (d) Luo, J. W.; Oliver, A. G.; McIndoe, J. S. *Dalton T.*, **2013**, *42*, 11312-11318; (e) Vikse, K.; Naka, T.; McIndoe, J. S.; Besora, M.; Maseras, F. *Chemcatchem*, **2013**, *5*, 3604-3609.
- (43) Zhu, X. F.; Henry, C. E.; Kwon, O. *J. Am. Chem. Soc.*, **2007**, *129*, 6722-6723.
- (44) Petzold, L. *SIAM J. Sci. Stat. Comput.*, **1983**, *4*, 136-148.
- (45) Peters, E. F.; Zletz, A.; Evering, B. L. *Ind. Eng. Chem.*, **1957**, *49*, 1879-1882.
- (46) Eleuterio, H. S. Polymerization of cyclic olefins. U.S. Patent 3,074,918, January 22, 1963.
- (47) Zielger, K.; Breil, H.; Martin, H.; Holzkamp, E. *US Patent*, 3574138 A 19710406., **1971**.
- (48) Banks, R. L.; Bailey, G. C. *Ind. Eng. Chem. Prod. RD.*, **1964**, *3*, 170-173.
- (49) Natta, G.; Dall'asta, G.; Mazzanti, G. *Angew. Chem. Int. Ed.*, **1964**, *3*, 723-729.
- (50) Bradshaw, C. P.; Howman, E. J.; Turner, L. *J. Catal.*, **1967**, *7*, 269-270.
- (51) Calderon, N.; Chen, H. Y.; Scott, K. W. *Tetrahedron Lett.*, **1967**, 3327-3328.
- (52) (a) Doering, W. V. E.; Knox, L. H. *J. Am. Chem. Soc.*, **1956**, *78*, 4947-4950; (b) Herisson, J. L.; Chauvin, Y. *Makromolekul. Chem.*, **1971**, *141*, 161.

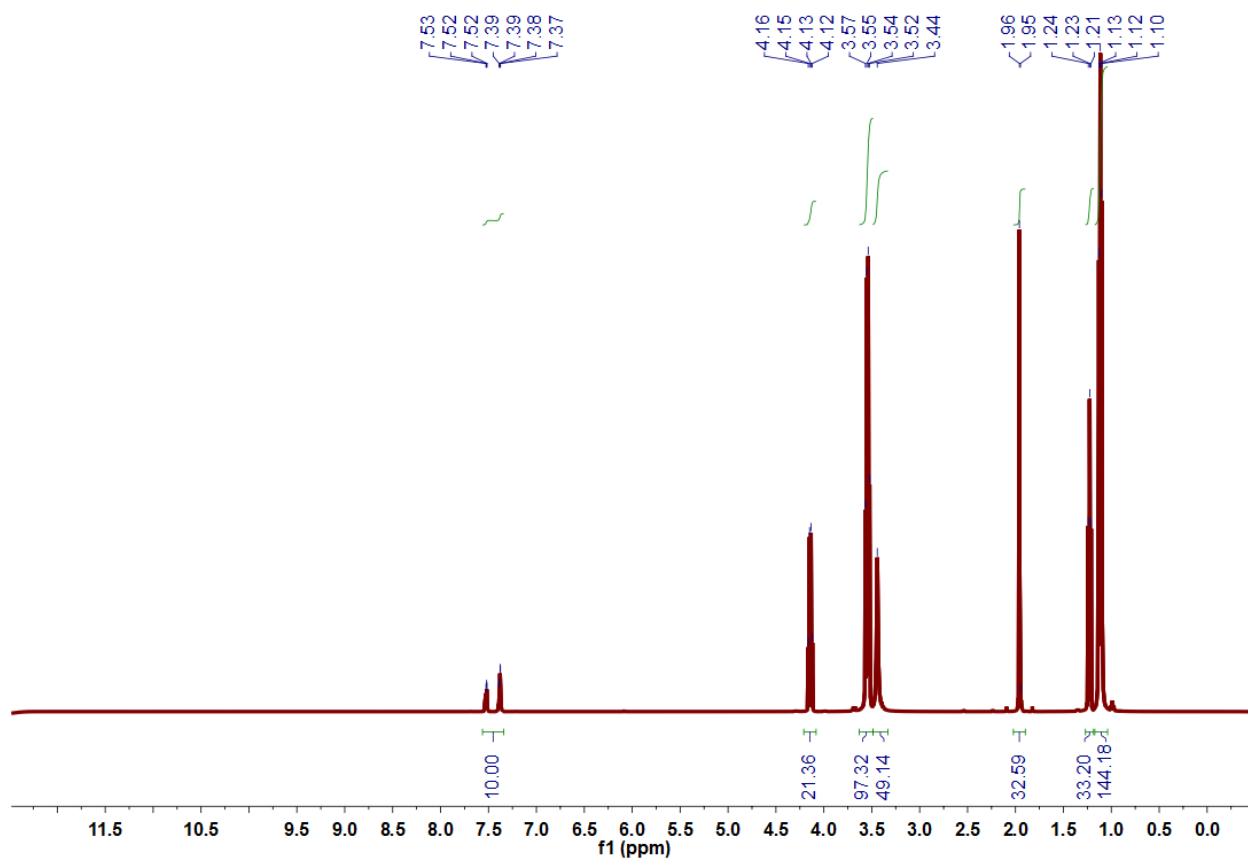
- (53) Arduengo, A. J.; Dias, H. V. R.; Harlow, R. L.; Kline, M. *J. Am. Chem. Soc.*, **1992**, *114*, 5530-5534.
- (54) Chauvin, Y. *Angew. Chem. Int. Ed.*, **2006**, *45*, 3740-3747.
- (55) Grubbs, R. H. *Angew. Chem. Int. Ed.*, **2006**, *45*, 3760-3765.
- (56) Schrock, R. R. *Angew. Chem. Int. Ed.*, **2006**, *45*, 3748-3759.
- (57) Szwarc, M. *Nature*, **1956**, *178*, 1168-1169.
- (58) GPC resource page, Agilent technologies. An introduction to gel permeation chromatography and size exclusion chromatography.
<https://www.chem.agilent.com/Library/primers/Public/5990-6969EN%20GPC%20SEC%20Chrom%20Guide.pdf> (accessed June 20, 2014).
- (59) Slugovc, C.; Burtscher, D.; Stelzer, F.; Mereiter, K. *Organometallics*, **2005**, *24*, 2255-2258.
- (60) (a) Novak, B. M.; Grubbs, R. H. *J. Am. Chem. Soc.*, **1988**, *110*, 7542-7543; (b) Novak, B. M.; Grubbs, R. H. *J. Am. Chem. Soc.*, **1988**, *110*, 960-961.
- (61) Monsaert, S.; Villa, A. L.; Drozdak, R.; Van Der Voort, P.; Verpoort, F. *Chem Soc Rev*, **2009**, *38*, 3360-3372.
- (62) Thoi, H. H.; Ivin, K. J.; Rooney, J. J. *J. Mol. Catal.*, **1982**, *15*, 245-270.
- (63) (a) Schrock, R. R. *Science*, **1983**, *219*, 13-18; (b) Schrock, R. R.; Hoyveda, A. H. *Angew. Chem. Int. Ed.*, **2003**, *42*, 4592-4633; (c) Schrock, R. R.; Murdzek, J. S.; Bazan, G. C.; Robbins, J.; Dimare, M.; Oregan, M. *J. Am. Chem. Soc.*, **1990**, *112*, 3875-3886.
- (64) Nguyen, S. T.; Johnson, L. K.; Grubbs, R. H.; Ziller, J. W. *J. Am. Chem. Soc.*, **1992**, *114*, 3974-3975.
- (65) Fu, G. C.; Nguyen, S. T.; Grubbs, R. H. *J. Am. Chem. Soc.*, **1993**, *115*, 9856-9857.
- (66) (a) Dias, E. L.; Grubbs, R. H. *Organometallics*, **1998**, *17*, 2758-2767; (b) Lynn, D. M.; Mohr, B.; Grubbs, R. H.; Henling, L. M.; Day, M. W. *J. Am. Chem. Soc.*, **2000**, *122*, 6601-6609; (c) Ulman, M.; Belderrain, T. R.; Grubbs, R. H. *Tetrahedron Lett.*, **2000**, *41*, 4689-4693.
- (67) Dias, E. L.; Nguyen, S. T.; Grubbs, R. H. *J. Am. Chem. Soc.*, **1997**, *119*, 3887-3897.
- (68) Adlhart, C.; Chen, P. *Helv. Chim. Acta*, **2000**, *83*, 2192-2196.
- (69) Straub, B. F. *Angew. Chem. Int. Ed.*, **2005**, *44*, 5974-5978.
- (70) Garber, S. B.; Kingsbury, J. S.; Gray, B. L.; Hoveyda, A. H. *J. Am. Chem. Soc.*, **2000**, *122*, 8168-8179.
- (71) (a) Alcaide, B.; Almendros, P. *Chem-Eur J.*, **2003**, *9*, 1259-1262; (b) Hong, S. H.; Wenzel, A. G.; Salguero, T. T.; Day, M. W.; Grubbs, R. H. *J. Am. Chem. Soc.*, **2007**, *129*, 7961-7968; (c) Schmidt, B. *Eur. J. Org. Chem.*, **2004**, 1865-1880; (d) Ulman, M.; Grubbs, R. H. *J. Org. Chem.*, **1999**, *64*, 7202-7207.
- (72) Courchay, F. C.; Sworen, J. C.; Ghiviriga, I.; Abboud, K. A.; Wagener, K. B. *Organometallics*, **2006**, *25*, 6074-6086.
- (73) Hong, S. H.; Sanders, D. P.; Lee, C. W.; Grubbs, R. H. *J. Am. Chem. Soc.*, **2005**, *127*, 17160-17161.
- (74) Trnka, T. M. *Ph.D. Thesis, California Institute of Technology*, **2003**.
- (75) (a) Huang, J. K.; Stevens, E. D.; Nolan, S. P. *Organometallics*, **2000**, *19*, 1194-1197; (b) Jazzar, R. F. R.; Macgregor, S. A.; Mahon, M. F.; Richards, S. P.; Whittlesey, M. K. *J. Am. Chem. Soc.*, **2002**, *124*, 4944-4945; (c) Trnka, T. M.; Morgan, J. P.; Sanford, M. S.; Wilhelm, T. E.; Scholl, M.; Choi, T. L.; Ding, S.; Day, M. W.; Grubbs, R. H. *J. Am. Chem. Soc.*, **2003**, *125*, 2546-2558.
- (76) Romero, P. E.; Piers, W. E.; McDonald, R. *Angew. Chem. Int. Ed.*, **2004**, *43*, 6161-6165.
- (77) Choi, T. L.; Grubbs, R. H. *Angew. Chem. Int. Ed.*, **2003**, *42*, 1743-1746.

- (78) Romero, P. E.; Piers, W. E. *J. Am. Chem. Soc.*, **2005**, *127*, 5032-5033.
- (79) Leitao, E. M.; Dubberley, S. R.; Piers, W. E.; Wu, Q. McDonald, R.; *Chem.-Eur. J.*, **2008**, *14*, 11565-11572.
- (80) Patiny, L.; Borel, A. *J. Chem. Inf. Model.*, **2013**, *53*, 1223-1228.
- (81) Connon, S. J.; Blechert, S. *Angew. Chem. Int. Ed.*, **2003**, *42*, 1900-1923.
- (82) Chatterjee, A. K.; Choi, T. L.; Sanders, D. P.; Grubbs, R. H. *J. Am. Chem. Soc.*, **2003**, *125*, 11360-11370.
- (83) McDougall, G. J.; Fyffe, S.; Dobson, P.; Stewart, D. *Phytochemistry*, **2007**, *68*, 1285-1294.
- (84) Charron, C. S.; Clevidence, B. A.; Britz, S. J.; Novotny, J. A. *J. Agr. Food Chem.*, **2007**, *55*, 5354-5362.
- (85) Coultate, T. P., Editor, *Food: The Chemistry of Its Components, 5th Edition*. Royal Society of Chemistry: **2009**; p 501.
- (86) Curtright, R. D.; Rynearson, J. A.; Markwell, J. *J. Chem. Ed.*, **1994**, *71*, 682.
- (87) (a) Borer, L. L. *J. Chem. Educ.*, **1987**, *64*, 446; (b) Forster, M.; *J. Chem. Educ.*, **1978**, *55*, 107; (c) Fortman, J. J.; Stubbs, K. M. *J. Chem. Ed.*, **1992**, *69*, 66; (d) Selco, J. I.; Bruno, M.; Chan, S. *J. Chem. Educ.*, **2012**, *89*, 206-210; (e) Tracy, H. J.; Collins, C.; Langevin, P. *J. Chem. Educ.*, **1995**, *72*, 1111.
- (88) Lech, J.; Dounin, V. *J. Chem. Ed.*, **2011**, *88*, 1684-1686.
- (89) Fanis, L. N. *J. Chem. Educ.*, **2008**, *85*, 1172.
- (90) Suzuki, C. *J. Chem. Educ.*, **1991**, *68*, 588.
- (91) Skinner, J. F. *J. Chem. Educ.*, **1981**, *58*, 1017.
- (92) Solomon, S.; Oliver-Hoyo, M.; Hur, C. *J. Chem. Educ.*, **1998**, *75*, 1581.
- (93) Mebane, R. C.; Rybolt, T. R. *J. Chem. Ed.*, **1985**, *62*, 285.
- (94) Epp, D. N. *J. Chem. Ed.*, **1993**, *70*, 326.
- (95) Dawson, R. M. C.; Elliott, D.; Elliott, W. H.; Jones, K. M., *Data for Biochemical Research*. 2nd ed. Oxford Univ. Press: **1969**; p 655.
- (96) Mazza, G.; Kay, C.D.; Cottrell, T.; Holub, B. J. *J. Agric. Food Chem.*, **2002**, *50*, 7731-7737.

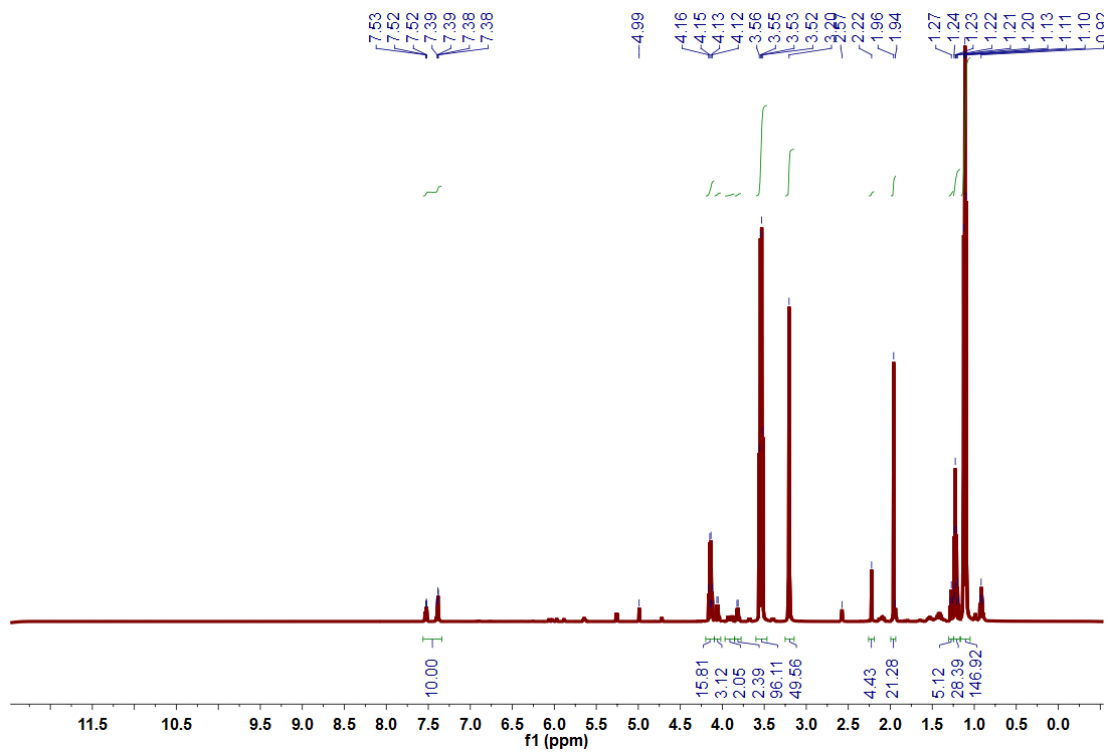
1 Appendix A

NMR spectra for phosphine catalysis

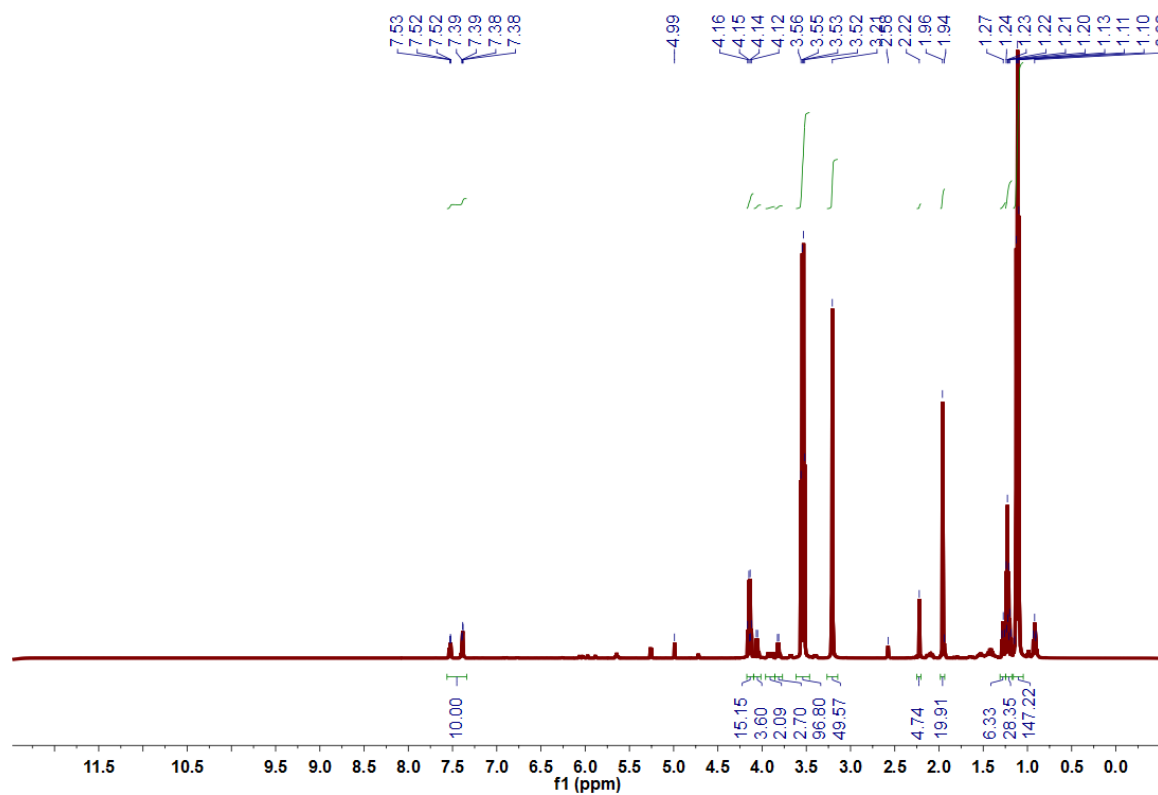
^1H NMR spectra for phosphine catalysis with ethyl-butynoate and ethanol in CD_3CN



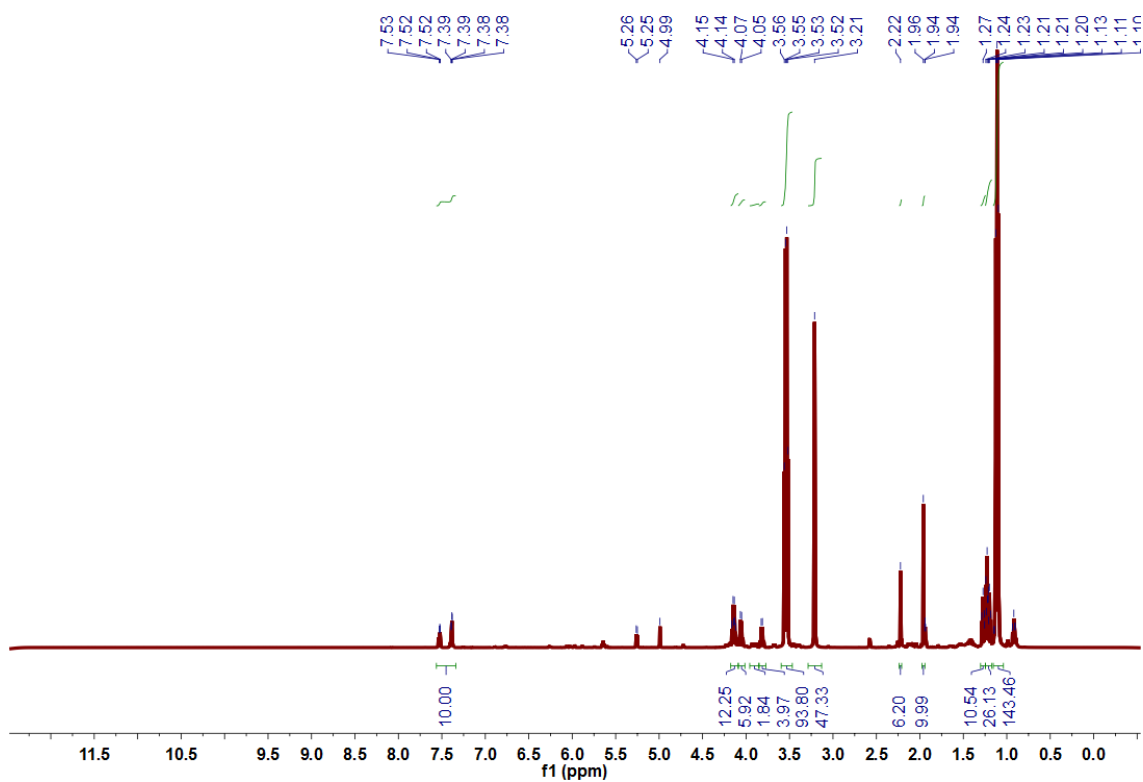
Spectra shows starting alkyne 4.14 (2H, q) (depicted as 1 in the stacked plot below), 1.96 (3H, s), 1.23 (3H, t), and EtOH (3.54 (2H, q), 3.44 (1H, br s), 1.11 (3H, t) before the addition of catalyst. Diphenylacetylene δ 7.53-7.37 (10 H, dm), was used as an internal standard. The integration of the peaks at 4.14 and 3.82 ppm were used to generate the traces seen in Figure 2.1.



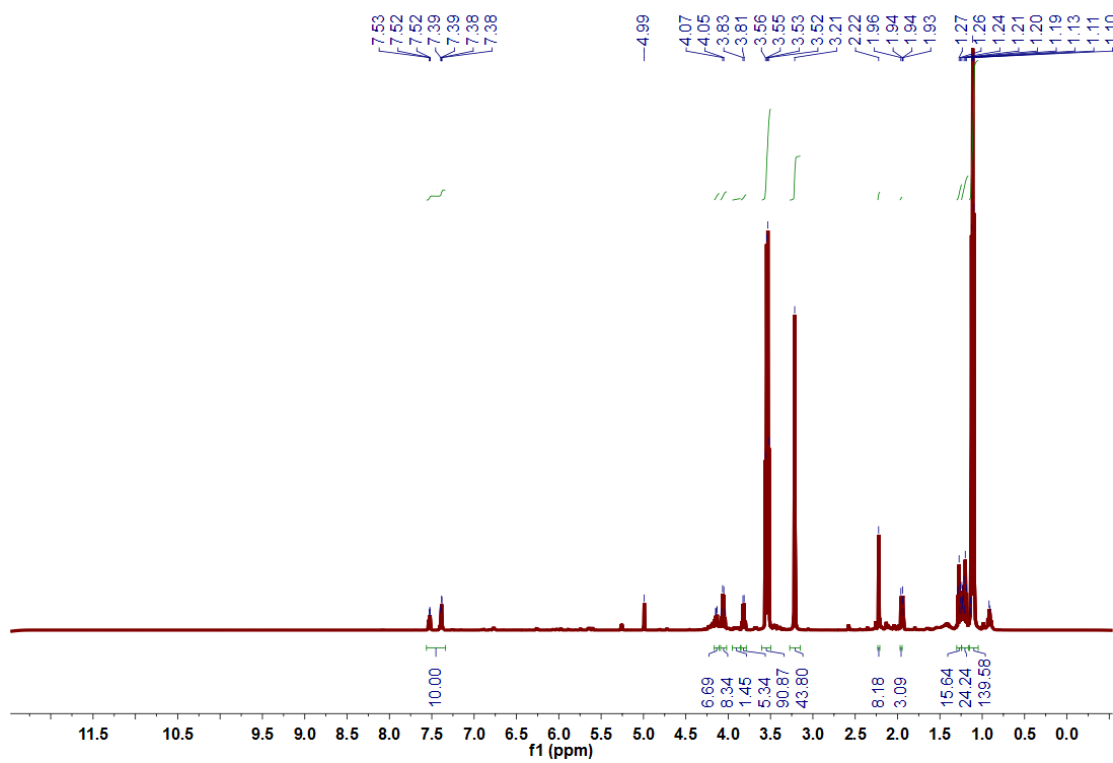
7 minutes after catalyst addition



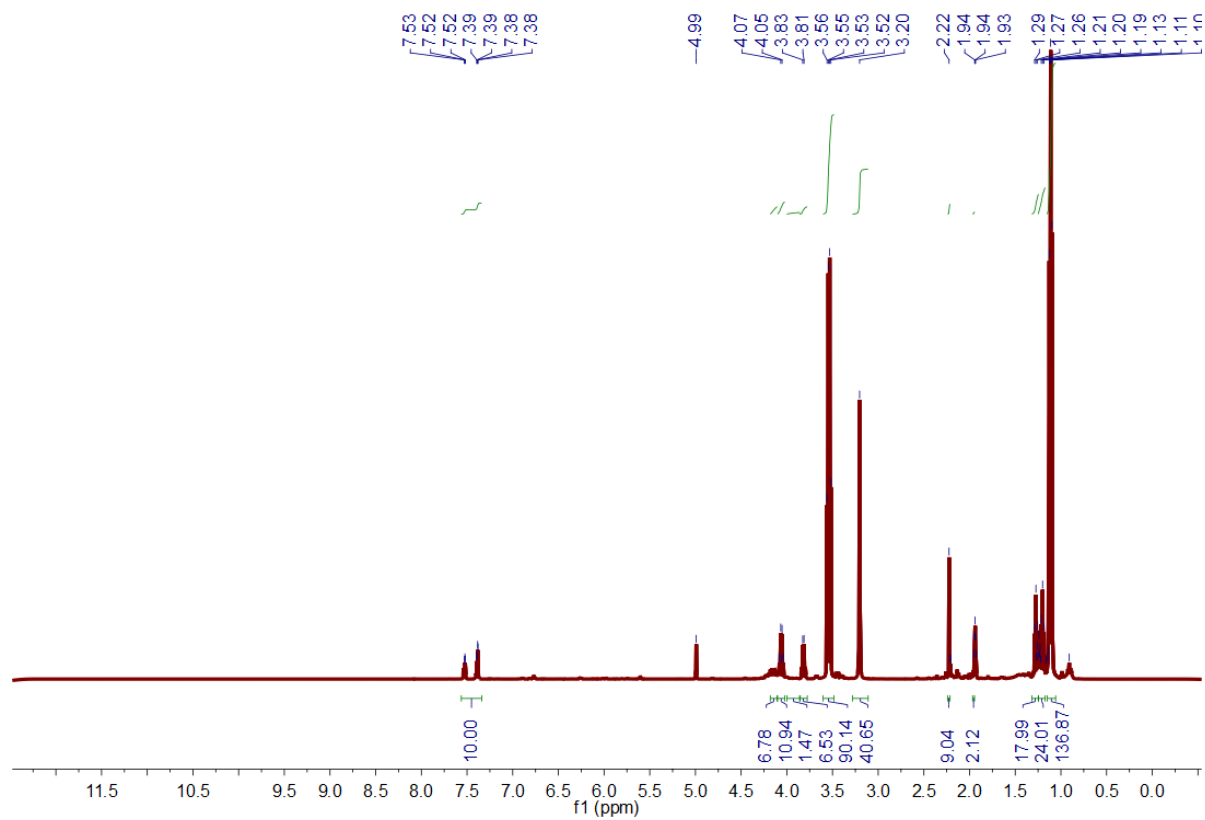
14 minutes after catalyst addition



61 minutes after catalyst addition

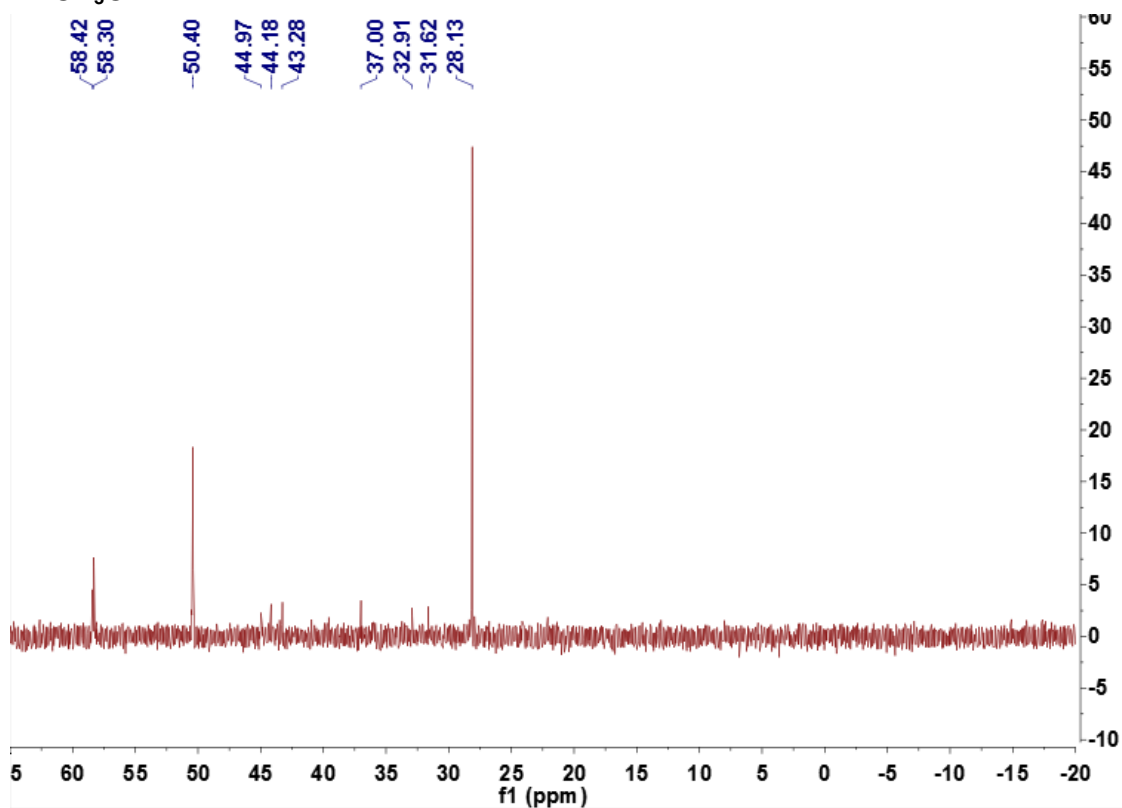


34 minutes after catalyst addition

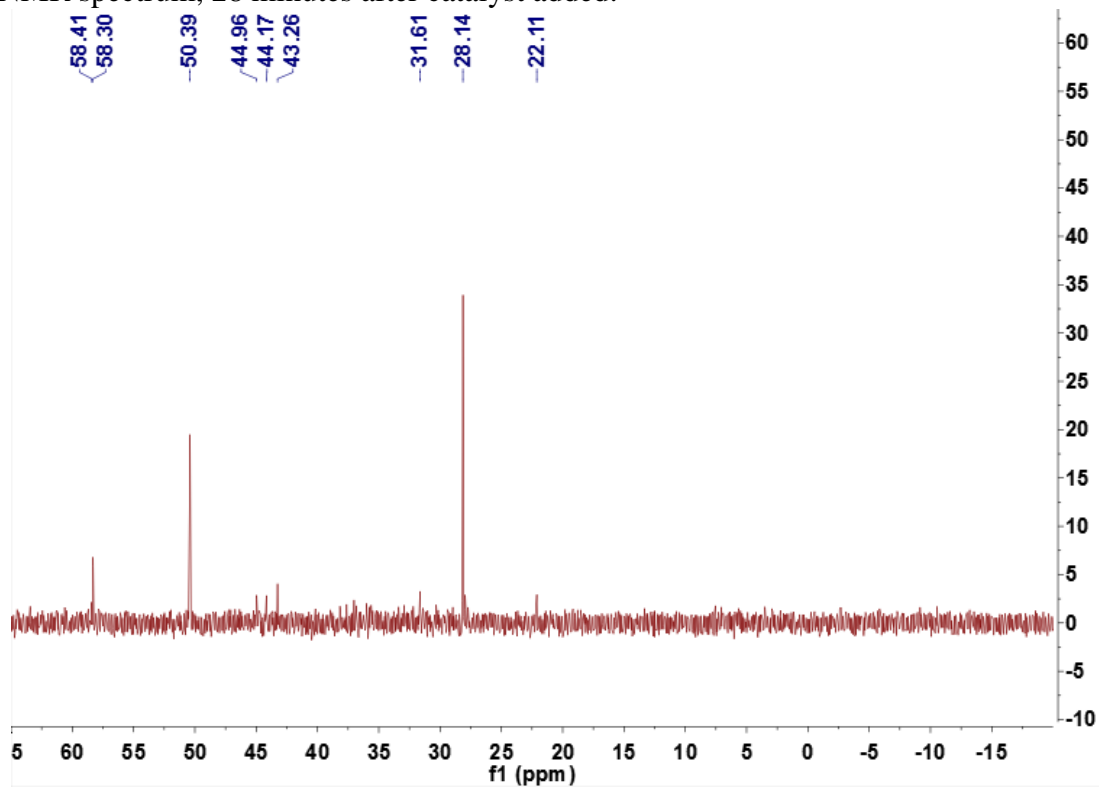


244 minutes after catalyst addition

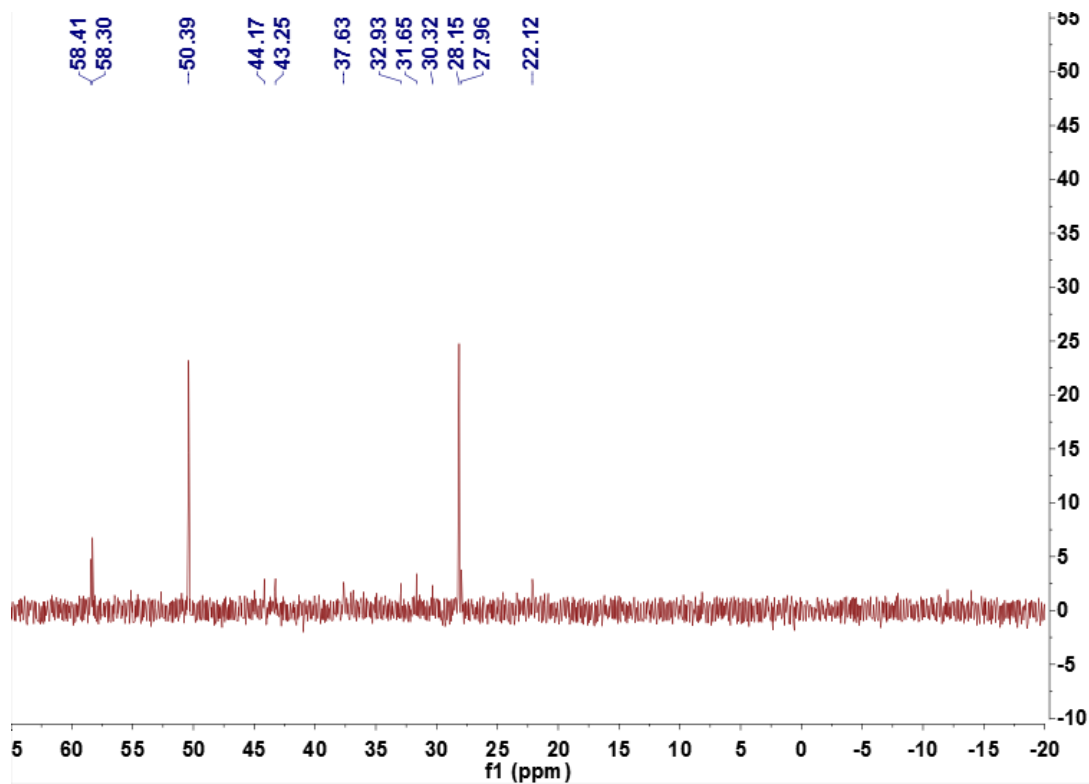
..1 ^{31}P NMR spectra for phosphine catalysis with ethyl-butynoate and ethanol in CD_3CN



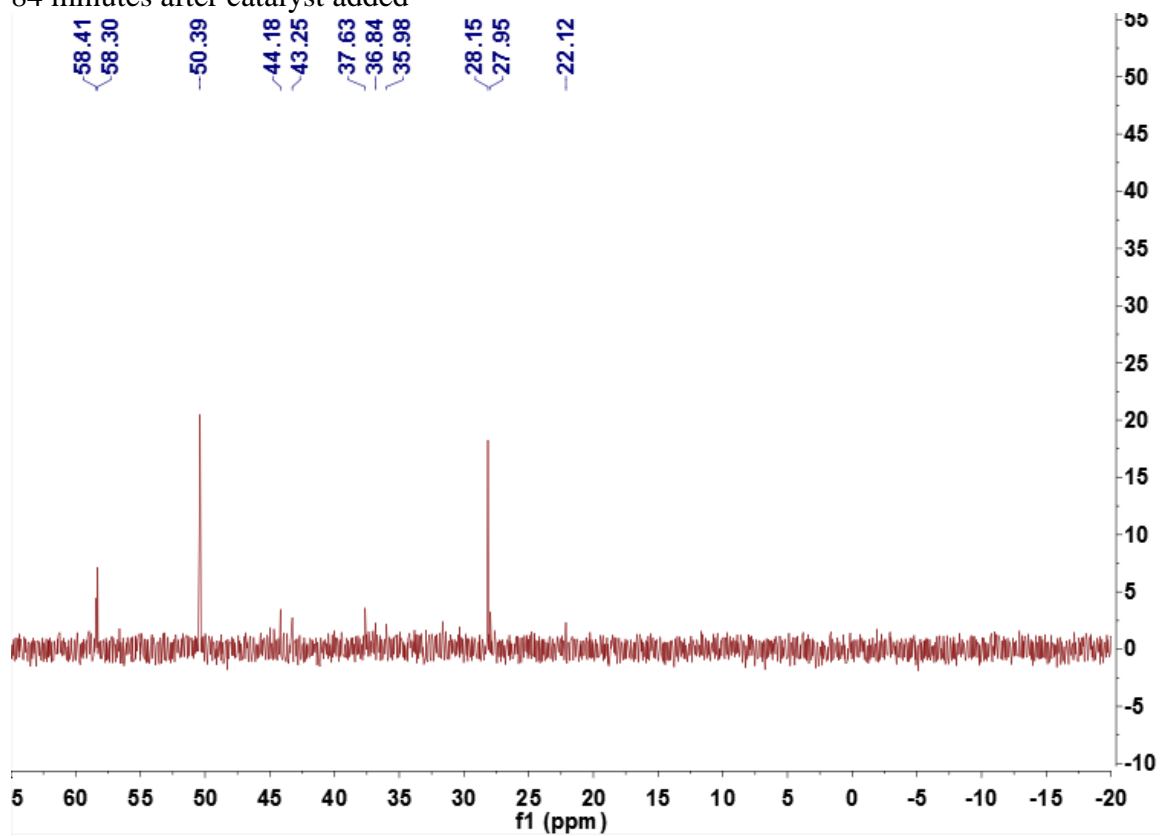
^{31}P NMR spectrum, 28 minutes after catalyst added.



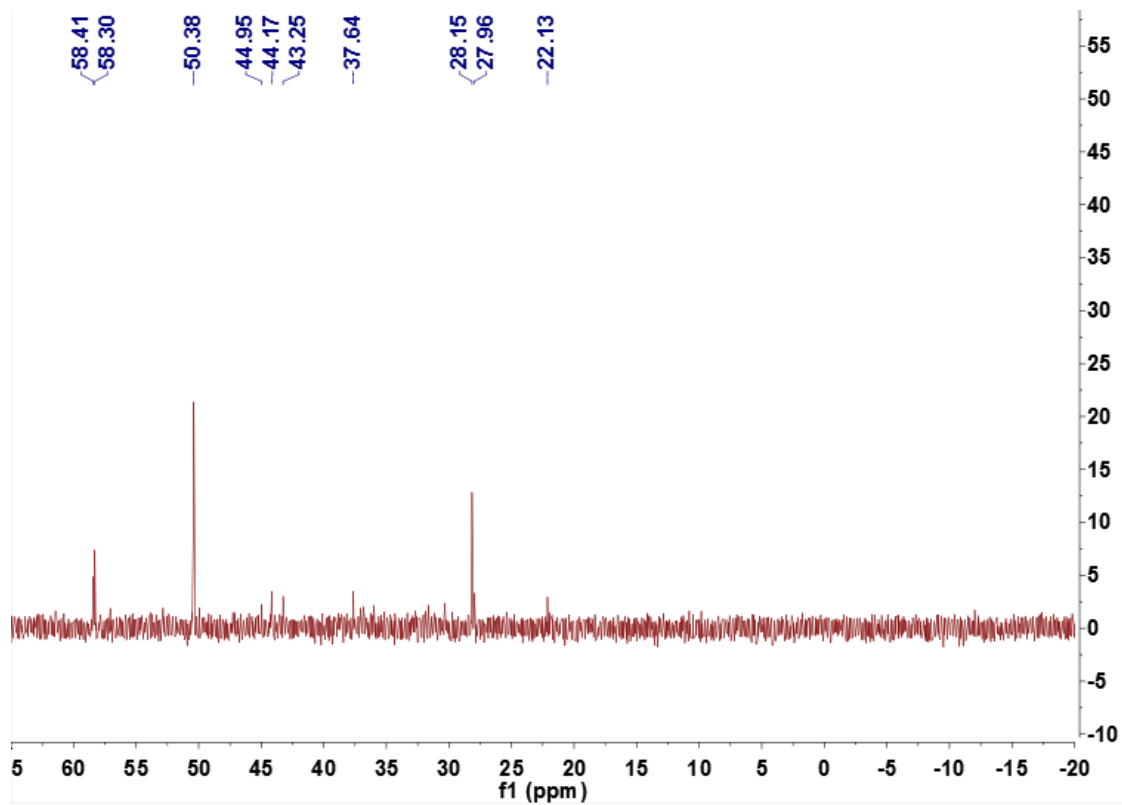
56 minutes after catalyst added



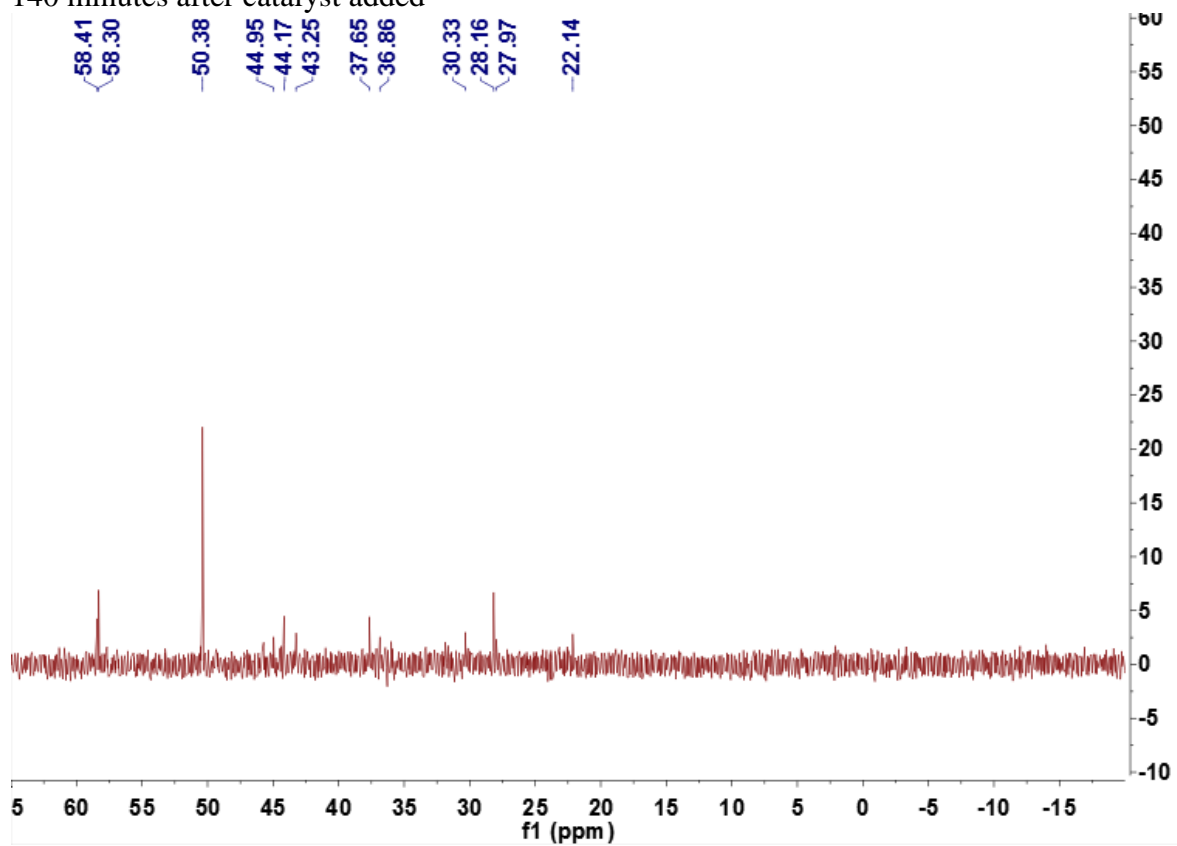
84 minutes after catalyst added



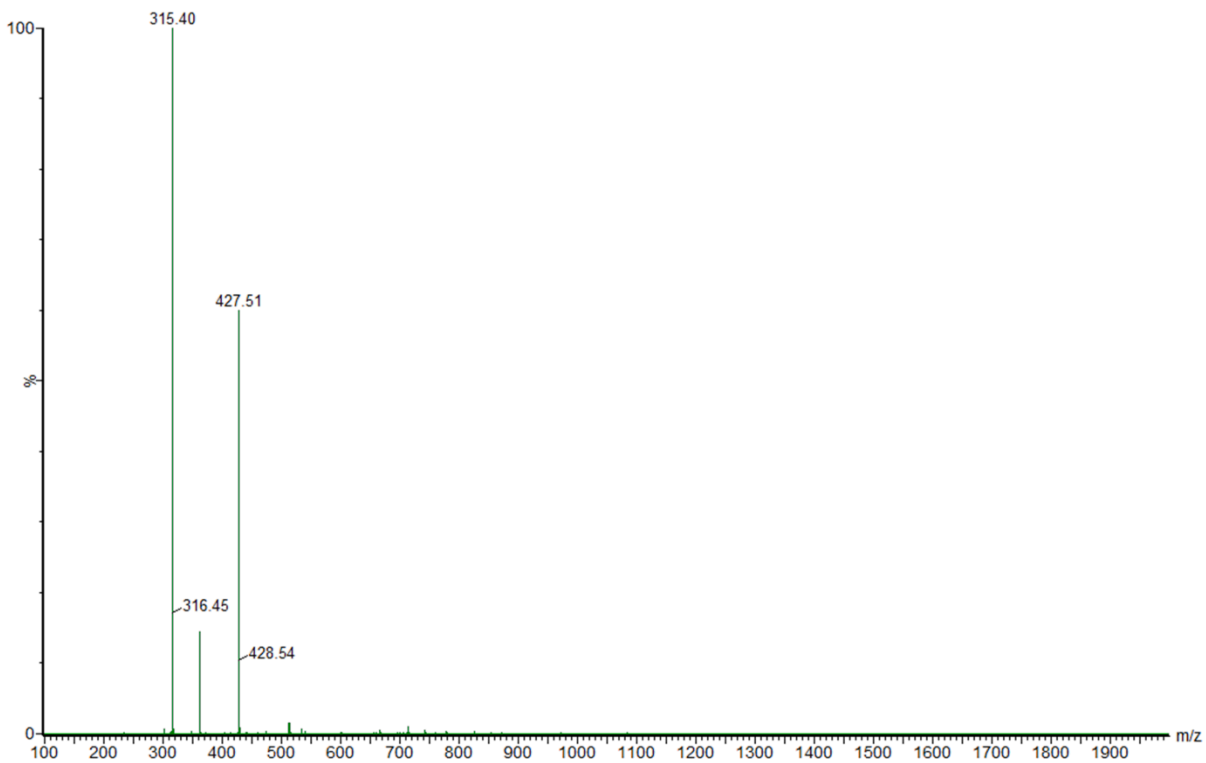
112 minutes after catalyst added



140 minutes after catalyst added



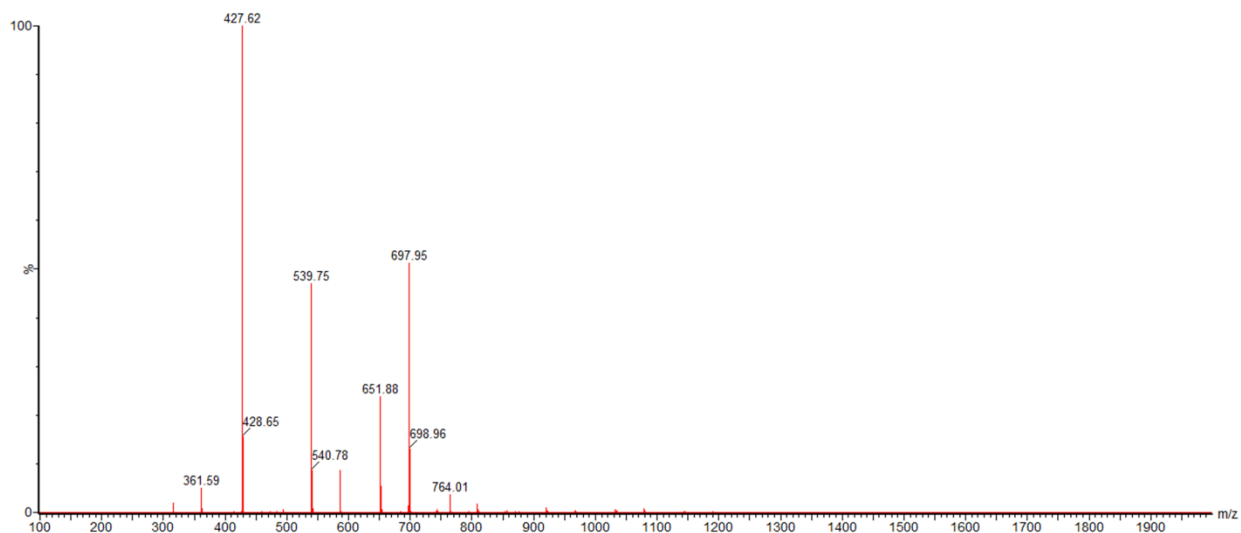
252 minutes after catalyst added

..2 ESI-MS spectra

MS combined spectra, first minute after catalyst was added to alkyne, ethanol and solvent mixture.

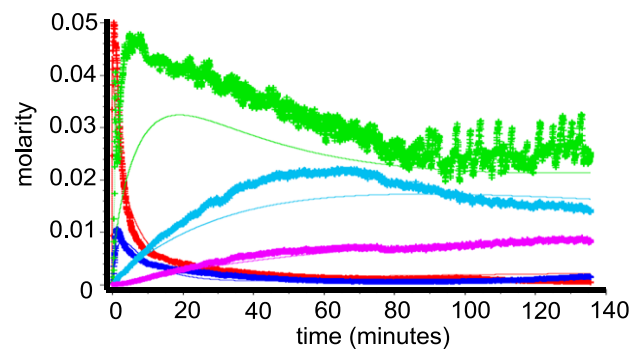
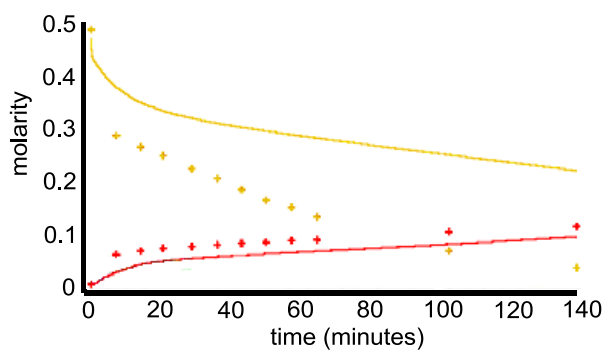


MS combined spectra over 3 minutes, 20 minutes after catalyst addition.

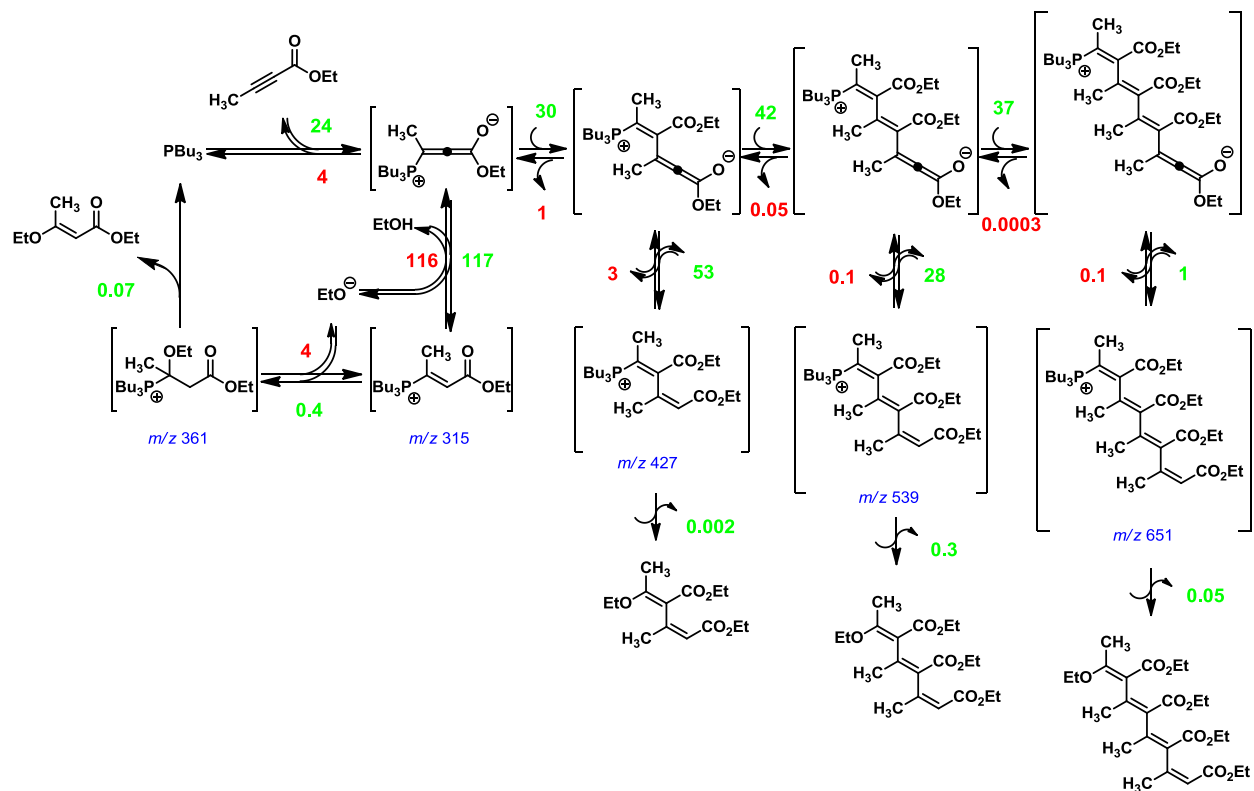


MS combined spectra over 3 minutes, 140 minutes after catalyst addition. EtOH aggregates (m/z 585, 697) are also visible. Collision induced dissociation (CID) of 15 volts caused fragmentation to a loss of 46 Da.

..3 Parameter optimization with Copasi



Optimized parameter estimated traces generated by Copasi (thin lines), compared with experimental ^1H NMR data for SM + P (left, crosses) and oligomer MS data (right, thick lines with estimated parameter traces as thin lines).



Rate constants generated by Copasi using parameter estimation for the starting alkyne/product and oligomer traces.